Design of Polyelectrolytes for use in Flocculation: Effect of Ionic Strength, pH, and Monomer Concentration on Reaction Kinetics and Copolymer Microstructure

by

Ian Desmond Conrod

Submitted in partial fulfilment of the requirements
for the degree of Master of Applied Science

at

Dalhousie University
Halifax, Nova Scotia
November 2023

Dalhousie University is located in Mi'kma'ki, the ancestral and unceded territory of the Mi'kmaq. We are all Treaty people.

Table of Contents

List of Tables

List of Figures

Abstract

Flocculation is a technology used for removing contaminants from liquids in various processes, including municipal wastewater treatment. Minimal attention has been paid to controlling the polymer microstructure using polymer reaction engineering techniques. A method was developed to study copolymerization kinetics of AMPS – AAm using in situ ^{1}H NMR. Altering the ionic strength of both AMPS – AAm and DADMAC – AAm comonomer solutions altered reactivity ratios and the resulting copolymer microstructure. From flocculation trials, it was found that varying microstructures improved flocculation performance. Next, two copolymerization models for design of experiments and reactivity ratio estimation were studied; it was found that the penultimate model may be more accurate. Finally, a 2^2 factorial design was employed for DADMAC – AAm copolymerization to understand effects of pH and monomer concentration on reactivity ratios, molecular weight averages, and flocculation performance. It was found pH and monomer concentration impacted copolymer microstructure, which in turn affected flocculation performance.

Acknowledgements

First and foremost, I thank Dr. Alison Scott for her years of guidance, support, and patience to help me become the engineer I am today. She encouraged all my ideas no matter how ambitious they were. It was a unique and exciting opportunity to be her first graduate student where I was able to learn how to train others and develop methods and procedures, I am grateful for her trust in me. Most importantly, she supported my journey of becoming a father by encouraging a paternity leave for a whole semester and ensuring there is no expectation of work after hours so I can be present and spend time with my family.

I would also like to thank my committee members Dr. Stanislav Sokolenko and Dr. Amina Stoddart. Their support with NMR knowledge and peak deconvoluting and wastewater treatment knowledge were instrumental in my degree.

I would like to thank Dr. Mike Lumsden for his aid with the NMR. His advice and training on the NMR was invaluable where I was able to log over 200 hours on the NMR.

I would like to acknowledge those that helped me experimentally. Baris Topcuoglu acquired some vial polymerization data that is used in this thesis. I would also like to acknowledge Carolina Ontiveros and Kayleigh Dunphy for their knowledge in wastewater treatment and helping acquire flocculation trial measurements.

I would also like to acknowledge my colleague Kiera for making it enjoyable working in the lab and all the discussions inside and outside academia.

To my Fiancé and daughter, Julie and Elena, your constant love and support made this possible. Despite finding out she was pregnant 1 month before the start of my masters, she encouraged me the whole way, this would not be possible without her. You girls are my motivation that helped me push to the end.

Last but not least, I would also like to express my gratitude to my parents and sisters who supported and encouraged me my whole life to pursue my dreams. I would not be who I am today without your support

1. Introduction

1.1. Motivation

Flocculants are long-chain water-soluble polymers used to separate non-settling fine particles from aqueous suspension [1]. Flocculants are used in multiple industries and one of the more common applications is in wastewater treatment. Almost all wastewater treatment plants use flocculation processes [1]. Water-soluble polymeric flocculants are high molecular weight polymers that promote the formation of bridges between particles or attract the contaminants to the flocculant via electrostatic attraction [2]. The technology has unique advantages in that there are no phase transitions, operation is straightforward and cost effective, and treatment efficiency is high for many applications [3].

The properties of flocculants, such as molecular weight distribution and charge density, are crucial factors impacting flocculation performance [1]. Flocculants with higher molecular weights will have longer chains to adsorb onto more contaminants. Adding a charged monomer can further improve flocculation using electrostatic attraction, and create more entanglement creating larger flocs [1]. Charge density also impacts flocculation performance, as polymers with higher charge density will be able to treat contaminants more effectively due to its stronger attraction (for example, between a cationic polymer flocculant and negatively charged contaminants) [4]. Therefore, the selection and development of flocculants with polymer properties that will yield effective and efficient flocculation performance is an important aspect of water treatment [5]. Despite continued advancements in novel polymer flocculants, such as incorporating biopolymers [6–8], little attention has been paid to controlling the microstructure of these materials using polymer

reaction engineering techniques that are well-established and widely used to produce other types of polymers [1]. There is a critical need to save water resources for future generations and to protect the environment from pollutants; designing novel polymer flocculants using polymer reaction engineering principles is expected to improve flocculation efficiency and minimize cost, while simultaneously reducing the resources required during product development [1].

To evaluate the potential to design polymer flocculants at a microstructural level, anionic copolymers of 2-acrylamido-2-methylpropane sulfonic acid (AMPS) and acrylamide (AAm), and cationic copolymers of diallyldimethylammonium chloride (DADMAC) and AAm are investigated in the current work. AMPS – AAm copolymers are already widely studied for enhanced oil recovery and hydrogels [9–12], therefore the system is investigated herein as a proof of concept for manipulating the polymer microstructure. In parallel, many papers have evaluated DADMAC – AAm copolymers for use in flocculation [2,3,5,13–15]. Currently, there are a handful of studies that have investigated the reaction conditions and polymerization kinetics of DADMAC – AAm [3,15–17] or studied the flocculation properties [13,14]. However, to the best of our knowledge, there is only one study correlating molecular weight averages and copolymer composition to flocculation performance [18]. The current study aims to expand on this knowledge by connecting the synthesis conditions, reaction kinetics, and flocculation performance for DADMAC – AAm.

1.2. Objectives

The primary objective of this study was to develop relationships between polymerization conditions, copolymer microstructure, and flocculation performance. If these relationships are quantified and well-understood, the copolymers can be reverse-engineered. Essentially, polymerization conditions can be manipulated to create desirable polymer properties for optimal use in specific applications. The target application for this study was to design water-soluble copolymers via free-radical copolymerization to be used in wastewater treatment facilities as flocculants. Therefore, the objectives were:

1. To study copolymerization kinetics using in situ ^{1}H NMR. In situ ^{1}H NMR is not the most widely used method, but it can be very accurate and time efficient. In situ ^{1}H NMR provides the ability to acquire a lot of information with minimal materials and time.
2. To demonstrate the potential to manipulate copolymer microstructure by changing polymerization conditions. In particular, the goal was to investigate the impact of changing conditions such as ionic strength, monomer concentration, and pH. These conditions are known to impact polyelectrolyte synthesis, either by impacting the comonomer propagation or the rigidity of the microstructure.
3. To design, synthesize, characterize, and test copolymers as flocculants in wastewater treatment. Results of the design of experiments can be used in future to determine optimal conditions to synthesize ideal copolymer flocculants. This relies on a detailed understanding how the copolymer characteristics can impact flocculation performance.

4. To utilize statistics to yield optimal copolymerization results and parameter estimates. Choosing the best models to find optimal feed fractions for copolymerization and performing statistically accurate reactivity ratio estimations are important for polyelectrolyte development.

1.3. Thesis Organization

In this thesis, there are eight chapters. The thesis contains a total of four projects related to polymer reaction engineering. The projects include AMPS – AAm copolymerization and DADMAC – AAm copolymerization. Flocculation jar testing is also discussed and tested to explore application performance of custom-made flocculants. A brief overview of each chapter is provided here.

Chapter 1 is the introduction to the thesis. The motivation, objectives, and the thesis organization are provided. The motivation discusses why this project was pursued and the objectives describe the goals of this project.

Chapter 2 contains the background information. The four main sections in Chapter 2 are flocculation and coagulation (2.1), monomers for polyelectrolyte synthesis (2.2), polymerization kinetics and polymer microstructure (2.3), and effects of changing reaction conditions (2.4). Section 2.1 regarding flocculation and coagulation largely describes the use of flocculants and coagulants in industry and the mechanisms involved. Section 2.2, monomers for polyelectrolyte synthesis, focuses on AMPS – AAm copolymerization and DADMAC – AAm copolymerization. Section 2.3 subsections include free radical copolymerization, the error-in-variables model for reactivity ratio estimation, the non-linear least squares approach for reactivity ratio estimation, design of experiments for

reactivity ratio estimation, and copolymer microstructure. Finally, Section 2.4 discusses the effect of pH, the effect of monomer concentration, and the effect of ionic strength on polyelectrolyte synthesis.

Chapter 3 details the experimental procedures used for the projects described in this thesis. Section 3.1 describes the chemicals used, while Section 3.2 describes the solution preparation procedure for Chapters 4 to 7. Section 3.3 describes the degassing procedure, which was used in all polymerizing samples to remove dissolved O_2. The nuclear magnetic resonance (NMR) procedure is discussed in Section 3.4, which includes transferring pre-polymer solution to NMR tubes, running in situ ^{1}H NMR polymerizations, and performing C^{13} NMR measurements. Gel permeation chromatography (GPC) procedures, to measure the molecular weight distribution of polymers, are provided in Section 3.5. Section 3.6 describes the procedure used for flocculation jar tests performed at the Dartmouth Wastewater Treatment Facility. Safety considerations are discussed in Section 3.7.

In Chapter 4, AMPS – AAm copolymerization kinetics were studied using in situ ^{1}H NMR. The results were compared to gravimetric methods. The effect of ionic strength on AMPS – AAm copolymerization kinetics was also investigated, specifically the impact on reactivity ratio estimates.

Chapter 5 describes an investigation of DADMAC – AAm copolymerization kinetics using in situ ^{1}H NMR. The effect of ionic strength on reactivity ratios and copolymer microstructure was investigated. The ionic strength effect on molecular weight averages and flocculation performance was also studied.

In Chapter 6, the terminal copolymerization model was compared to the penultimate copolymerization model. This chapter outlines program development for design of experiments and reactivity ratio estimation for the penultimate model, including program validation. Two case studies were explored: AMPS – AAm and DADMAC – AAm copolymerization were both investigated. The model predictions were compared to experimental data using cumulative copolymer composition and triad fractions. C^{13} NMR was used to measure triad fractions.

Chapter 7 explores the effect of pH and monomer concentration on the copolymerization of DADMAC – AAm, using a factorial design with center points. The effects of these variables on reactivity ratio estimates, triad fractions, molecular weight averages, and flocculation performance were investigated. For all of these results, 3D surface response plots were used to understand the effects of pH and monomer concentration on polymer properties.

Chapter 8 presents the thesis conclusions and recommendations. The thesis is summarized in this section, with specific comments about each chapter. Recommendations for future studies are also discussed in Chapter 8.

Finally, the Appendix is used to show sample calculations for ionic strength concentrations, chain lengths, and surface response plots.

2. Background

2.1. Flocculation and Coagulation

Flocculation is a technology often used for removing contaminants from liquids in a wide range of processes such as municipal drinking water and wastewater treatment, mineral processing, oil sands tailings dewatering, and paper making [1]. Polymer flocculants are large molecules that cause contaminants to form large particles ("flocs") using either bridging, electrostatic attraction, or both. As contaminants are attracted to the flocculant, flocs form and fall out of solution based on their large size and weight (see Figure 1). The bridging mechanism relies on adsorption, and is observed with long chain (high molecular weight) polymers. During bridging, a single polymer chain will adsorb onto multiple contaminants and become intertwined with other polymer chains, causing an increase in floc mass, therefore causing the floc to settle out of solution. The electrostatic attraction mechanism is observed using polyelectrolytes, where charged polymers attract contaminants with an opposite charge, and therefore increases the floc mass. Most common polymer flocculants are acrylamide based, usually copolymerized with anionic or cationic monomers [19]. The most common anionic monomer is acrylic acid and the most common cationic monomer is DADMAC [20,21].

(a) (b)

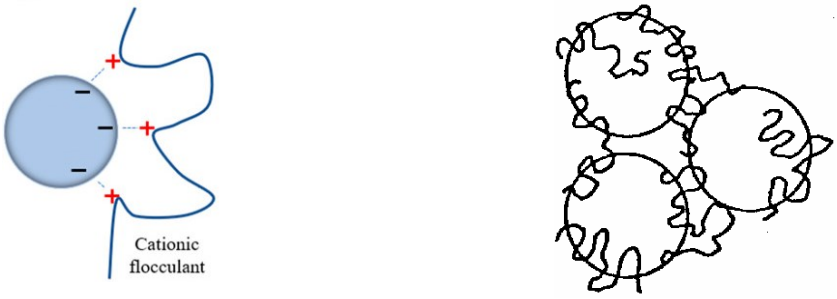

Figure 1: Examples of a) an ionic (cationic) flocculant using electrostatic attraction [22] and b) a non-ionic polymer using adsorption [23]

Coagulation is also commonly used alongside (or instead of) flocculation. Coagulants are small, charged molecules that create flocs when added to wastewater treatment processes [1]. While slightly different definitions of flocculation and coagulation are sometimes used (depending on the field), the terminology mentioned above will be used in the current project. Often, the term "flocculation" is also used to describe the slow mixing stage that occurs after adding a flocculant and/or coagulant and fast mixing. Flocs can be created by both flocculants and coagulants (used either individually or together), and are the agglomerates of contaminants and coagulant or flocculant molecules.

Commonly used coagulants are alum (Figure 2a) and ferric sulfate (Figure 2b). In drinking water plants, coagulants are generally more common than flocculants due to lower associated costs [1]. However, coagulants are generally not used alone in wastewater because large doses are required for treatment to be effective. An additional consideration is that coagulants can release aluminum or iron in the treated water, depending on the coagulant used; aluminum exposure may be linked to Alzheimer's disease [24] and iron can cause undesirable water discolouration. Therefore, in wastewater treatment, where high coagulant doses are needed, polymer flocculants are generally used along with coagulants.

Figure 2: Representative coagulants a) alum [25] and b) ferric sulfate [26]

Effective polymer flocculants will have the capacity to promote both the bridging and electrostatic attraction mechanisms. Generally, it is more challenging to prepare ionic homopolymers with high molecular weight averages (especially compared to neutral polymers), therefore copolymers are ideal as they can be synthesized to promote both mechanisms. Neutral comonomers will allow for the development of high molecular weight polymers, while the charged comonomers will ensure that electrostatic attraction is possible; it is anticipated that desirable polymers will have high molecular weight averages and will include ionic monomers with sufficient charge density [1]. Another consideration is the polymer microstructure (for example, forming a gradient or block copolymer), as studies have shown that block copolymers may improve flocculation performance [5,14]. Flocculation performance can be studied by investigating turbidity, settling velocity, and other flocculation properties; this will be discussed further in Section 3.6.

2.2. Monomers for Polyelectrolyte Synthesis

Polyelectrolytes are polymers that contain anionic and/or cationic charges. The presence of charged comonomers is especially impactful in copolymerization kinetics. For example, during the synthesis of anionic polyelectrolytes, anionic monomers and non-ionic (neutral) monomers may be combined to create copolymers. These monomers form the copolymer

backbone of the polyelectrolytes, therefore monomer selection should be carefully considered.

Non-ionic (neutral) polymers can also be used for flocculation [27–29]. Monomers used for this application are typically highly reactive and create high molecular weight polymers ($10^6 – 3\times10^7$ g/mol) [28,30]. The high molecular weight (long chain) molecules promote a bridging mechanism between the contaminant particles. As the long chain molecules adsorb onto the surface of multiple particles, the particles are more likely to agglomerate and settle out of solution.

Cationic polymers contain positively charged structural units and can be used to flocculate negatively charged particles. It is well known that most natural organic matter is negatively charged and is commonly removed via flocculation [31]. To synthesize cationic polyelectrolytes, cationic monomers are often copolymerized with non-ionic, inexpensive, and reactive comonomers such as acrylamide. Since cationic monomers are generally not as reactive and not as stable as non-ionic monomers, their homopolymers typically have lower molecular weight averages, so copolymerization of cationic and neutral comonomers is preferable [1,32].

Anionic polymers contain negatively charged structural units and can be used to flocculate positively charged particles [10,33]. Often, positively charged coagulants are added to make flocs, and anionic polymer flocculants may be added after to create larger flocs from the positively charged coagulant flocs [34].

Polyacrylamide (PAAm) is arguably the most important water-soluble non-ionic flocculant because its constituent monomer, acrylamide (AAm, Figure 3), is highly water-soluble,

cost-effective, and very reactive. Although researchers have tried to replace polyacrylamide with other flocculants due to the carcinogenic potential and toxic nature of acrylamide [1], there have not been any other monomers that have surpassed AAm in industry. PAAm does not present the same hazards as the monomer from which it is derived [35] and is therefore widely used for flocculation applications.

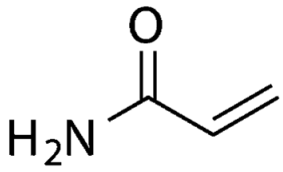

Figure 3: Molecular structure of AAm

2-Acrylamido-2-methylpropanesulfonic acid (AMPS) is a highly acidic, anionic, water-soluble monomer [36], as shown in Figure 4. AMPS homopolymers are sometimes used as hydrogels [37]. Due to its reactivity and acidity, AMPS hydrogels have been explored for electrical applications. AMPS hydrogels have electroresponsive characteristics and may be used as skin contact electrodes [37]. Copolymers containing AMPS are known to be used in enhanced oil recovery, as anionic flocculants, and as hydrogels [1,36,38]. In the current work, AMPS is copolymerized with AAm as a proof-of-concept, to compare polymerization techniques and to study the effect of ionic strength during synthesis on the resulting polymer microstructure and flocculation performance. While AMPS – AAm copolymers have the potential to be used as anionic flocculants, their evaluation was beyond the scope of the current project.

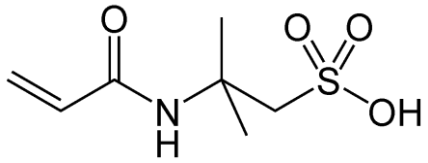

Figure 4: Molecular structure of AMPS

DADMAC is a cationic water-soluble monomer, as shown in Figure 5. DADMAC is one of the most commonly used cationic monomers for the synthesis of polymer flocculants [1], despite the monomer's potential to cause harm to aquatic life and to create carcinogenic disinfection by-products during reactions with chlorine (chlorine is often used in water treatment plants as a disinfectant) [39]. However, once polymerized, poly(DADMAC) is considered safe for use in water treatment [14]. DADMAC is almost always copolymerized with AAm to create polymers with higher molecular weight averages, which can promote the bridging effect described previously; the homopolymerization of DADMAC typically does not obtain high enough molecular weight averages to promote bridging [40].

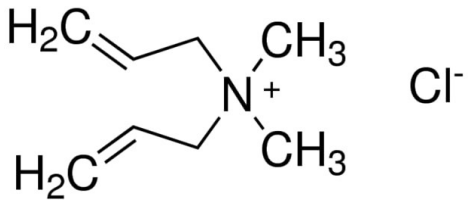

Figure 5: Molecular structure of DADMAC

Combining acrylamide with anionic or cationic monomers to create copolymer polyelectrolytes ensures the advantages of both the electrostatic and the bridging effects for a variety of wastewater treatment applications. The two specific acrylamide-based copolymers investigated in the current work, anionic AMPS – AAm and cationic DADMAC – AAm, are described in what follows.

2.2.1. AMPS – AAm Copolymerization

AMPS – AAm copolymerization has been widely studied [9,10,12,38,41,42]. This copolymer system is often investigated for hydrogel and enhanced oil recovery applications [9,11,30,41]. It has been demonstrated that application-specific properties are dependant on the microstructure of the copolymer, which can be influenced by the polymerization conditions [10,39,42,43]. Therefore, there have been studies developed to improve understanding of the polymerization kinetics [10,12,38,42], polymer characterization [11,41,44], and polymer application performance [30,45]. Although it is not common for AMPS to be used in flocculation, one study has been identified using AMPS-containing terpolymers in flocculation [33].

Therefore, in the current work, the AMPS – AAm copolymer system is used as a "proof-of-concept" to validate the methods used to investigate the DADMAC – AAm copolymerization. The effect of ionic strength on the copolymerization kinetics of AMPS – AAm is also studied.

2.2.2. DADMAC – AAm Copolymerization

One of the challenges in DADMAC – AAm copolymerization is that DADMAC does not incorporate as readily as AAm. From the literature (summarized in Table 1), it has been observed that reactivity ratios range from 5 to 7 for AAm and from 0.03 to 0.6 for DADMAC. As shown in Figure 6, the copolymerization strongly favours the AAm monomer, and the DADMAC demonstrates minimal incorporation until the AAm monomer is depleted.

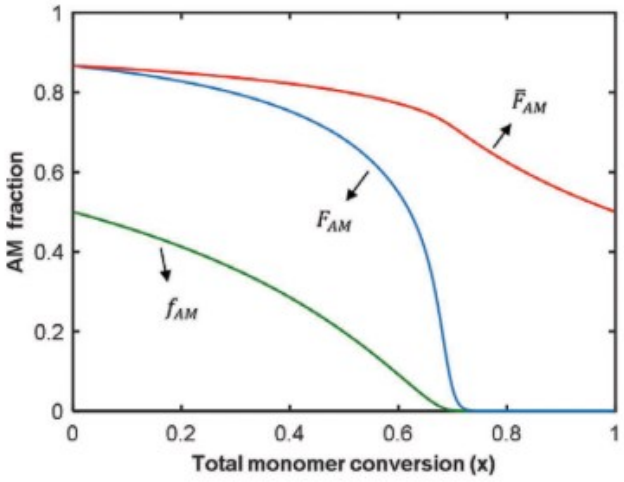

Figure 6: Acrylamide fraction as a function of conversion [1]

In Figure 6, AM represents acrylamide, f_{AM} is the acrylamide fraction in the monomer feed, F_{AM} is the instantaneous copolymer composition of acrylamide, $\overline{F}_{AM}$ is the cumulative copolymer composition of acrylamide, and the balance is DADMAC.

The following two paragraphs discuss articles by Abdollahi et al. [3] and Baade et al. [15]. These two articles were taken from Table 1, these papers were selected due to either similarities to the method, reaction conditions, and/or analysis methods used in this study. Abdollahi et al. [3] used in-situ ^{1}H NMR copolymerization and polymerized at 50°C. Baade et al. [15] is also discussed as they are the only articles that used EVM. Abdollahi et al. [3] studied the homo- and copolymerization kinetics of DADMAC and AAm. In this work, all polymer synthesis was conducted at 50°C using potassium persulfate (KPS) as the initiator in a D_2O solution. Total monomer, NaCl, and KPS concentration were set to 1 M, 0.1 M, and 3×10^{-2} M, respectively. Based on the information provided in the study, pH did not seem to be controlled. Samples were then measured in situ using ^{1}H NMR to obtain conversion versus time plots and to estimate reactivity ratios. The reactivity ratios were

calculated using the Mao-Huglin [46] and extended Kelen-Tudos [47] methods at medium to high conversions. The estimated reactivity ratios were reported as $r_{DADMAC} = 0.12 \pm 0.04$ and $r_{AAm} = 6.9 \pm 2.0$.

Baade et al. [15] also studied the copolymerization kinetics of DADMAC – AAm. In this study, copolymer synthesis was performed in a continuous stirred tank reactor to allow for constant composition in the monomer phase. The pH of all monomer solutions was 5.2 pH, the reaction temperature was maintained at 50°C, and the initiator used was azodimethylvaleronitrile. Polymer samples' reactivity ratios were estimated using the error-in-variables model (EVM); while this approach is the most statistically correct method for reactivity ratio estimation, EVM is rarely used [48]. This will be discussed further in Section 2.3.3. Colloid titration and high-performance liquid chromatography (HPLC) were used to measure remaining monomer from the reaction [15]. For HPLC, a CN column was used, which is known to separate amines and amides. Polymers were retained in the guard column and the unreacted monomer concentration was measured. Colloid titration was observed to be very unprecise, so HPLC was the main method employed. Interestingly, this was the only paper identified during the literature review that used EVM for parameter estimation in DADMAC – AAm copolymerization. The reactivity ratio estimates obtained using this approach were $r_{DADMAC} = 0.06 \pm 0.03$ and $r_{AAm} = 6.4 \pm 0.4$. However, the authors did not indicate whether they used the cumulative or instantaneous model. Since the data that they provided was the instantaneous copolymer composition, the instantaneous model was likely used.

There are many more papers that have estimated reactivity ratios for DADMAC – AAm copolymerization using linear estimation methods such as the Kelen-Tudos method [16,49,50]. These papers, along with the studies described previously, are summarized in Table 1.

Table 1: DADMAC – AAm reactivity ratios from the literature

r_{DADMAC}	r_{AAm}	Monomer Concentration	Initiator	Temp.	pH	Solvent	Measurement Method	Reactivity Ratio Estimation	Reference
0.12±0.03	7.09±1.4	1 M	KPS	50°C	N/A	D_2O	In situ NMR	Mao-Huglin	[3]
0.12±0.04	6.9±2.0	1 M	KPS	50°C	N/A	D_2O	In situ NMR	Extended Kelen-Tudos	[3]
0.12	6.664	40%	$K_2S_2O_8$	40°C	buffer (5.5-6.5)	Water:EtOH 50%:50%	Ion Chromatography	Fineman-Ross	[52]
0.58	6.7	1.5 M	$K_2S_2O_8$-isopropanol	40°C	6.1	Water/ 0.9% Isopropanol	Titration	Fineman-Ross	[50]
0.05	6.06	3 M	S_2O_8	35°C	N/A	Water	Electrometric Titration	Kelen-Tudos (KT)	[49]
0.11	5.95	4 M	S_2O_8	35°C	N/A	Water	Electrometric Titration	KT	[49]
0.14	6.11	2.5 M	ammonium persulfate, sodium bisulfate	45°C	N/A	Water	Titration	Linear method	[17]
0.03±0.02	6.0±1.0	0.5 M	V50	50°C	N/A	Water	Potentiometric Titration	KT	[51]
0.03±0.01	6.7±0.7	1.5 M	V50	50°C	N/A	Water	Potentiometric Titration	KT	[51]
0.04±0.01	4.6±1.2	3.0 M	V50	50°C	N/A	Water	Potentiometric Titration	KT	[51]
0.06±0.03	6.4±0.4	0.5 M	ACVA	50°C	5.2	Water	HPLC	EVM	[15]

EtOH = ethanol, D_2O = deuterium oxide, NMR = nuclear magnetic resonance, ACVA = 4,4′-azobis(4-cyanovaleric acid), V50 = 2,2-azobis(2-amidinopropane) dihydrochloride, HPLC = high pressure liquid chromatography, EVM = error-in-variables method, KT = Kelen-Tudos method

2.3. Polymerization Kinetics and Polymer Microstructure

Despite growing interest and advancements in polymer flocculants, there have been few studies exploring the impact of polymer microstructure on flocculant performance [1]. In the current study, one of the goals was to investigate the ability to manipulate polymer microstructure by changing the reaction conditions to alter the reaction kinetics.

2.3.1. Free Radical Polymerization

Free radical polymerization is a common method for synthesizing polymers from vinyl monomers. Free radical polymerization has 3 main steps, initiation, propagation, and termination. All of the studies summarized in Table 1 employed free radical polymerization for the synthesis of DADMAC – AAm copolymers [3,15,17,49–52]. Multiple techniques for initiating the polymerization exist; in the studies shown in Table 1, the most common initiation methods were thermal [15,16,50,51,53] and ultraviolet [8] initiation, while some studies used ultrasonic initiation [5,39,53].

Free radical polymerization is well understood and equations have been established to predict polymerization rate (R_p), as seen in Equation 1 [54]. Equation 2 to 12 will discuss how the polymerization rate equation is derived.

$$R_p = k_p[M]\left(\frac{R_i}{k_t}\right)^{\frac{1}{2}} = k_p[M]\left(\frac{f k_d[I]}{k_t}\right)^{\frac{1}{2}} \qquad \text{Equation 1}$$

Where k_d is the initiator decomposition rate constant, f is the initiator efficiency, k_t is the overall termination rate constant, k_p is the propagation rate constant, [M] is the monomer concentration, and [I] is the initiator concentration [55].

To initiate free radical polymerization, free radicals are needed. Free radicals are unpaired valence electrons. In the current work, free radicals are introduced to the pre-polymerization solution using a thermolabile compound called an initiator. When the initiator temperature is increased, the initiator decomposes and two free radicals are created. Equation 2 demonstrates the reaction for initiator decomposition [56].

$$I \overset{k_d}{\rightarrow} 2R^{\blacksquare} \qquad \text{Equation 2}$$

Where *I* represents the initiator, $R^{\blacksquare}$ represents the free radical. The free radicals then react with monomers in the initiation step, as shown in Equation 3 [56].

$$R^{\blacksquare} + M \overset{k_i}{\rightarrow} M_1^{\blacksquare} \qquad \text{Equation 3}$$

Where *M* represents the (unbound) monomer, $M_1^{\blacksquare}$ represents the single monomer unit (subscript 1) with a radical at its end, and k_i represents the initiation rate constant. The rate of initiation can be expressed in Equation 4.

$$R_i = 2fk_d[I] \qquad \text{Equation 4}$$

Where *f* is the initiator efficiency.

The propagation step is where the polymer chains grow and is the focus of this study. Through successive addition reactions, monomers are added to the polymer chain end. The free radical then moves along the polymer chain as propagation occurs, and the free radical is always at the end of the chain. A representative propagation reaction is shown in Equation 5.

$$M_i^{\blacksquare} + M \overset{k_p}{\rightarrow} M_{i+1}^{\blacksquare} \qquad \text{Equation 5}$$

Where $M_i^{\blacksquare}$ is a monomer chain with i monomer units, with the i^{th} monomer having a radical end, and $M_{i+1}^{\blacksquare}$ is a monomer chain with i+1 units, now with the added monomer having a radical end. This addition reaction happens continuously to form a chain, where each addition step has the same rate constant, k_p, based on the assumption that k_p is independent of the size of the propagating polymer chain. R_p, the rate of propagation, is represented in Equation 6.

$$R_p = k_p[M^{\blacksquare}][M] \qquad \text{Equation 6}$$

Where k_p is the propagation rate constant and $[M^{\blacksquare}]$ represents the sum of the concentrations of all monomer-ended radicals in the system [56].

The chain growth sequence that occurs during propagation can end when two radicals from two chains come together, creating a paired electron bond. This is called termination by combination, an example of which is shown in Equation 7.

$$M_n^{\blacksquare} + M_m^{\blacksquare} \xrightarrow{k_{tc}} M_{(n+m)} \qquad \text{Equation 7}$$

Termination is also possible by a disproportionation reaction; this occurs when a hydrogen is transferred. The reaction is shown in Equation 8.

$$M_n^{\blacksquare} + M_m^{\blacksquare} \xrightarrow{k_{td}} M_m + M_n \qquad \text{Equation 8}$$

The rate of reaction for termination can be calculated using Equation 9. k_t can be calculated by adding together k_{tc} and k_{td}.

$$R_t = 2k_t[M^{\blacksquare}]^2 \qquad \text{Equation 9}$$

It is assumed that at steady-state the rate of initiation is equal to the rate of termination. This relationship is showed in Equation 10.

$$\frac{d[M^{\blacksquare}]}{dt} = 0 \text{ at steady state} \qquad \text{Equation 10}$$

And

$$R_i = R_t \text{ at steady state} \qquad \text{Equation 11}$$

Therefore substituting Equation 4 and Equation 9 into Equation 11, you get Equation 12.

$$2fk_d[I] = 2k_t[M^{\blacksquare}]^2 \qquad \text{Equation 12}$$

Equation 6 can be used to substitute $[M^{\blacksquare}]$ in Equation 12. The equation can then be rearranged to get Equation 1 to complete the derivation.

2.3.1.1. Terminal Copolymerization Model

During copolymerization, the polymerization kinetics become more complex. According to the terminal model to describe copolymerization kinetics, monomer reactivities are based on the terminal unit $[M_i^{\blacksquare}]$ and the monomer being added to the chain, which means that there are four possible propagation reactions, as seen in Figure 7 [57].

$$\sim\sim M_1^{\blacksquare} + M_1 \xrightarrow{k_{11}} \sim\sim M_1 - M_1^{\blacksquare}$$

$$\sim\sim M_1^{\blacksquare} + M_2 \xrightarrow{k_{12}} \sim\sim M_1 - M_2^{\blacksquare}$$

$$\sim\sim M_2^{\blacksquare} + M_1 \xrightarrow{k_{21}} \sim\sim M_2 - M_1^{\blacksquare}$$

$$\sim\sim M_2^{\blacksquare} + M_2 \xrightarrow{k_{22}} \sim\sim M_2 - M_2^{\blacksquare}$$

Figure 7: Terminal model for free-radical copolymerization

Where $M_i^{\blacksquare}$ is the propagating species with terminal monomer *i*. The reactivity ratios, r_1 and r_2, are the ratios of the homo-propagation rate constant (k_{ii}) relative to cross-propagation rate constant (k_{ij}), as shown in Equation 13 [54].

$$r_1 = \frac{k_{11}}{k_{12}} \qquad r_2 = \frac{k_{22}}{k_{21}} \qquad \text{Equation 13}$$

A copolymerization model and experimental data can be used to estimate reactivity ratios for a given copolymerization. At minimum, monomer (feed) composition and copolymer composition are required to calculate reactivity ratios.

Obtaining reactivity ratios makes it possible to predict the copolymer composition and microstructure using the feed composition. The chain composition of copolymers impacts the chemical, physical, and mechanical properties of materials, so estimating reliable reactivity ratios is extremely important [58]. There have been numerous publications about reactivity ratio estimation for various copolymer systems, including references [3,15,17,38,43,49,50,53,58,59] and the studies shown in Table 1. The most widely used model for copolymerization is the Mayo-Lewis model (Equation 14), which was developed in 1944 for multicomponent polymerization systems [60]. The Mayo-Lewis equation

relates the instantaneous copolymer composition (F_i) to the free (unbound) monomer composition (f_i) using reactivity ratios.

$$F_1 = \frac{r_1 f_1^2 + f_1(1-f_1)}{r_1 f_1^2 + 2f_1(1-f_1) + r_2(1-f_1)^2} \qquad \text{Equation 14}$$

$$F_1 = \frac{d[M_1]}{d[M_1]+d[M_2]} \text{ and } f_1 = \frac{[M_1]}{[M_1]+[M_2]} \qquad \text{Equation 15}$$

Where $[M_1]$ is the monomer concentration of species 1 and $[M_2]$ is the monomer concentration of species 2.

Although linear methods should not be used to solve non-linear equations, many publications that estimate reactivity ratios have used linear methods such as Fineman-Ross and Kelen-Tudos [2,12,53,61–65,16,17,42,48–52]. Behnken and Tidwell-Mortimer were the first to estimate reactivity ratios using a non-linear approach; these groups also emphasized that using linear estimation methods is statistically incorrect [58,66]. Linearizing a kinetic model that is inherently non-linear requires assumptions that are not accurate (aside from statistical issues related to the error structure) [58]. Polymerizations must also be kept at very low conversions to ensure that the assumption of no composition drift is valid [38], but polymerizations at low conversion are very error-prone, and are therefore not ideal. The estimation method that is believed to be the most statistically correct approach is the error-in-variables model (EVM) [48], as it employs cumulative copolymer composition up to high conversions and takes composition drift into account [48]. This will be discussed further in Section 2.3.3.

2.3.1.2. Penultimate Copolymerization Model

The penultimate model to describe copolymerization kinetics relies on more complex relationships than the terminal model. The terminal model only considers the monomer at the end of the propagating polymer chain (that is, the terminal unit) and the monomer propagating onto the chain (Figure 7). In contrast, the penultimate model considers the last two monomers on the propagating polymer chain (that is, the penultimate unit and the terminal unit; see Figure 8). The penultimate model can be beneficial if there are effects beyond the terminal monomer that need to be considered. In the current study, large ionic monomers are employed that may demonstrate penultimate effects.

Since the final two monomers on the propagating chain are considered in the penultimate model, there are now twice as many rate constants, and therefore twice as many reactivity ratios [57].

$$\sim\sim M_1M_1^{\blacksquare} + M_1 \xrightarrow{k_{111}} \sim\sim M_1M_1M_1^{\blacksquare}$$

$$\sim\sim M_1M_1^{\blacksquare} + M_2 \xrightarrow{k_{112}} \sim\sim M_1M_1M_2^{\blacksquare}$$

$$\sim\sim M_2M_2^{\blacksquare} + M_1 \xrightarrow{k_{221}} \sim\sim M_2M_2M_1^{\blacksquare}$$

$$\sim\sim M_2M_2^{\blacksquare} + M_2 \xrightarrow{k_{222}} \sim\sim M_2M_2M_2^{\blacksquare}$$

$$\sim\sim M_2M_1^{\blacksquare} + M_1 \xrightarrow{k_{211}} \sim\sim M_2M_1M_1^{\blacksquare}$$

$$\sim\sim M_2M_1^{\blacksquare} + M_2 \xrightarrow{k_{212}} \sim\sim M_2M_1M_2^{\blacksquare}$$

$$\sim\sim M_1M_2^{\blacksquare} + M_1 \xrightarrow{k_{121}} \sim\sim M_1M_2M_1^{\blacksquare}$$

$$\sim\sim M_1M_2^{\blacksquare} + M_2 \xrightarrow{k_{122}} \sim\sim M_1M_2M_2^{\blacksquare}$$

Figure 8: Penultimate model for free-radical copolymerization

The Mayo-Lewis equation has also been extended for the penultimate model to calculate the instantaneous copolymer composition, as shown in Equation 16 [67]. The four reactivity ratios are defined in Equation 17.

$$F_1 = \frac{r_{21}f_1^2\left(\frac{r_{11}f_1+f_2}{r_{21}f_1+f_2}\right)+f_1f_2}{r_{21}f_1^2\left(\frac{r_{11}f_1+f_2}{r_{21}f_1+f_2}\right)+2f_1f_2+r_{12}f_2^2\left(\frac{r_{22}f_2+f_1}{r_{12}f_2+f_1}\right)} \quad \text{Equation 16}$$

$$r_{11} = \frac{k_{111}}{k_{112}} \quad r_{21} = \frac{k_{211}}{k_{212}} \quad r_{12} = \frac{k_{122}}{k_{121}} \quad r_{22} = \frac{k_{222}}{k_{221}} \quad \text{Equation 17}$$

Although the terminal model has been shown to be accurate [38], the penultimate model provides the ability to improve accuracy, especially for monomer structural units that may affect monomers being incorporated two structural units away. The penultimate model also identifies penultimate effects if the two reactivity ratios for one of the monomers are significantly different. An example can be seen in a paper by Burke et al. [68] where the penultimate reactivity ratios for styrene-acrylonitrile copolymerization are r_{11}=0.229, r_{21}=0.634, r_{22}=0.039, and r_{12}=0.091 (1 = styrene). When comparing r_{11} and r_{21}, the reactivity ratio more than doubles when the monomer two structural units away is not styrene.

2.3.2. Molecular Weight Estimation

The kinetic chain length, v, can be estimated using Equation 18 [56]. The kinetic chain length represents the average number of monomers that react with an active center from initiation to termination. The equation is the ratio of rate of polymerization to the rate of

initiation under steady-state conditions. Typically, free radical copolymerization is terminated by combination, therefore $\overline{DP}_n = 2v$, where $\overline{DP}_n$ is the number-average degree of polymerization.

$$v = \frac{k_p[M]}{2(fk_d[I]k_t)^{\frac{1}{2}}} \quad \text{Equation 18}$$

The number-average molecular weight, $\overline{M}_n$, can then be calculated by using Equation 19.

$$\overline{M}_n = M_0\overline{DP}_n \quad \text{Equation 19}$$

Where M_0 is the monomer molecular weight.

2.3.3. Error-in-Variables Model (EVM) for Reactivity Ratio Estimation

The error-in-variables model (EVM) is a non-linear parameter estimation technique that considers the error present in all variables [54,58]. The nested-iterative algorithm has two iterative loops, the inner and outer loops. At each iteration step, the outer loop searches for parameter estimates while the inner loop finds the 'true' values of the variables. As shown in Equation 20, $\underline{x_i}$ is the vector of obtained measurements, $\underline{\xi_i}$ is the vector of unknown 'true' values of the measurements (estimated within the inner loop of the nested-iterative loop), *k* is a constant that reflects the uncertainty of the variables, and $\underline{\varepsilon_i}$ is the error term for the i^{th} trial [58]. A copolymerization model is used for the outer loop, as seen in Equation 21, to relate the estimated 'true' variables ($\underline{\xi_i}$) and the parameters ($\underline{\theta}$; that is, the reactivity ratio estimates) [48,54].

$$\underline{x_i} = \underline{\xi_i}(1 + k\underline{\varepsilon_i}) \quad \text{Equation 20}$$

$$\underline{g}\left(\underline{\xi_i}, \underline{\theta}\right) = 0 \qquad \text{Equation 21}$$

EVM minimizes the sum of squares between the observed and predicted values, both in terms of the parameter estimates and the independent variables, using the nested-iterative approach. When Equation 22 (the objective function) is minimized, the best estimates for the parameters (here, the reactivity ratios) and the independent variables have been determined [48].

$$\Phi = \frac{1}{2}\sum_{i=1}^{n} r_i(\underline{\overline{x}}_i - \underline{\hat{\xi}}_i)'\underline{V}^{-1}(\underline{\overline{x}}_i - \underline{\hat{\xi}}_i) \qquad \text{Equation 22}$$

Where n is the number of experimental trials, r_i is the number of replicates for the i^{th} trial, $\underline{\overline{x}}_i$ is the average of the r_i measurements ($\underline{x_i}$), $\underline{\hat{\xi}_i}$ is an estimate of the true values of the variables ($\underline{\xi_i}$) and $\underline{V}$ is the variance-covariance matrix of the variables [54,58]. Graphically, as shown in Figure 9, the data points represent the observed/measured variables and $\underline{\hat{\xi}}$ from Equation 22 is the estimated true value. The estimates of the true values are represented by the tangent points of the ellipses and the model prediction.

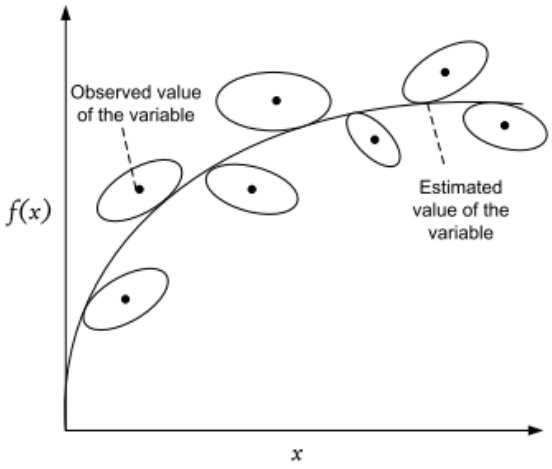

Figure 9: Graphical representation of EVM [58]

A user-friendly version of the EVM program [48] was used in this study for estimating reactivity ratios using the terminal model; full conversion data were used and the cumulative copolymer composition model was applied. The conversion, feed compositions, cumulative copolymer compositions, error tolerance, and initial reactivity ratios estimates (from the literature) were the program inputs. More information about the program can be found in the following references [48,58]. The cumulative copolymer composition ($\bar{F}_1$), can be calculated using the Skeist equation, Equation 23, using the initial feed fraction (f_{10}), the monomer (free or unbound) fraction (f_1) in the reacting mixture, and molar conversion (X_n).

$$\bar{F}_1 = \frac{f_{10} - f_1(1 - X_n)}{X_n} \qquad \text{Equation 23}$$

$$\frac{df_1}{dX_n} = \frac{f_1 - F_1}{1 - X_n} \qquad \text{Equation 24}$$

As the reaction occurs, the differential copolymer composition equation is required, as shown in Equation 24. X_n will change during polymerization and is used to estimate the fraction of unreacted monomer.

2.3.4. Non-Linear Least Squares (NLLS) for Reactivity Ratio Estimation

Non-linear least squares (NLLS) is a common and widely accepted method of estimating parameters in non-linear models from experimental data [58]. NLLS minimizes the sum of residuals squared to find the optimal parameter estimates. For NLLS, there are 3 assumptions: 1, the model perfectly describes the system, 2, the error in the independent variables is negligible, and 3, the error is assumed to be independent and identically

normally distributed with mean zero and variance σ^2 [58]. The general equation for NLLS is shown in Equation 25.

$$\underline{y_i} = g\left(\underline{x_i}, \underline{\theta}\right) + \underline{\varepsilon_i} \qquad i=1,2,\ldots,n \qquad \text{Equation 25}$$

The minimum of the sum of residuals squared was determined using shuffled complex evolution (SCE). This method uses a natural evolution as a global search; it starts with a lower and upper boundary and then fills a population of samples [58]. These samples are divided into groups or complexes, and then each of the complexes evolves and iterates to the optimum point(s) [69]. The SCE program is the same code that is referenced by Kazemi et al. [70].

2.3.5. Design of Experiments for Reactivity Ratio Estimation

Employing design of experiments (DOE) is extremely important in reactivity ratio estimation. Collecting undesigned data will create more error, especially if experimental conditions are chosen at random [54,58]. Effective use of DOE allows the user to acquire more information from fewer experiments. For example, DOE can be used to estimate the optimal feed compositions for reactivity ratio estimation experiments; this makes it possible to determine the two monomer feed compositions that have the least amount of variance/covariance. In contrast, with no design, some articles have reported using five different feed compositions to collect reactivity ratio estimation data. Using DOE makes it possible to use less materials and save experimentation time.

Tidwell and Mortimer developed one of the first non-linear design of experiments approaches for reactivity ratio estimation [66]. The Tidwell-Mortimer method applies an approximate D-optimality criterion to the Mayo-Lewis copolymerization equation (Equation 14) [54,58,66]. The Tidwell-Mortimer design gives the following experimental conditions as optimal suggestions.

$$f_{1,1} \cong \frac{r_2}{2+r_2} \qquad f_{1,2} \cong \frac{2}{2+r_1} \qquad \text{Equation 26}$$

Where $f_{1,1}$ and $f_{1,2}$ are the two feed compositions (feed fractions) for species 1. When starting a new project, r_1 and r_2 are acquired using literature data collected under similar reaction conditions (temperature, monomer concentration, pH, ionic strength, initiator, etc.).

The EVM method can be used for both reactivity ratio estimation and DOE as it takes both the independent (feed compositions), dependant (copolymer compositions), and experimental limitations into account [54,58]. The EVM design criterion maximizes the determinant of the information matrix ($\underline{G}$), which is the inverse of the variance-covariance matrix of the parameters (see Equations 27 through 29).

$$\underline{G} = \sum_{i=1}^{n} r_i \underline{Z'}_i \left(\underline{B}_i \underline{V} \, \underline{B'}_i \right)^{-1} \underline{Z}_i \qquad \text{Equation 27}$$

$$\underline{B}_i = \left[\frac{\partial g(\underline{\xi}_i, \underline{\theta})}{\partial (\underline{\xi}_i)_t} \right]_{\underline{\xi}_i = \underline{\xi}_i^{(k)}} \text{ for the t}^{\text{th}} \text{ element} \qquad \text{Equation 28}$$

$$\underline{Z}_i = \left[\frac{\partial g(\underline{\xi}_i, \underline{\theta})}{\partial \theta_m} \right] \text{for the m}^{\text{th}} \text{ element} \qquad \text{Equation 29}$$

Where r_i is the number of replicates at the i^{th} trial (out of n trials), $\underline{Z_i}$ is the vector of partial derivatives of the copolymerization model with respect to the parameters (that is, the reactivity ratios), $\underline{B_i}$ is the vector of partial derivatives of the copolymerization model with respect to the variables (that is, the feed composition (f_i) and copolymer composition (F_i)), k is the iteration step, and $\underline{V}$ is the variance-covariance matrix of the measurements. Further information on the EVM design of experiments approach is provided in the following papers [58,70].

For the evaluation of the penultimate copolymerization model, D-optimality was used to find the optimal feed compositions. SCE was used again to search for the optimal points [71,72].

$$\varphi = \max\left(\sum_{i=1}^{p}\sum_{j=i}^{p}\sigma^{ij}J'_{i}J_j\right) \qquad \text{Equation 30}$$

$$J_i = \begin{bmatrix} \frac{dF_1}{dr_{11}} & \frac{dF_1}{dr_{21}} & \frac{dF_1}{dr_{22}} & \frac{dF_1}{dr_{12}} \\ \frac{dF_2}{dr_{11}} & \frac{dF_2}{dr_{21}} & \frac{dF_2}{dr_{22}} & \frac{dF_2}{dr_{12}} \\ \frac{dF_3}{dr_{11}} & \frac{dF_3}{dr_{21}} & \frac{dF_3}{dr_{22}} & \frac{dF_3}{dr_{12}} \\ \frac{dF_4}{dr_{11}} & \frac{dF_4}{dr_{21}} & \frac{dF_4}{dr_{22}} & \frac{dF_4}{dr_{12}} \end{bmatrix} \qquad \text{Equation 31}$$

Where φ represents the maximum of the multivariate D-optimal criterion for the parameter estimates, p is the number of measured responses, σ^{ij} is the ij^{th} element of the true covariance matrix for the number of measurements available from a single experiment, and J_i is the Jacobian of the i^{th} response with respect to the parameters [71]. i and j relate to the row and column number.

2.3.6. Copolymer Microstructure

In terms of copolymer microstructures, there are four basic types: random, alternating, block and graft. Random copolymer microstructure is self-explanatory; the distribution of comonomers is random (e.g., AABABBA). Alternating copolymers have regularly alternating comonomers (e.g., ABABABAB). Block copolymers are copolymers with long uninterrupted chains of one comonomer type (e.g., AAAABBBBB). Gradient copolymers are a slight variation on block copolymers, where the chain primarily contains one comonomer and gradually becomes dominated by the other comonomer. Finally, graft copolymers are copolymers that contain one comonomer type within the backbone (as a repeating unit), and a second comonomer forms chains attached to the polymer backbone to create branching. An overview of copolymer microstructures is provided in Figure 10.

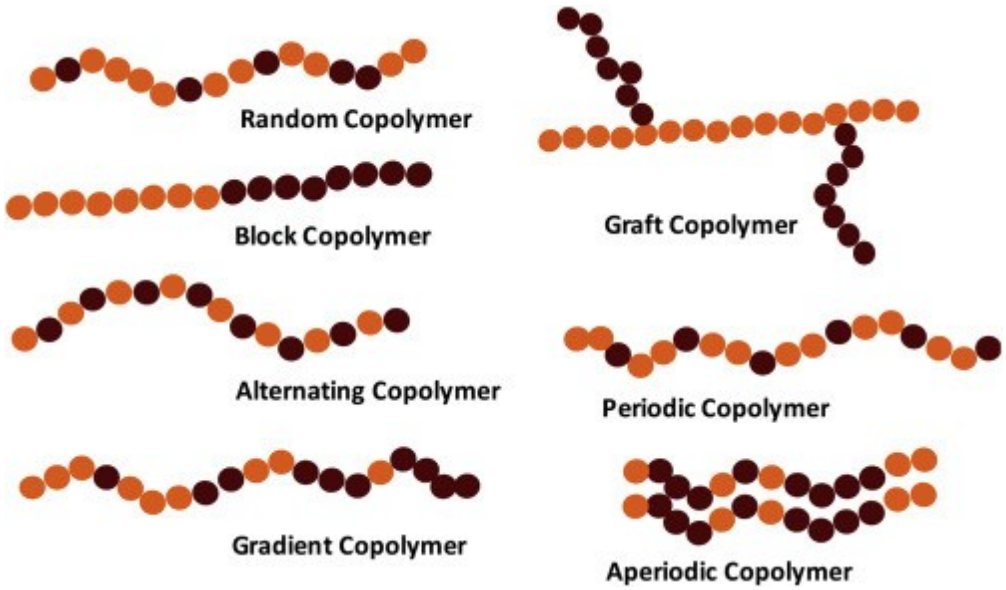

Figure 10: Different types of copolymer structures, including random, block, alternating, gradient, and graft copolymers [73]

Some studies have shown that block copolymers are the most effective copolymer structures to flocculate negatively charged particles [2,5,14,39]. Figure 11 demonstrates the impact of random and block copolymer microstructures on flocculation. Chen et al. suggest that since random copolymers will have charged comonomers between the contaminant particles and at the polymer "tails", this can result in some charges not being used or charged sections of the polymer backbone being "wasted" [2]. This can also result in fewer charges at the adsorption site, leading to weaker electrostatic effects. In contrast, when block copolymers are employed for flocculation (where one of the blocks contains charged comonomers), the centralized charges ensure that most of the charged comonomers are participating in adsorption, leading to fewer charged comonomers being "wasted" and creating stronger adsorption sites, as seen in Figure 11 [5]. Therefore, Chen et al. suggest that block copolymer flocculants allow for a more efficient flocculation process.

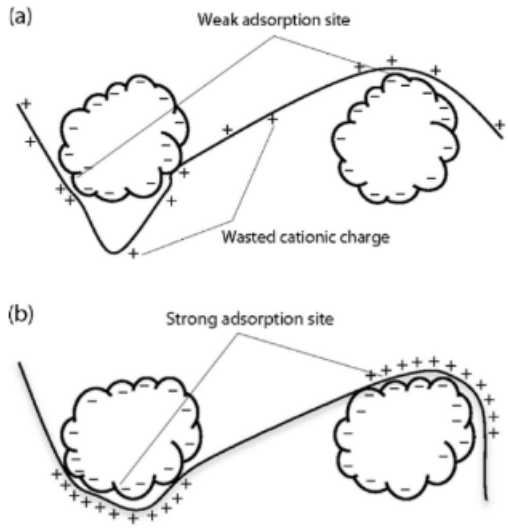

Figure 11: Comparison of (a) random vs. (b) block copolymers in flocculation [2]

Reactivity ratio estimates can be used to predict how polymerization conditions will impact the resulting copolymer microstructure. For copolymerizations with reactivity ratios where $r_1 << 1 << r_2$, gradient copolymers are likely to form. As shown in Figure 10, gradient copolymers are similar to block copolymers, except there is a gradual transition between comonomers; in contrast, for block copolymers there is a sudden transition. For $r_2 >> 1$, monomer 2 will have a very high likelihood of homo-propagation rather than cross-propagation (recall Equation 13). As such, monomer 1 will primarily be added to the propagating polymer chain once the monomer 2 concentration is almost (or completely) depleted.

Triad fractions are important for studying copolymer microstructure and can be used to quantify the copolymer microstructure. Instantaneous triad fractions estimate the fraction of three consecutive monomers having a certain order, or how a 'centered' monomer is related to surrounding monomers. Instantaneous triad fraction calculations are statistically based and are determined using reactivity ratios and feed composition. For example, if a copolymer has a high fraction of A_{111} and A_{222} triads, the polymer is likely to have "blocky" copolymer sections. In contrast, if there is a high fraction of A_{121} and A_{212}, the polymer is likely alternating or random. Equations for instantaneous triad fractions (developed using the terminal copolymerization model) are shown in Equations 32 through 34. The following equations are shown for monomer species 1 centered triads; monomer species 2 centered triads can be calculated by exchanging the 1s and 2s, giving a total of 6 equations.

$$A_{111} = \left(\frac{r_1 f_1}{r_1 f_1 + f_2}\right)^2 \qquad \text{Equation 32}$$

$$A_{212} = \left(\frac{f_2}{r_1 f_1 + f_2}\right)^2 \qquad \text{Equation 33}$$

$$A_{112} = A_{211} = \frac{r_1 f_1 f_2}{(r_1 f_1 + f_2)^2}$$ Equation 34

When the penultimate copolymerization model is considered, triad fractions can be calculated using Equations 35 through 37 [67]. Again, the complementary triad fractions can be determined by replacing 1s with 2s and vice versa.

$$A_{111} = \frac{r_{11} r_{21} f_1^2}{r_{11} r_{21} f_1^2 + 2 r_{21} f_1 f_2 + f_2^2}$$ Equation 35

$$A_{212} = \frac{f_2^2}{r_{11} r_{21} f_1^2 + 2 r_{21} f_1 f_2 + f_2^2}$$ Equation 36

$$A_{211} = A_{112} = \frac{2 r_{21} f_1 f_2}{r_{11} r_{21} f_1^2 + 2 r_{21} f_1 f_2 + f_2^2}$$ Equation 37

2.4. Effects of Changing Reaction Conditions

2.4.1. Effect of pH

Acrylamide homopolymerization studies have been performed extensively [27–29,74,75]. The effect of pH on acrylamide homopolymerization kinetics has been studied by Lacik et al. [27], Kurenkov et al. [74], Currie et al. [75], and many others (see, for example, [29]). In general, studies show that pH has no significant effect on polymerization rate in the range of pH 3 to pH 11. According to Lacik et al., the rate of propagation is increased above pH 11 [27]. However, Lin reported conflicting results, and found no change in rate of polymerization in the range of pH 1 to pH 13 [29]. The maximum pH used in the current study is pH 9, so these conflicting results are not expected to affect the current study.

When AMPS is used as a comonomer, it is not expected that pH will have a significant effect on the rate of polymerization, as AMPS is completely deprotonated at pH 7, since the pKa is 2.3 [76]. Therefore, no significant effects are expected to occur due to changes in pH [36].

The homopolymerization of DADMAC, on the other hand, is significantly impacted by pH. The pKa of DADMAC is 7, meaning that at pH 7, DADMAC is 50% dissociated [77]. Results in the literature have shown that a higher pH increases the rate of propagation, as the monomer is deprotonated and reduces electrostatic repulsion among and between molecules [77]. This is important for polyelectrolytes; when the ions are protonated and DADMAC is positively charged, any propagating like charges will repel each other. In other words, electrostatic repulsion will decrease the rate of propagation. As such, at higher pH (such as pH 9), the DADMAC charges will be neutralized, and any electrostatic repulsion is negligible (sample calculations are shown in Appendix A.1). Reducing or removing the electrostatic repulsion also allows the polymer chain conformation in solution to be a random coil structure instead of a rigid structure. Polymer microstructures with high concentrations of charges are more likely to repel themselves and form a rigid geometry in solution. Additionally, a study on the homopolymerization of DADMAC reported that pH can impact the molecular weight of PDADMAC, especially at conversions below 50% [77]. The study showed that as pH increased, so did the molecular weight, although the highest pH tested was pH 5. The lowest pH tested in this work was pH 1, which means that the effect of pH when DADMAC is deprotonated is still unknown, but is expected to be minimal as the charges are neutral.

To the best of our knowledge, no studies to date have investigated the effect of pH on the copolymerization of DADMAC – AAm. However, the impact of pH is expected to be significant as the pKa of DADMAC is 7. It is expected that DADMAC will be more likely to propagate and have a higher molecular weight averages as the pH increases.

2.4.2. Effect of Monomer Concentration

In multiple studies, the effect of monomer concentration on AAm homopolymerization kinetics was investigated [27,29,74,75]. One study found that the propagation rate peaked when the concentration was ~0.422 M, and that higher or lower monomer concentrations decreased the rate of propagation [27]. It is believed that the propagation rate decreases at higher monomer concentrations due to stronger dipole interactions that restrict the internal rotational mobility of the transition state structure [27,78].

The total monomer concentration can impact the kinetics of homopolymerization and copolymerization, especially for polyelectrolytes, as the monomer concentration can also impact the ionic strength of the polymerizing mixture. For the homopolymerization of AMPS, Beuermann et al. found that a monomer concentration of 1.04 M in water demonstrated significantly higher propagation rates than a monomer concentration of 2.79 M [36]. This difference was believed to be caused by reduced chain mobility and repulsion between the charged monomers (to be added to the propagating chain) and the charges along the macroradical.

For DADMAC homopolymerization, it has been shown that increasing monomer concentration increases the rate of polymerization [77]. This can be explained using Equation 1, as monomer concentration increases the rate of polymerization.

The effect of monomer concentration on DADMAC – AAm copolymerization kinetics has been studied by Brand et al. [51] and Wandrey et al. [49]. Both found that increasing total monomer concentration increased r_{DADMAC} and decreased r_{AAm}. This can be explained using the relevant homopolymerization results in the literature; it has been shown that increasing monomer concentration decreases the rate of polymerization for AAm [27] and increases the rate of polymerization for DADMAC [77]. Total monomer concentrations in the copolymerization study by Brand et al. were 0.5 M, 1.5 M, and 3 M, while the study by Wandrey et al. explored 4 M and 5 M [49,51].

2.4.3. Effect of Ionic Strength

For polyelectrolytes, ionic strength is an important variable during copolymerization [59,79]. Since the copolymer has like-charges along the propagating polymer chain, these charges will repel each other and limit the propagation of charged monomers onto the charged macroradical. Counter-ions can be added to solution to create a shielding effect and reduce the electrostatic repulsion from like-charges, as demonstrated in Figure 12 [59,79]. The shielding effect neutralizes the charges from the monomer molecules as opposite charges from salt are added to solution. As such, the shielding effect impacts both the ions along the polymer chain and any like-charged monomers that are propagating onto the polymer chain, subsequently affecting the reactivity ratios. Ionic strength also affects the rigidity of copolymer chains in solution. When the ionic strength in solution is low (that is, no ionic shielding), the polymer will create a more rigid geometry to maximize the distance between like-charges. In contrast, if the ionic strength is higher, ionic shielding will allow the polymer to form a random coil structure, due to reduced electrostatic repulsion along the polymer chain [59,79].

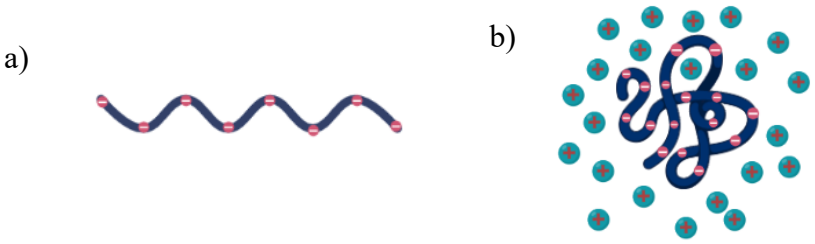

Figure 12: Examples of polyelectrolytes without (a) and with (b) ionic shielding.

The effect of ionic strength on acrylamide homopolymerization was studied by Lacik et al. [27], and it was found that there were no ionic strength effects until the concentration of NaCl reached 1 M. Even at this concentration, little effect on the propagation rate was observed. This is because AAm is non-ionic, and therefore no ionic shielding or repulsion effects are present.

For AMPS, there are limited studies about the effects of ionic strength on homopolymerization kinetics. However, due to the strong acidic nature of AMPS, it is expected that there will be some ion shielding when salts are added to the pre-polymerization mixture. Thus, increasing the ionic strength should theoretically increase the rate of polymerization of AMPS. In a terpolymerization study for AAm-AMPS-AAc, it was found that increasing ionic strength increased the $r_{AMPS/AAm}$, improving AMPS propagation [80].

For DADMAC homopolymerization, it is believed that increasing the ionic strength will increase reactivity when the monomer is protonated by creating ionic shielding and reducing the repulsion between monomers and the propagating macroradical chain. When the monomers are deprotonated, effects are not expected to be significant due to the

absence of DADMAC charges. The pKa of DADMAC is at 7 pH and is 99% deprotonated at 9 pH, therefore a pH below 9 is expected to be impacted by ionic strength.

There are no known studies about the effect of ionic strength on DADMAC – AAm copolymerization kinetics. However, based on anticipated homopolymerization behaviour of DADMAC, increasing ionic strength is expected to increase r_{DADMAC}.

3. Experimental Procedures

3.1. Materials

3.1.1. Chemicals

Acrylamide (99% purity), diallyldimethylammonium chloride solution (DADMAC, 65% by weight in water), 2-acrylamido-2-methylpropanesulfonic acid (99% purity), HPLC grade methanol (99.9% purity), hydroquinone (99% purity), sodium chloride (99% purity), sodium hydroxide (97% purity), 3-(trimethylsilyl)-1-propanesulfonic acid sodium salt (DSS; 97% purity), 4,4′-azobis(4-cyanovaleric acid) (98% purity), sodium phosphate dibasic heptahydrate (98.0% purity), sodium phosphate monobasic monohydrate (98% purity), sodium nitrate (99.0% purity), hydrochloric acid (HCl, ACS reagent, 37% purity), acetone (99.5% purity), and HPLC grade H_2O were all purchased from Sigma-Aldrich. Ultra High Purity (5.0) nitrogen was purchased from Linde.

For gel permeation chromatography (GPC), polyethylene glycol (PEG) and polyethylene oxide (PEO) standards were used, with peak-average molecular weight ($\overline{M}_P$) ranging from 8.5×10^3 g/mol to 1.250×10^6 g/mol. All GPC standards were acquired from Agilent Technologies.

3.2. Solution Preparation

3.2.1. Homopolymerization

2-acrylamido-2-methylpropane sulfonic acid (AMPS) or acrylamide (AAm) stock solutions were made at 2 M total monomer concentration in HPLC grade H_2O. When preparing a 20 mL solution to be polymerized, 10 mL of the 2 M stock solution was added to a beaker. Next, 22.3 mg of 4,4′-azobis (4-cyanovaleric acid) (ACVA) initiator was added

to the formulation to achieve a final initiator concentration of 0.004 M. A pH probe was placed in the beaker, while the monomer solution was stirred on a stir plate. NaOH solution was then added to the 10 mL of monomer stock solution using a micropipette, under constant stirring, until the desired pH (± 0.5) was obtained. In some cases, NaCl was also added to the solution to achieve the desired ionic strength. For NMR experiments, DSS (which acts as a reference peak) was added to the pre-polymerization mixture at 1 mM. Once the desired pH was obtained, HPLC grade H_2O was added to the solution until a total volume of 20 mL was obtained; this brought the total monomer concentration for each experiment to 1 M.

3.2.2. AMPS – AAm copolymerization

2-acrylamido-2-methylpropane sulfonic acid (AMPS) – acrylamide (AAm) stock solutions were made at 2 M total monomer concentration in HPLC grade H_2O. The molar compositions in the feed for this study were $f_{AMPS,0} = 0.84$ and $f_{AMPS,0} = 0.10$, with the balance AAm. These compositions were chosen to replicate prior work by Scott et al. to facilitate comparison of results [38]. When preparing a 20 mL solution to be polymerized, 10 mL of the 2 M stock solution was added to a beaker. Next, 22.3 mg of 4,4′-azobis (4-cyanovaleric acid) (ACVA) initiator was added to the formulation to achieve a final initiator concentration of 0.004 M. A pH probe was placed in the beaker, while the monomer solution was stirred on a stir plate. NaOH solution was then added to the 10 mL of monomer stock solution using a micropipette, under constant stirring, until pH 7 ± 0.5 was obtained. For NMR experiments, DSS (which acts as a reference peak) was added to the pre-polymerization mixture at 1 mM. Once the desired pH was obtained and any necessary additives were incorporated, HPLC grade H_2O was added to the solution until a

total volume of 20 mL was obtained; this brought the total monomer concentration for each experiment to 1 M.

3.2.3. DADMAC – AAm Ionic Strength Study

To investigate the DADMAC – AAm copolymerization kinetics, monomer stock solutions containing a total monomer concentration of 4 M were prepared in HPLC grade H_2O. The molar compositions in the feed for this study were $f_{DADMAC,0} = 0.851$ and $f_{DADMAC,0} = 0.100$, with the balance acrylamide; design of experiments for the feed composition is explained in Section 5.1. A similar process to Section 3.2.2 was developed for DADMAC – AAm copolymer synthesis and is outlined here for clarity. When preparing a 20 mL solution to be polymerized, 10 mL of the 4 M stock solution was added to a beaker. A 0.1327 g/mL solution of ACVA in 2 M NaOH was created by adding 66.35 mg of ACVA to 0.5 mL of 2 M NaOH. 222.2 µL of ACVA solution was added to the beaker using a micropipette to achieve a final initiator concentration of 0.00526 M. A pH probe was placed in the beaker, while the monomer solution was stirred on a stir plate. HCl solution was added to the monomer stock solution using a micropipette, until a pH of 7 ± 0.1 was reached. DSS (which again acted as a reference peak) was added at 1 mM. Once the desired pH was obtained and any necessary additives were incorporated, HPLC grade H_2O was added to the solution until a total volume of 20 mL was obtained; this brings the total monomer concentration for each experiment to 2 M. These experimental decisions are explained further in Section 5.1.

3.2.4. DADMAC – AAm pH and Monomer Concentration ([M]) Study

The procedure used to study the impact of pH and monomer concentration on DADMAC – AAm copolymerization kinetics was very similar to that described in Section 3.2.3. One major difference was the amount of monomer stock solution and ACVA initiator added to each pre-polymerization solution. For 3 M monomer concentration experiments, 15 mL of stock solution was added, and a final initiator concentration of 0.0118 M was targeted. For 1 M monomer concentration experiments, 5 mL of stock solution was added, and a final initiator concentration of 0.00132 M was targeted. The initiator concentration was not varied linearly with monomer concentration, in an effort to achieve similar molecular weight averages. These relationships were based on Equations 18 and 19, where R_p was used to calculate molecular weight.

A 10 mL aliquot was taken from the beaker to separate the pre-polymerization solution into 2 separate vials. Using high concentrations of HCl and NaOH solutions, one of the samples was brought to pH 5 and the other was brought to pH 9. The amount of volume added was ~5-20 μL and was deemed to have an insignificant effect on final monomer and initiator concentrations.

3.3. Degassing

Once solutions were at the desired ionic strength, pH and monomer concentration, they were degassed using nitrogen gas. Each solution was placed in a round bottom flask and sealed with a rubber septum and a zip tie, as shown in Figure 13.

Figure 13: Representative pre-polymerization solution in a 50 mL round bottom flask; sealed with an orange septum and black zip tie

The pre-polymerization solution was kept cool for the duration of the degassing step using an ice bath; this prevented premature polymerization. The solution had an inlet feed of nitrogen pierced through the septum (on the round bottom flask) and an outlet feed (using a double-tipped needle) into a 20 mL vial that also had a polytetrafluoroethylene septum, as shown in Figure 14.

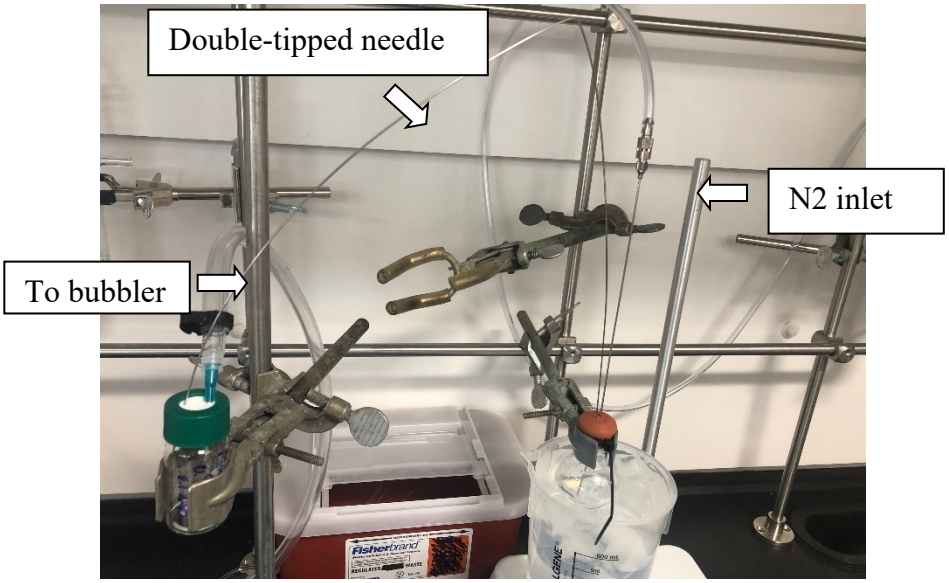

Figure 14: Pre-polymer solution degassing system

The 20 mL vial outlet was attached to a gas bubbler (containing mineral oil) to prevent any air from entering the vial and to avoid pressure buildup within the vial. Nitrogen gas was fed at a rate of ~100 mL/min for 60 minutes, and then the polymer solution was transferred from the round bottom flask to the 20 mL vial using the double-tipped needle connecting the round bottom flask and the 20 mL vial (cannula transfer method). The degassed solution, once entirely in the 20 mL vial, was placed in the glove box for subsequent transfer (see Section 3.4.1).

For samples that involved adding NaCl to increase ionic strength, the 20 mL vials were prepared with pre-weighed NaCl powder inside. Within the glove box, 5 mL aliquots from the monomer solution were transferred to the vials with NaCl powder, using a micropipette. Each vial then represented a new experiment. For example, 20 mL of prepared prepolymer solution was added to glove box with the vial and NaCl, and then 5 mL of solution was added to vial with NaCl powder. This led to the preparation of two solutions (for two experiments), where one of them has ionic strength adjustment.

3.4. Nuclear Magnetic Resonance (NMR)

The glove box in which NMR samples were prepared was under a nitrogen atmosphere to avoid any oxygen contamination. Samples were handled in the glove box when the $\%O_2$ was below 0.5%. It was found that samples prepared with higher $\%O_2$ either had very long initiation delays or did not polymerize at all. A study by Cutie et al. showed that the presence of oxygen can create a delay in inhibition time, but should not affect the conversion profile of the polymerization [81].

^{1}H NMR was used to measure alkene bonds during polymerization. This allowed the tracking of conversion and all monomers' concentration in the monomer and polymer phase in parallel. Protons of the monomers were measured via Bruker AV300 (2002) NMR at 300 MHz.

3.4.1. Transfer to NMR Tubes

Within the glove box, ~0.2 mL pre-polymerization solution samples were transferred into NMR (Ø = 5 mm) tubes. Each NMR tube must be well-sealed using the standard lid, parafilm, and a Ziploc bag to prevent oxygen from entering the tube; oxygen can act as an inhibitor and can compromise the polymerization reaction. Once the NMR tubes were filled, samples were placed in a fridge at 5°C until polymerization to avoid premature polymerization. For transport to the Dalhousie NMR facility (NMR3, Department of Chemistry, Dalhousie University), NMR tubes were placed on ice in an insulated container.

3.4.2. In situ ^{1}H NMR Operation and Data Collection

To begin each in situ NMR polymerization, the NMR cavity was preheated to the desired polymerization temperature (typically 50°C) and allowed to sit for 10 minutes to ensure that the NMR probe was at equilibrium. For AMPS – AAm copolymerization, there was an initiation delay of 10-30 minutes, therefore no reference solution was needed as the initial measurement was used as the reference at 0% conversion. DADMAC polymerization tended to have no initiation delay, therefore any solutions containing DADMAC were placed in two separate NMR tubes during the preparation stage. One of the NMR tubes was taken out of the glove box and intentionally exposed to oxygen; this sample was used as a monomer reference that would not polymerize. This 'reference

sample' was added and measured first so that a measurement at 0% conversion could be acquired. After ejecting the non-polymerizing sample, the other sample was injected, so that in situ polymerization progress could be monitored. Once the samples were placed in the NMR, they were measured every ~6 minutes. The exact time of day was recorded when the solution was inserted into the NMR (for example, August 31, 2023, 6:09:27 am). This was done for at least 10 total measurements for each run; AMPS-rich and DADMAC-rich samples often had approximately 15-20 measurements since the reactions were generally slower than AAm-rich polymerizations.

Once the solution was inserted into the NMR, the probe was locked, shimmed and tuned. Locking and shimming also occurred before every measurement. Each measurement had a relaxation delay of 10 seconds and had 8 scans. It was found that the optimal quantitative relaxation delay was at least 10 seconds. Only 8 scans were used because of the high relaxation delay and high monomer concentration; having more scans was not found to be significantly more accurate. Since we used H_2O instead of D_2O, solvent peak suppression was used to remove the H_2O peak. The method is detailed in a paper by McKay et al. [82].

Acrylamide peaks were measured in the range of 5.42 to 5.54 ppm, AMPS peaks were measured in the range of 5.30 to 5.37 ppm, and DADMAC peaks were between 5.65 and 5.8 ppm. Once the data were collected for each run, the monomer concentration and monomer fractions were calculated at each time point. This made it possible to calculate the cumulative copolymer composition, which in turn made it possible to estimate the reactivity ratios. This methodology is similar to that described by Preusser et al. [83]. This method made it possible to acquire a significant amount of data while using limited material quantities.

3.4.3. C^{13} NMR Measurements

The Bruker AV300 (2002) NMR was also used for C^{13} measurements. C^{13} measurements were used to measure triad fractions of select copolymers. For all measurements, there were 400 scans with a relaxation delay of 1 second. Scans were performed at 25°C.

3.5. Gel Permeation Chromatography (GPC)

GPC is the most accurate method for measuring molecular weight averages and polydispersity. For GPC characterization, a buffer is used for the mobile phase. For AMPS – AAm copolymers, a pH 7 buffer was used as the mobile phase. The pH 7 buffer contained 0.2 M sodium nitrate and 0.01 M sodium phosphate in HPLC water. For DADMAC – AAm copolymers, a pH 3.2 buffer was used as the mobile phase; this was selected due to the cationic nature of the copolymers. The same buffer solution was used as described above, except pH was adjusted to 3.2 using HCl.

For samples measured via GPC, solutions had to be polymerized in 20 mL vials instead of NMR tubes so that the polymer could be isolated. Remaining solutions in the 20 mL vials (that is, after ~0.2 mL was taken out for NMR as described in Section 3.4.1) were placed in a 50°C water bath to polymerize. For AAm- and AMPS-rich solutions, polymerizations were performed for 24 to 48 hours. DADMAC-rich solutions were polymerized for 4 to 10 days due to the slower reaction kinetics, especially at [M] = 1 M. All AAm- and AMPS-rich copolymers are expected to have a conversion greater than 0.95, and all DADMAC-rich copolymers are expected to have a conversion of at least 0.40.

After polymerization, the vial contents were transferred into an excess of acetone to precipitate the polymer product. Samples were then filtered (paper filter grade number 41,

Whatman; Sigma-Aldrich, Oakville, ON, Canada) and left for 24 hours for any acetone in the filter paper to evaporate. Finally, polymer samples were dried in a vacuum oven at 50°C for 1 week. The polymers were then dissolved in buffer solution in the range of 0.33 – 0.5 mg/mL, depending on the solubility of the polymer. Once dissolved, samples were filtered into HPLC vials using 0.45 μm PTFE syringe filters.

The GPC was operated at 1 ml/min for 35 minutes and took 100 μL aliquots for each sample. For each day the GPC was used, a blank, 6 calibration standards (in a range from 8.5×10^3 g/mol to 1.250×10^6 g/mol), and a known sample (poly(acrylamide-co-acrylic acid)), were measured. The samples synthesized as described above were then characterized in random order.

The GPC used a guard column and two PL aquagel-OH MIXED-H 8 μm 300 x 7.5 mm columns from Agilent Technologies. Triple detection was used to measure molecular weight averages. The detectors employed were dual angle light scattering, a refractive index detector, and a viscometer. With the data collected, the weight-average molecular weights ($\overline{M}_w$) and the entire molecular weight distribution were determined.

3.6. Flocculation Jar Tests

Polymer samples isolated in Section 3.5 were also used in flocculation jar tests. All samples were tested at Halifax Water's Dartmouth Wastewater Treatment Facility. All polymer samples were dissolved in HPLC grade H_2O at a concentration of 1 mg/mL, 24 hours before testing. Flocculation trials were done at either 1.0 mg/L or 2.0 mg/L, therefore either 1.0 mL or 2.0 mL of polymer solution was added to the jar. ~40 L of influent (post coarse

screen, fine screen, and grit removal) was collected at the beginning of the day and was used for all experiments within that day to ensure consistency. The 40 L bucket of influent was stirred before taking samples, and 1 L of influent was added to each jar using a graduated cylinder. A standard jar tester was used (Phipps & Bird PB-900 Programmable Jar Tester). The jar test protocol is shown in Table 2.

Table 2: Jar test program used for all flocculation tests

Stage	**Time**	**RPM**	**G-value**	**Notes**
Pre-mix	30 s	240	300	
Coagulation (rapid mix)	5 min	180	200	Polymer added at beginning of this stage
Flocculation (slow mix)	10 min	40	30	
Settling	20 min	0	0	

The G-value is the velocity gradient for mixing, therefore a higher G-value represents more intense mixing. The pre-mix stage is for mixing and suspending the contaminants and solids in the jar. The coagulation or rapid mix stage is when the flocculants were added; this stage is to mix the flocculants into the influent. The flocculation stage is slow compared to pre-mix and coagulation stage, as this stage is for creating larger flocs; mixing too rapidly will break the flocs. Finally, the settling stage has no mixing, and the objective is to have the flocs settle to the bottom during this stage.

After the settling was completed, the supernatant was collected, along with an aliquot of the sampled influent. The influent was characterized by measuring temperature, alkalinity, turbidity, pH, conductivity, zeta potential, ultra-violet transmission (UVT) 254, biochemical oxygen demand (BOD), and chemical oxygen demand (COD). Similarly, the supernatant was characterized by measuring the turbidity, UVT254, zeta potential, and

conductivity. Temperature, alkalinity, pH, conductivity, zeta potential, BOD, and COD were tested by Kayleigh Dunphy and Carolina Ontiveros from the Centre for Water Resources Studies.

3.7. Safety Considerations

One of the main safety considerations throughout this project was related to chemical handling, as this project required working with strong acids, strong bases, and monomers. All chemicals were handled within the fumehood and all required personal protective equipment (PPE) were used, including wearing a lab coat, safety glasses, gloves, long pants (covering legs and ankles), and closed toed shoes. To weigh AAm on the analytical balance, AAm was placed in pre-weighed vials and sealed within the fume hood, then the AAm mass within the vial was measured on the analytical balance outside the fume hood. This was done for all AAm measurements because acrylamide is carcinogenic.

Another safety consideration was handling the pressurized nitrogen tank. N_2 tank handling rules include: always have the lid on when moving the tank and have the tank secured at all times (except when moving). A sudden release in pressure could either cause an explosion or cause the tank to become a flying object [84].

There were also several needles required during the experimental steps described previously (see Section 3.3). All needles were handled with caution and were not recapped for safety reasons. All sharps were placed directly in the designated sharps container after use.

4. Impact of Ionic Strength (Sodium Chloride Concentration) on Homopolymerization and Copolymerization Kinetics of Acrylamide and AMPS

The first goal of Chapter 4 was to validate copolymerization kinetics of AMPS – AAm using in situ ^{1}H NMR. The in situ ^{1}H NMR results are compared to vial homo- and copolymerization. The chapter also describes a study investigating the effects ionic strength on AMPS – AAm copolymerization. In situ ^{1}H NMR was used because previous results by Scott [54] show salt retention in the polymer product, affecting gravimetric results used in vials. Although a mathematical model was built to address salt retention in gravimetric conversion measurements, in situ ^{1}H NMR is not affected by salt retention and may be more accurate [54].

Experimental results from Section 4.1.1 are from the thesis of Scott [54], and provided here for context. Experimental results in Section 4.1.2 and vial copolymerization data in Section 4.2.1 were performed by co-op student Baris Topcuoglu.

4.1. Homopolymerization

4.1.1. Vial Homopolymerization of Polyacrylamide

As reported by Scott, conversions of over 100% were reached when using gravimetric methods to evaluate terpolymerizations of 2-acrylamido-2-methylpropane sulfonic acid, acrylamide, and acrylic acid at high ionic strength [54]. To investigate this issue, several homopolymerizations of AAm were performed at 1 M monomer concentration, with ACVA as an initiator at 40°C (see Table 3).

Table 3: PAAm salt study experiments prepared by Scott [54]

Run #	NaOH	NaCl	pH	IS
PAAm1			3	0.0 M
PAAm2	✓		7	0.0 M
PAAm3	✓	✓	7	1.8 M
PAAm4	✓	✓	11	1.8 M

Originally prepared by Scott [54], the conversion vs. time plots are shown in Figure 15. In Figure 15(a), it can be seen that PAAm1 and PAAm2 were polymerized without the addition of NaCl and the profiles are similar. Lacik et al. had similar results, where ionic strength had minimal or no effect on AAm homopropagation [27]. Samples PAAm3 and PAAm4 were polymerized with the addition of NaCl, and the measured conversion reached up to 200%. Based on these results, it was hypothesized that NaCl was incorporating at a 1:1 molar ratio with acrylamide through a weak physical bond. Therefore, the mass was adjusted based on an assumption that 45.1% of each sample is NaCl and the remaining portion is PAAm. The adjusted conversion vs. time plot is shown in Figure 15(b).

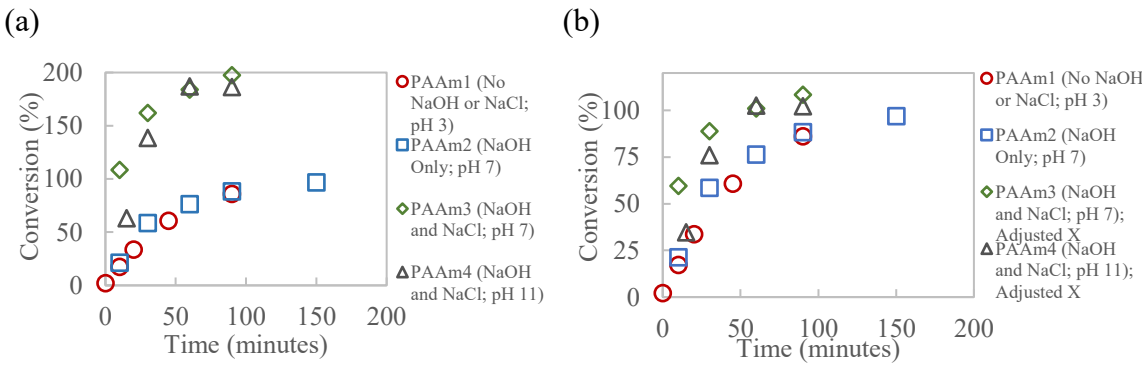

Figure 15: Effect of NaOH and high NaCl content on conversion vs. time for PAAm at [M] = 1.0 M, (a) without adjustment (for NaCl addition) and (b) with adjustment (NaCl consideration); results and analysis from Scott [54]

After the adjustment for NaCl, the salt retention assumption was confirmed for related terpolymer studies by evaluating the polymer composition [80]. This result is one of the motivating reasons for the in situ polymerization approach that is described in what follows (see Section 4.1.3).

4.1.2. Vial Homopolymerization of Poly(AMPS)

A similar homopolymerization study was also performed with AMPS as the monomer; these data were collected by co-op student B. Topcuoglu. The experiments conducted are summarized in Table 4.

Table 4: PAMPS salt study experiments

Run #	NaOH	NaCl	pH	IS
PAMPS1			0	0.0 M
PAMPS2	✓		7	0.0 M
PAMPS3	✓	✓	7	1.0 M

As shown in Figure 16, increasing pH decreased the rate of polymerization slightly, whereas increasing the ionic strength slightly decreased the rate of polymerization. Changing the pH is not expected to have significant impacts as the AMPS monomer is already deprotonated.

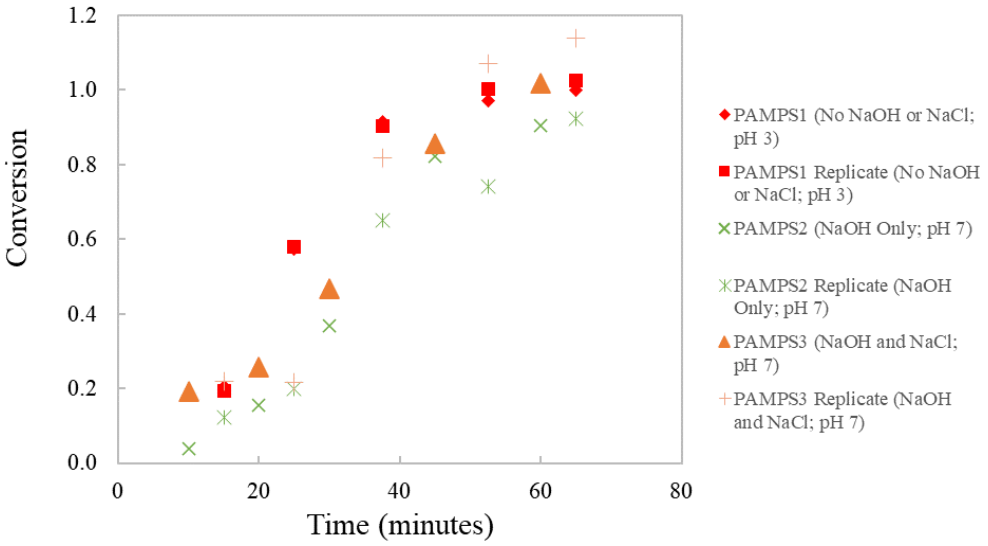

Figure 16: Effect of NaOH and NaCl content on the conversion of PAMPS at [M] = 1.0 M

Homopolymerization of AMPS was not as impacted by ionic strength as expected, considering AMPS is anionic and terpolymerization studies have shown that ionic strength impacts reactivity ratios that include AMPS [80].

4.1.3. ^{1}H NMR for In Situ Homopolymerization of PAAm and PAMPS

Homopolymerization was also studied using ^{1}H NMR, as described in Section 3.4. Representative spectra are shown in Figure 17 and Figure 18; with increasing time, the response in the alkene region is depleting and the response in the alkane region is increasing. This is as expected, as the alkenes are converted to alkanes as propagation occurs.

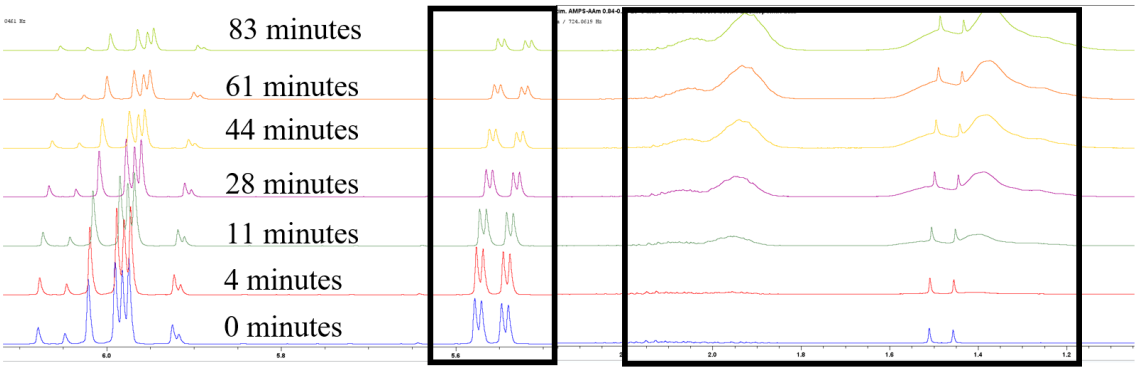

Figure 17: AAm homopolymerization at 40°C via in situ NMR

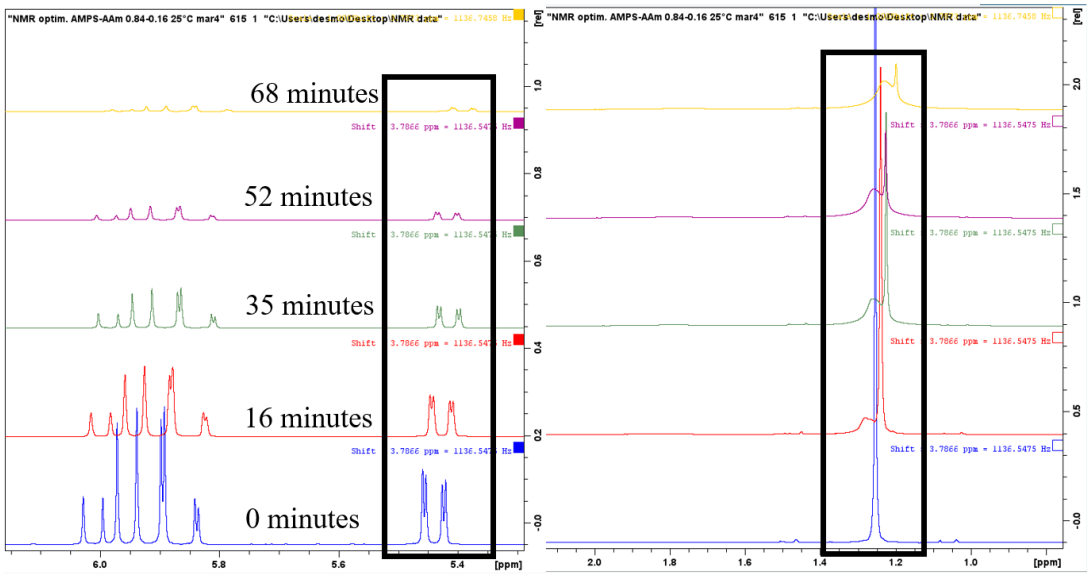

Figure 18: AMPS homopolymerization at 40°C via in situ NMR

Conversion vs. time profiles for both homopolymerization studies (under similar conditions in 20 mL vials and via in situ NMR) are shown in Figure 19. All homopolymerization data shown for comparison were collected at pH 7 with no ionic strength adjustment, unless stated otherwise. As shown in Figure 19(a), the vial scale conversion measurements are consistently higher than the NMR results for PAAm

synthesis, although they follow a similar trajectory. Although there was no NaCl added to this formulation, NaOH was used to increase the pH to 7; as discussed previously, there may be some Na^+ retention within the PAAm samples. Another potential factor is the mixing and geometry of the reaction vessel. All samples in the vials were polymerized in 20 mL vials with continuous mixing (100 rpm), whereas NMR samples were only 0.2 mL and were not mixed during polymerization. The improved mixing in the vial scale is likely to result in increased conversion values. It is also possible that the gravimetric data are subject to experimental error; the hydrophilic nature of the material may result in some water retention when the sample is weighed. Since water retention will not impact the in situ NMR measurements, it is reasonable that the vial results exhibit slightly higher conversion values than the NMR approach. For AMPS homopolymerization, however (Figure 19(b)), the conversion vs. time profiles for vials and NMR results are very similar.

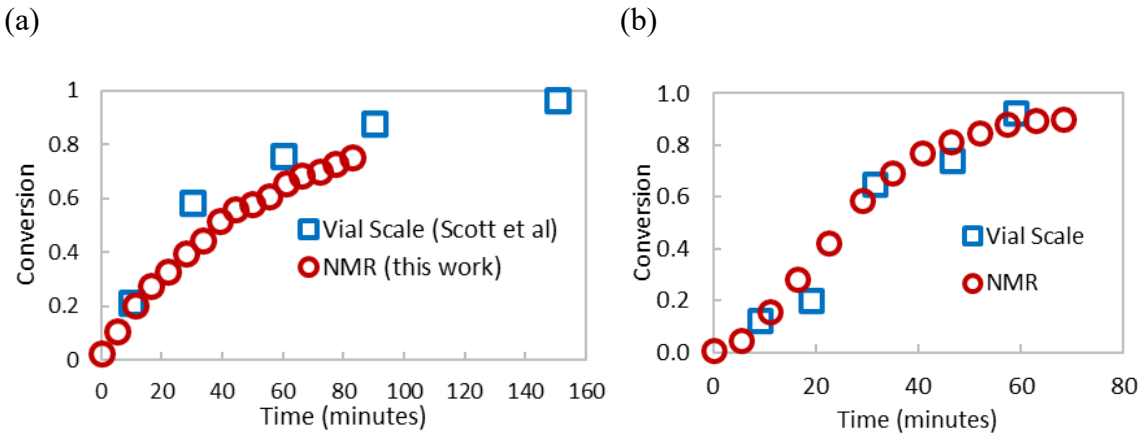

Figure 19: (a) AAm and (b) AMPS homopolymerization comparing vial to NMR polymerizations (with vial scale PAAm data from [54])

This demonstrates that in situ ^1H NMR is an effective technique to study the impact of ionic strength on the copolymerization kinetics of AMPS and AAm (see also references including Preusser et al. and Feng et al. [28,85]). Any retained salt will not affect the

conversion measurements, composition measurements can be collected in parallel, and smaller sample volumes are required compared to vial polymerizations. As such, in situ ^{1}H NMR is used for the copolymerization study that follows.

4.2. Copolymerization of AMPS – AAm

Six different copolymer formulations were prepared to determine the impact of ionic strength on reactivity ratio estimates. The feed compositions and ionic strengths were varied according to Table 5 and the AMPS monomer is fully dissociated (as pH is 7±0.5).

Table 5: Feed compositions and ionic strength of copolymerization experiments

Run	$f_{0,AMPS}$	**NaCl (M)**	**Ionic strength (M)**	**T (°C)**
1	0.10	0	0.10	50
2	0.10	0.74	0.84	50
3	0.10	1.48	1.58	50
4	0.84	0	0.84	50
5	0.84	0.74	1.58	50
6	0.10	0.37	0.47	50

All formulations were selected to facilitate ionic strength comparisons between reactivity ratio estimates. For example, 0.74 M NaCl was added to Run 2 to ensure that an AAm-rich and AMPS-rich feed composition (Runs 2 and 4) would have the same ionic strength (0.84 M). In the same way, the salt concentration for Run 5 was selected to compare the effects of adding the same amount of NaCl as in Run 2 (0.74 M). All combinations are summarized in Table 6, and are used in what follows to elucidate the effects of ionic strength on AMPS – AAm reactivity ratio estimates.

Table 6: Copolymerization combinations for AMPS – AAm and resulting reactivity ratio estimates

Pair	IS (M) (AAm- rich)	IS (M) (AMPS-rich)	r_{AMPS}	r_{AAm}	r_{AMPS}*r_{AAm}
1,4	0.10	0.84	0.549	0.870	0.477
2,4	0.84	0.84	0.557	0.993	0.553
3,4	1.58	0.84	0.483	0.825	0.398
4,6	0.47	0.84	0.536	0.915	0.491
2,5	0.84	1.58	0.456	0.923	0.421
3,5	1.58	1.58	0.465	0.815	0.379

4.2.1. Evaluation of In Situ ^{1}H NMR for Copolymerization Studies

All samples were run in quadruplicate except Run 6, which was done in duplicate. Figure 20 demonstrates the reproducibility of the conversion vs. time data collection, as the four data sets are shown for Run 2. The four independent replicates were done over a 2-month span.

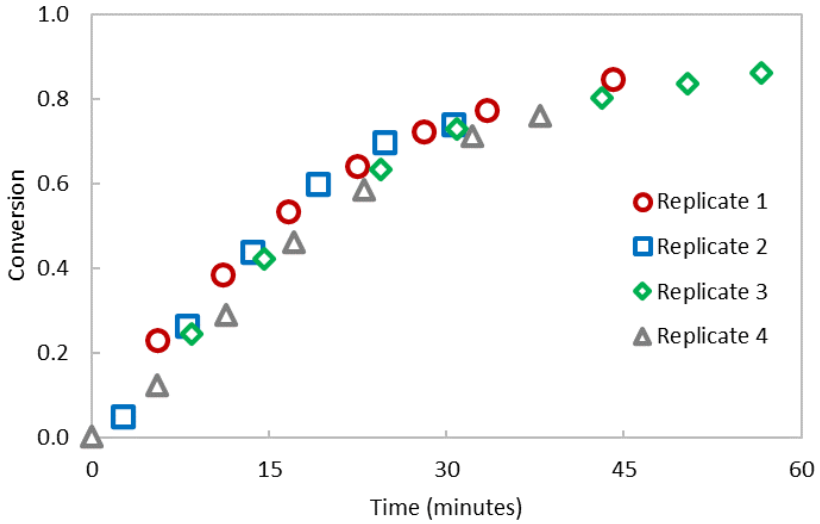

Figure 20: Representative reproducibility for conversion measurements using in situ ^{1}H NMR for Run 2 of Table 5

The results from in situ ^{1}H NMR were also compared to copolymerization performed in vials, as shown for Run 1 in Figure 21. As observed in the homopolymerization studies (recall Figure 19), vial polymerization results demonstrated a slightly higher propagation rate, which may be attributed to the mixing that occurred within the vial polymerizations. Despite the higher conversion levels in vial scale, both techniques follow the same general trajectory.

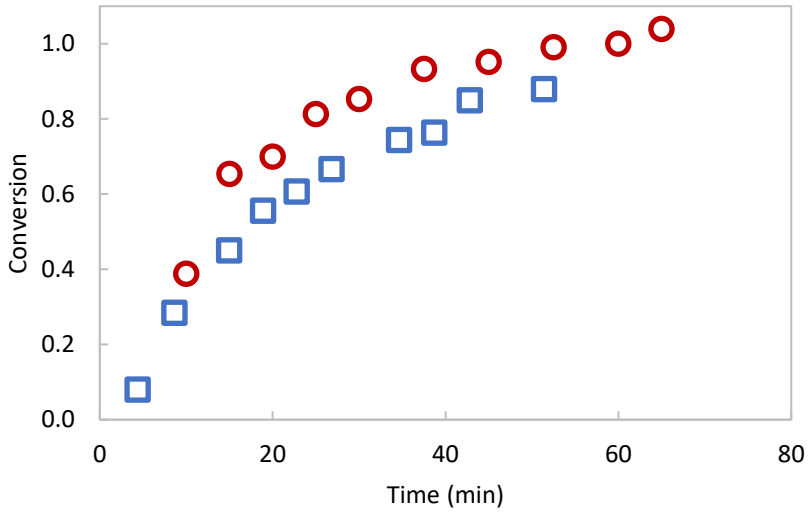

Figure 21: Conversion vs. time for copolymerization in vials and in situ ^{1}H NMR for Run 1 of Table 5

4.2.2. Effects of Ionic Strength

As explained earlier, the effect of ionic strength on AMPS – AAm copolymerization kinetics was evaluated by comparing reactivity ratio estimates obtained with varying monomer feed compositions and NaCl concentrations. The reactivity ratio estimates (RREs) and corresponding joint confidence regions (JCRs) are discussed below.

4.2.2.1. Varying Ionic Strength in AAm-rich Feeds

In comparing Runs (1,4) and Runs (2,4), there is a significant difference in the reactivity ratio estimates, as seen in Figure 22. This indicates that with increased ionic strength in the AAm-rich sample (0.10 M for Run 1 to 0.84 M in Run 2), r_{AMPS} remains relatively constant and r_{AAm} increases. Based on the literature, one might initially expect that r_{AAm} would decrease with increasing ionic strength due to ionic shielding (see, for example, [59,74]). On the other hand, Ponratnam and Kapur studied the copolymerization of methacrylic acid and acrylamide and observed an increase in both r_{AAm} and r_{MAA} with increasing NaCl concentration at pH =4 [86]. Despite conflicting results in the literature, it is well established that ionic shielding will occur when counter-ions are added to a polymerizing solution; reducing the repulsion between the anionic monomer and the anionic polymer is expected to increase the addition of AMPS monomer to the propagating chain (for example, increasing k_{21} and reducing r_{AAm}, where monomer 1 is AMPS and monomer 2 is AAm). It is expected that the homopropagation of AAm (k_{22}) is not affected by ionic strength, as AAm is non-ionic [27]. Therefore, any changes in r_{AAm} are likely due to cross-propagation (k_{21}).

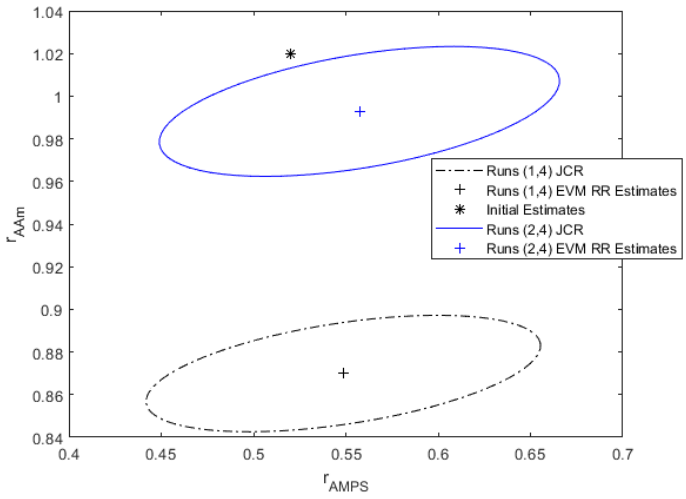

Figure 22: Reactivity ratio estimates and JCRs for Runs (1,4) and (2,4) (Runs (1,4) have no IS adjustment, while Runs (2,4) have IS adjustment such that IS=0.84 M); initial estimates from McCormick and Chen [42]

Since the expected behaviour for r_{AAm} is not observed in this case, both an explanation and experimental confirmation are in order. First, the explanation: since AMPS is a 'bulky' monomer, the concentration of counter-ions may not be sufficient for ionic shielding. However, the ions may be creating a steric effect, where they have caused the structure of the propagating polymer chain to transition from a rigid structure to a less rigid (coiled) structure, creating diffusional limitations for the bulky AMPS monomers moving through the coiled polymer. This has been reported previously by He et al., where they describe this behaviour as a "crowding effect" [87].

Second, the experimental confirmation: to validate the results, Run 6 was performed and replicated. The NaCl concentration for Run 6 was selected to create an ionic strength midpoint between Run 1 and Run 2 to confirm the observed increase. As shown in Figure 23, r_{AAm} from Runs (6,4) is approximately halfway between Runs (1,4) and Runs (2,4), which aligns with the midpoint expectation. While r_{AMPS} varies slightly between

copolymerization pairs, these differences are not significant and are attributed to experimental error.

Figure 23 also demonstrates the results when the ionic strength in the AAm-rich sample is further increased to 1.58 M (Run 3). Runs (3,4) show that r_{AAm} decreases significantly when the ionic strength of the AAm-rich feed is 1.58 M. This suggests that the rate of cross-propagation (k_{21}) is increasing at this salt concentration, resulting in a decrease in r_{AAm}. This is a more typical result; similar observations have been reported previously [59,74,80]. It is hypothesized that at 1.58 M ionic strength, the reduction of electrostatic repulsion becomes more impactful than the 'crowding effect', thus resulting in a lowered r_{AAm}. This transition is shown in Figure 24, where r_{AAm} increases with increasing ionic strength under moderate conditions, but ultimately decreases at higher ionic strength conditions.

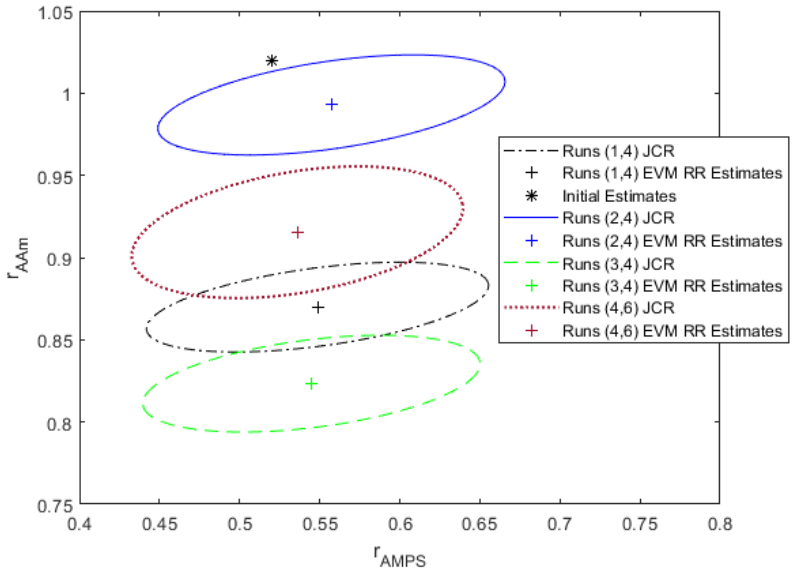

Figure 23: Reactivity Ratio Estimates and JCRs for Runs (1,4), Runs (2,4), Runs (3,4), and Runs (4,6); all AMPS-rich data collected with IS = 0.84 M, while AAm-rich data collected at varying IS; initial estimates from McCormick and Chen [42]

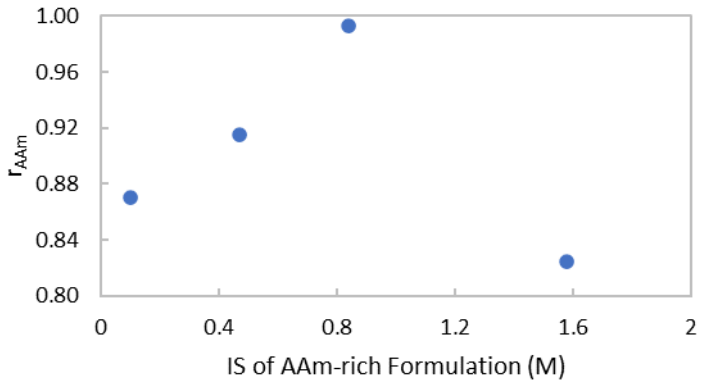

Figure 24: r_{AAm} vs. ionic strength (IS) in the AAm-rich formulation for Runs 1, 2, 3, and 6 (where Run 4 of Table 5 is used for all AMPS-rich feeds for reactivity ratio estimation)

4.2.2.2. Varying Ionic Strength in AMPS-rich Feeds

In addition to varying the ionic strength of the AAm-rich formulations, experiments were also performed to determine the effect of varying the ionic strength of the AMPS-rich formulations. The results of this study are shown in Figure 25, where the ionic strength of

AAm-rich formulations are varied (0.84 M in Run 2 vs. 1.58 M in Run 3) and the ionic strength of the AMPS-rich formulations are varied (0.84 M in Run 4 vs. 1.58 M in Run 5) in parallel.

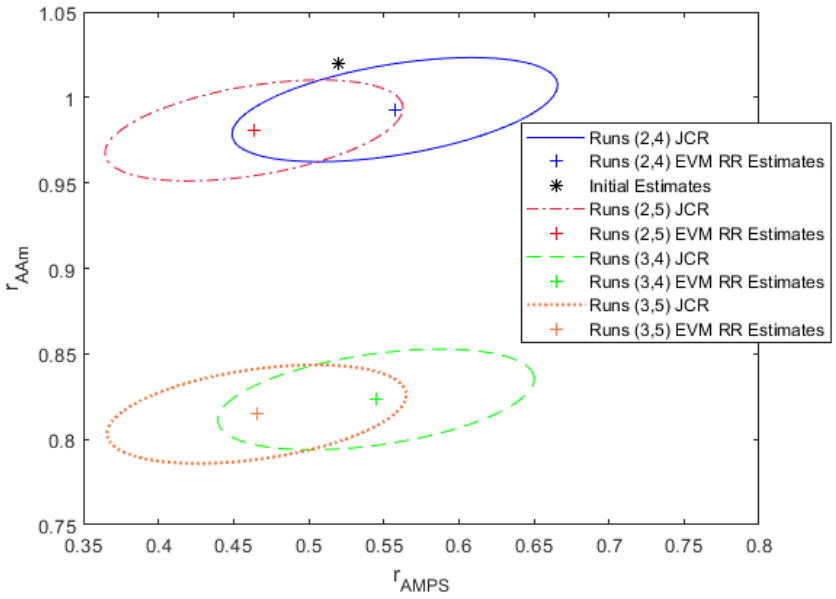

Figure 25: Reactivity ratio estimates and JCRs for Runs (2,4), Runs (2,5), Runs (3,4), and Runs (3,5); impact of varying the IS of AAm-rich and/or AMPS-rich formulations on reactivity ratios; initial estimates from McCormick and Chen [42]

In comparing Runs (2,4) to Runs (2,5) and Runs (3,4) to Runs (3,5), it is possible to evaluate the impact of increasing the ionic strength of the AMPS-rich feed. A slight decrease in r_{AMPS} is observed, but with overlapping JCRs. This shift may be due to increased cross-propagation (k_{12}) resulting from steric hindrance (where AAm is more likely to propagate than AMPS due the molecule's smaller size). Here, the ionic strength was not changed for the AAm-rich feed, showing that this shift is likely caused by ionic strength changes in the AMPS-rich feed.

In contrast, by comparing Runs (2,4) to Runs (3,4) and Runs (2,5) to Runs (3,5), we can evaluate the impact of increasing the ionic strength of the AAm-rich feed. While this was

done fairly extensively in Section 4.2.2.1 (recall Figure 23), the current comparison shows that the Runs (2,5) vs. Runs (3,5) behaviour follows the same trend as observed previously. With sufficient salt addition to ensure charge screening, the cross-propagation of r_{AAm} (that is, k_{21}) is expected to increase, thus decreasing r_{AAm}. Ultimately, for this copolymer system, the effects of ionic strength seem to be more profound for AAm-rich formulations. This demonstrates how the reactivity ratios can be impacted (or manipulated) by changing ionic strength within a reaction solution.

Riahinezhad et al. studied ionic strength effects for the copolymerization of acrylamide (AAm) and acrylic acid (AAc) [59]. They reported similar results in terms of r_{AAm}, where r_{AAm} decreased with increasing ionic strength as a result of increased cross-propagation. However, in the same study, they found that changing the ionic strength of the anionic AAc-rich feed had more significant effects on the reactivity ratios compared to changing the ionic strength of the AAm-rich feed. This differs from the current observations, where the AMPS – AAm reactivity ratios are more impacted by changing the ionic strength in the AAm-rich feed. This may be due to the impact of steric hindrance and diffusional limitations of the larger AMPS compared to AAc.

As a final comparison, the estimated cumulative copolymer composition for the AMPS-rich formulations as a function of conversion is shown in Figure 26. In the AMPS-rich feed, the cumulative copolymer composition exhibits a higher acrylamide fraction ($\overline{F}_{AAm}$) and more composition drift with higher ionic strength. This will affect how the anions are distributed along the chain, which again highlights the important influence of ionic strength in AMPS – AAm copolymerization.

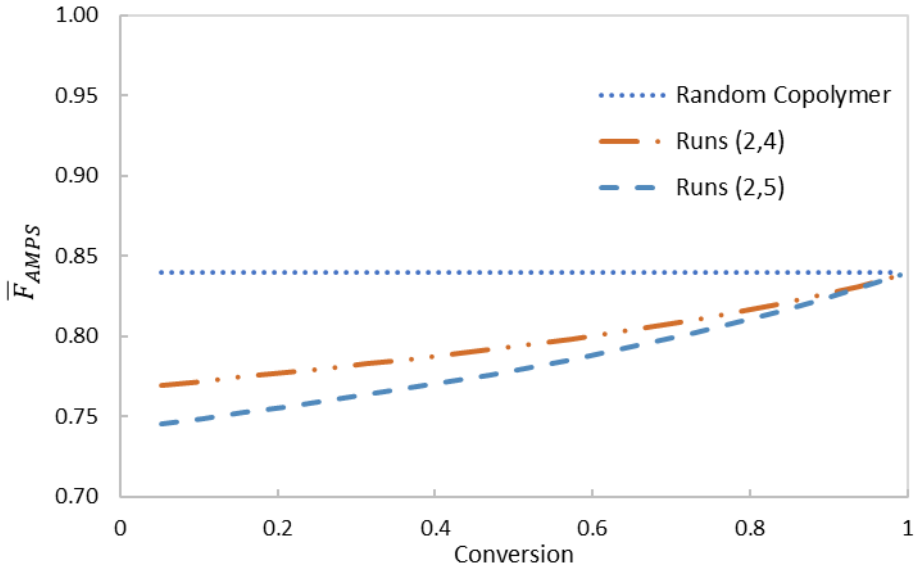

Figure 26: Estimated cumulative copolymer composition vs. conversion for AMPS-rich formulations (using RREs from Runs (2,4) and (2,5) (Table 6)); effect of increasing IS in AMPS-rich feed

4.2.2.3. Reactivity Ratio Comparisons at Constant Ionic Strength

Copolymerizations at constant ionic strength (where formulations are adjusted to ensure that both AAm- and AMPS-rich samples have the same ionic strength) were performed at 0.84 M (Runs 2,4) and 1.58 M (Runs 3,5). Reactivity ratio estimation results are shown in Figure 27. Increasing the ionic strength of copolymer pairs from 0.84 M to 1.58 M resulted in a decrease in both r_{AMPS} and r_{AAm}, but more so for r_{AAm}. These results align with observations reported in previous work, such as the terpolymerization of AMPS, AAm, and AAc [80].

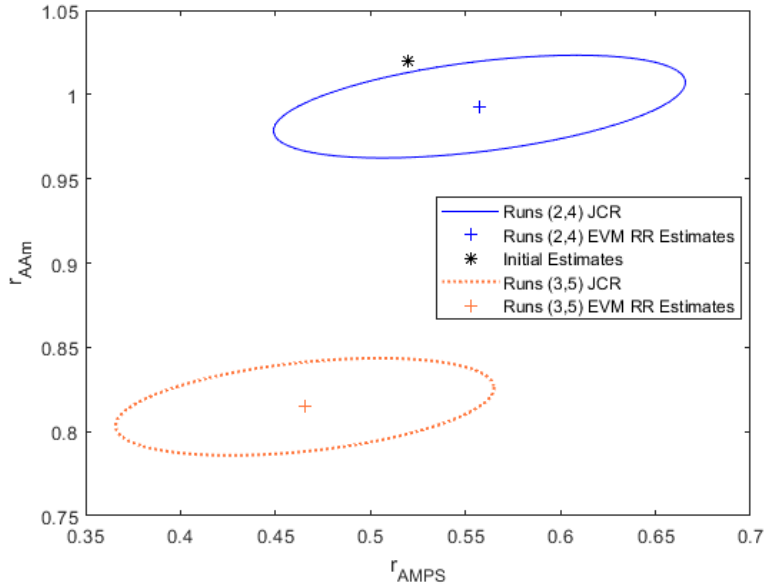

Figure 27: Reactivity ratio estimates and JCRs for Runs (2,4) and Runs (3,5); constant IS of 0.84 M (Runs 2,4) and 1.58 M (Runs 3,5); initial estimates from McCormick and Chen [42]

These changes in ionic strength impact the predicted cumulative copolymer composition, as shown in Figure 28. For copolymerizations with AAm-rich feed ($f_{AAm,0} = 0.90$), there is a significant difference in cumulative copolymer composition predictions at different ionic strengths. Using the reactivity ratios estimated at IS = 0.84 M (Runs 2,4), the model prediction indicates that AAm is more likely to propagate, as the cumulative copolymer composition is greater than the feed composition. In contrast, at IS = 1.58 M (Runs 3,5), the cumulative copolymer composition ($\overline{F}_{AAm}$) is below the feed composition. This is a significant result, as this means that AMPS is more likely to propagate at this ionic strength and composition.

The model predictions for the AMPS-rich feed ($f_{AAm,0} = 0.16$) indicate that AAm is more likely to propagate than AMPS, regardless of whether 0.84 M or 1.58 M ionic strength conditions are employed. However, in comparing the ionic strength effects, AAm will have

a higher incorporation when samples are prepared with an ionic strength of 1.58 M (Runs 3,5).

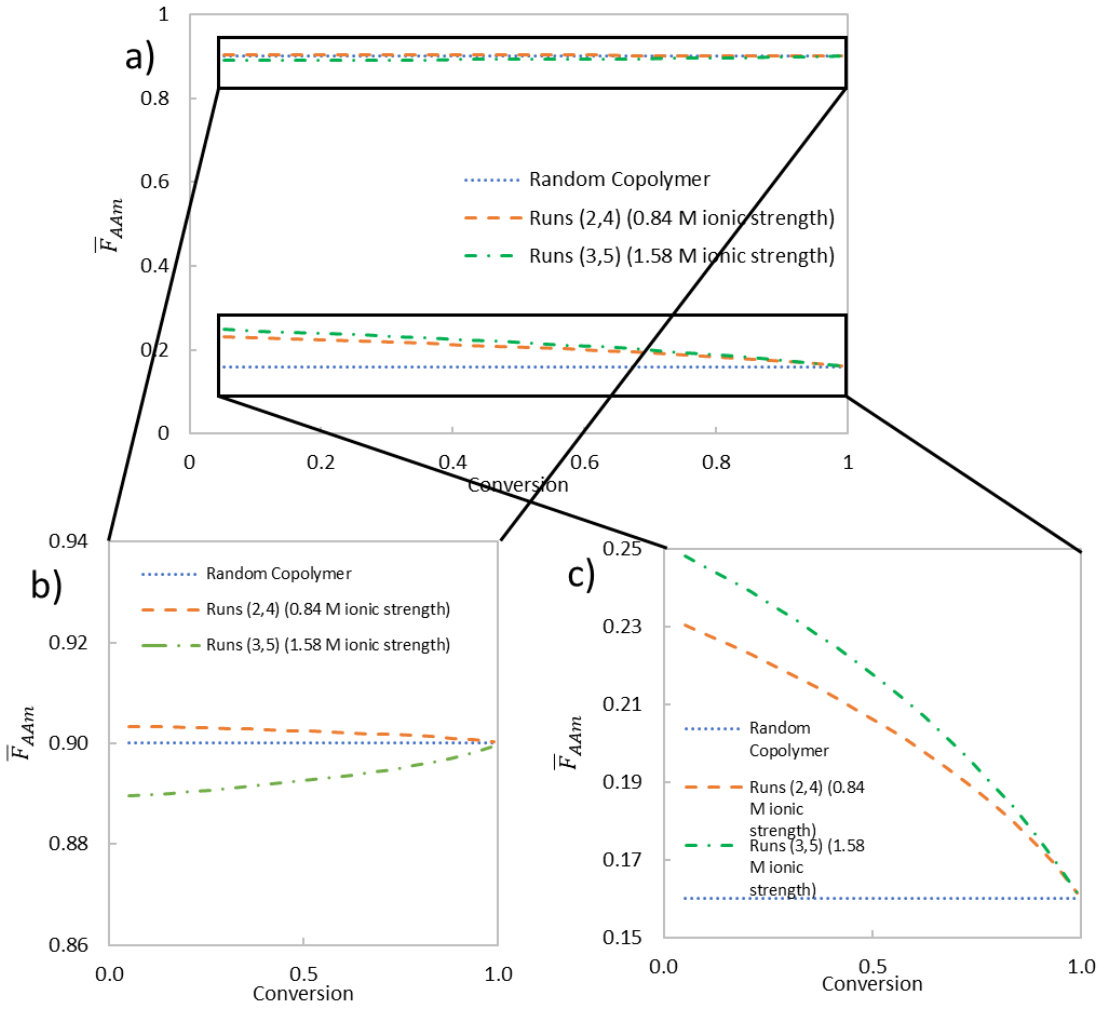

Figure 28: a) Estimated cumulative polymer composition vs. conversion at varying ionic strengths, with b) zoomed in on the AAm-rich feed and c) zoomed in on the AMPS-rich feed.

The shift in probability of propagation (instantaneous copolymer composition vs. feed composition) is shown in Figure 29. Specifically, at f_{AAm}= 0.9, the sample at the higher ionic strength is below that of a random copolymer, signalling that AMPS is more likely to propagate; this agrees with the results of Figure 28. For the conditions studied herein,

increasing the ionic strength also creates an azeotrope (represented by the intersection of the instantaneous copolymer composition curve with the random copolymer line). At the azeotrope, the copolymerization will create a random copolymer and there will be no composition drift.

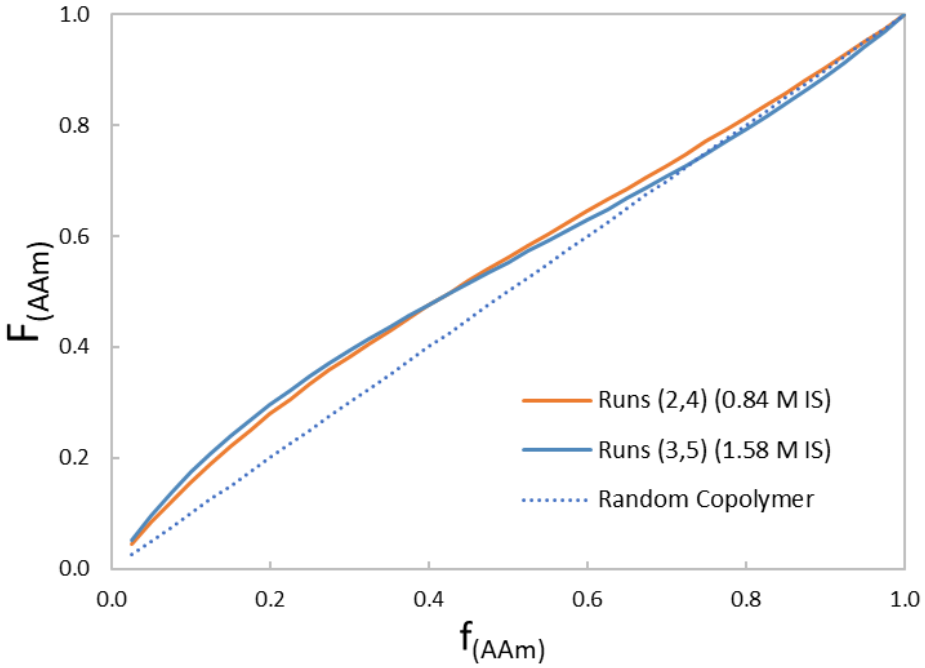

Figure 29: Instantaneous copolymer composition vs. monomer composition for Runs (2,4) (0.84 M ionic strength) and (3,5) (1.58 M ionic strength)

As described previously, Riahinezhad et al. [59] investigated the impact of ionic strength on the copolymerization of AAm and anionic AAc. In comparing 'constant IS' conditions at different feed compositions, they found that increasing the ionic strength increased r_{AAc} and decreased r_{AAm}, whereas in the current study both r_{AMPS} (also an anionic monomer) and r_{AAm} decreased. Despite both AMPS and AAc being anionic, the reactivity ratios were impacted differently by changes in ionic strength. This may be because AAc is a much smaller molecule than AMPS; as mentioned above, it is hypothesized that AMPS is more

significantly impacted by steric effects. Therefore, it is reasonable to conclude that AMPS and AAc would exhibit different results with the addition of counter ions.

4.3. Conclusions

Through the homopolymerization of AAm and AMPS, it was found that altering the ionic strength and pH had no significant effects on the conversion vs. time profile, although changes in reactivity ratios were observed in related AMPS – AAm copolymerizations. Copolymerization with no ionic strength adjustment yielded reactivity ratio estimates of $r_{AMPS} = 0.549$ and $r_{AAm} = 0.870$. Moderate ionic strength adjustment of the AAm-rich feed increased r_{AAm}, but higher concentrations of ionic strength ultimately reduced the r_{AAm}. When the ionic strength of the AAm-rich feed was adjusted to a 'constant ionic strength' of 0.84 M (same IS in both AAm-rich and AMPS-rich feeds), the reactivity ratios were $r_{AMPS} = 0.557$ and $r_{AAm} = 0.993$. However, when the 'constant IS' was increased to 1.58 M, the reactivity ratios decreased to $r_{AMPS} = 0.465$ and $r_{AAm} = 0.815$.

For the AMPS – AAm copolymerization system, it was also observed that changing the ionic strength of the AAm-rich feed had a stronger impact on reactivity ratio estimates than changing the ionic strength of the AMPS-rich feed. This study has demonstrated the various impacts that ionic strength can have on the composition and microstructure of anionic copolymers; it can promote more or less rigid structures in solution, impact propagation kinetics, and alter the comonomer distribution along the polymer chains. This is an important result in applications such as flocculation and enhanced oil recovery, as copolymer composition and microstructure will impact the ultimate application performance.

5. Effect of Ionic Strength on DADMAC–AAm Copolymerization Kinetics, Microstructure, and Flocculation Performance

Chapter 5 describes the study of DADMAC – AAm copolymerization kinetics using in situ ^{1}H NMR. The EVM design of experiments was used to find optimal feed compositions for reactivity ratio estimation, so that the effect of ionic strength on DADMAC – AAm copolymerization reactivity ratios and copolymer microstructure could be studied. GPC was used to measure the molecular weight averages of the synthesized copolymers, and flocculation performance was studied for the resulting copolymers. Flocculation trials were performed at the Dartmouth Wastewater Treatment Facility with support from Halifax Water and the Centre for Water Resources Studies (CWRS).

5.1. Design of Experiments and Experimental Preparation

The EVM design of experiments (DOE; as described in Section 2.3.5) was used in this study to calculate the optimal feed compositions for reactivity ratio estimation [70]. Initial estimates for the reactivity ratios were needed, and results from a study by Bi and Zhang were used [17]. Bi and Zhang reported a similar monomer concentration (2.5 M) and reaction temperature (45°C) to the current study, and their data yielded reactivity ratio estimates of r_{DADMAC}=0.14 and r_{AAm}=6.11 [17]. Using these values as preliminary reactivity ratio estimates, it was found that the maximum of the determinant of the information matrix (that is, the compositions at which the information for subsequent reactivity ratio estimation would be maximized) occurred at feed compositions of $f_{DADMAC,0}$ = 0.851 and $f_{DADMAC,0}$ = 0.1 (see Figure 30). Constraints were implemented in the EVM DOE program

to ensure that feed compositions did not exceed a minimum of $f_{DADMAC,0}$ = 0.1 and maximum of $f_{DADMAC,0}$ = 0.9.

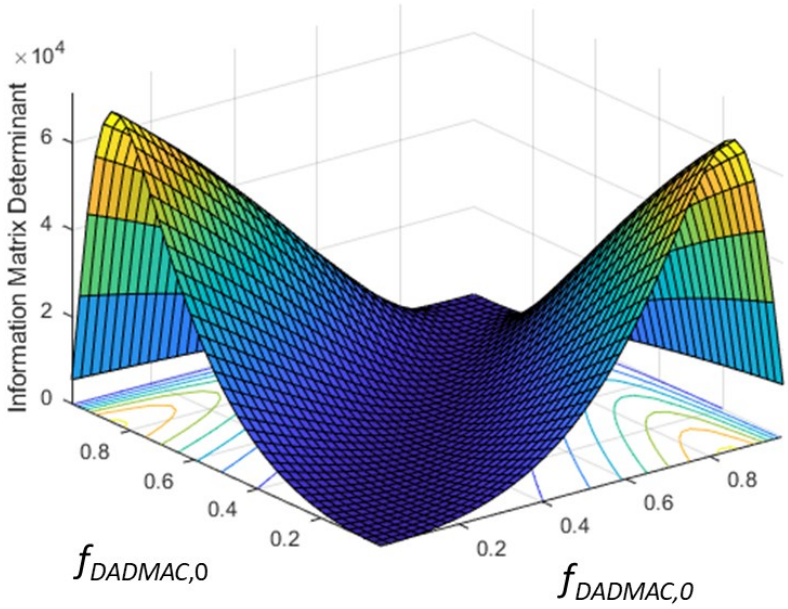

Figure 30: Determinant of information matrix for DADMAC – AAm copolymerization, plotted against feed composition, based on data from Bi and Zhang [17]

Initiator concentration was chosen so the $\overline{M}_w$ of the AAm-rich formulation would be approximately 14×10^6 g/mol. Using the rate constants from Abdollahi et al. [3] and Equations 16 and 18, it was calculated that the required initiator concentration would be 5.26 mM of ACVA. Sample calculations for estimating molecular weight are shown in Appendix A.2. Abdollahi et al. [3] used [M] =1 M, KPS as the initiator, and did not adjust the pH, hence there are likely differences in the rate of propagation compared to the current study.

2 M monomer concentration was selected for this study, so the results would also be relevant to the analysis described in Chapter 7. For the Chapter 7 design of experiments, where monomer concentration and pH impacts were studied, 2 M monomer concentration and pH 7 were used as the center point for the factorial design.

5.2. Results and Discussion

5.2.1. In Situ ^{1}H NMR for DADMAC – AAm Copolymerization Monitoring

The ^{1}H NMR spectra of DADMAC and AAm comonomers in pre-polymerization solution are shown in Figure 31. For DADMAC monomers, there are 2 doublets relating to the terminal alkenes in the range of 5.65 and 5.8 ppm. The average was taken to calculate the monomer concentration, as some overlap occurred between the responses. As mentioned in Section 3.4, acrylamide peaks were measured in the range of 5.42 to 5.54 ppm.

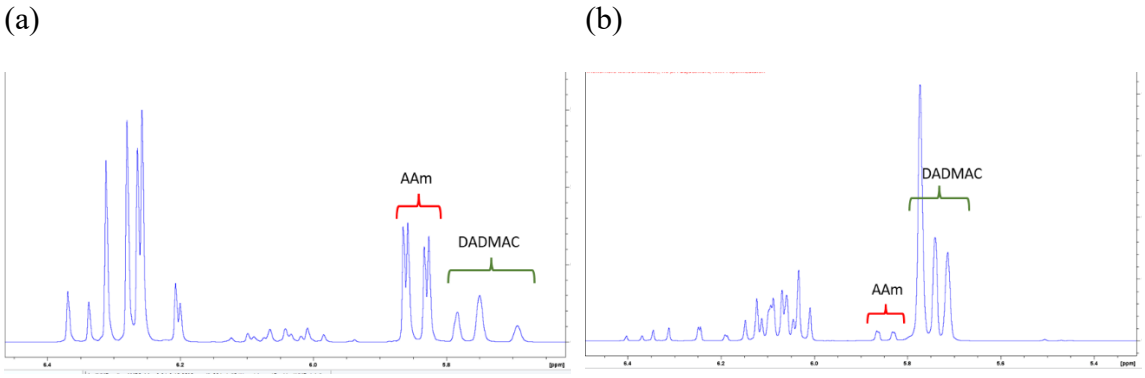

Figure 31: Representative ^{1}H NMR spectra measurements of comonomer mixtures of DAMDMAC and acrylamide, where (a) $f_{DADMAC,0}$ = 0.10 and (b) $f_{DADMAC,0}$ = 0.851

A standard curve at various monomer feed fractions was developed and is shown in Figure 32. This demonstrates that this method for analyzing NMR data is accurate and can be confidently used for calculating monomer concentrations in polymerizing mixtures.

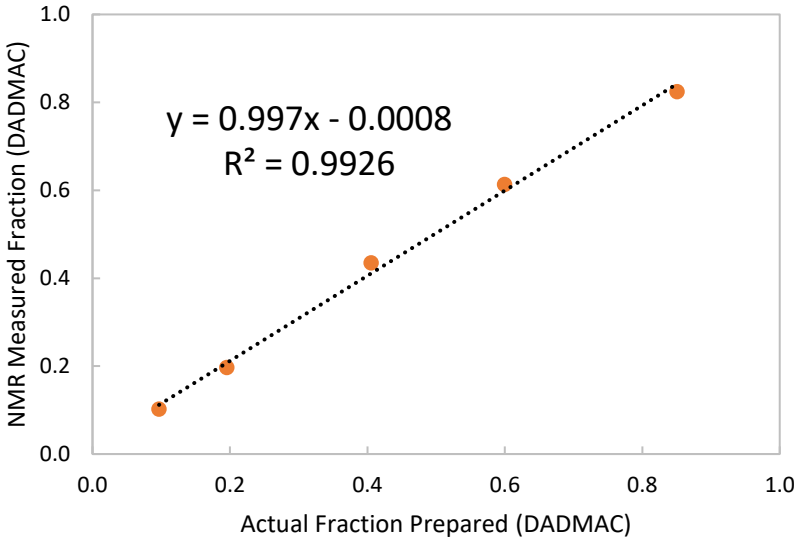

Figure 32: Standard curve for measuring DADMAC and AAm molar fractions via ^{1}H NMR

As described in Section 3.4, samples were inserted into the NMR at 50°C to initiate polymerization. Samples were measured approximately every 6 minutes. This was done for at least 10 total measurements for each sample, but DADMAC-rich samples often had approximately 20 measurements since the polymerization kinetics were generally slower. An example of NMR scans over time (as polymerization progresses) is provided in Figure 33.

(a)

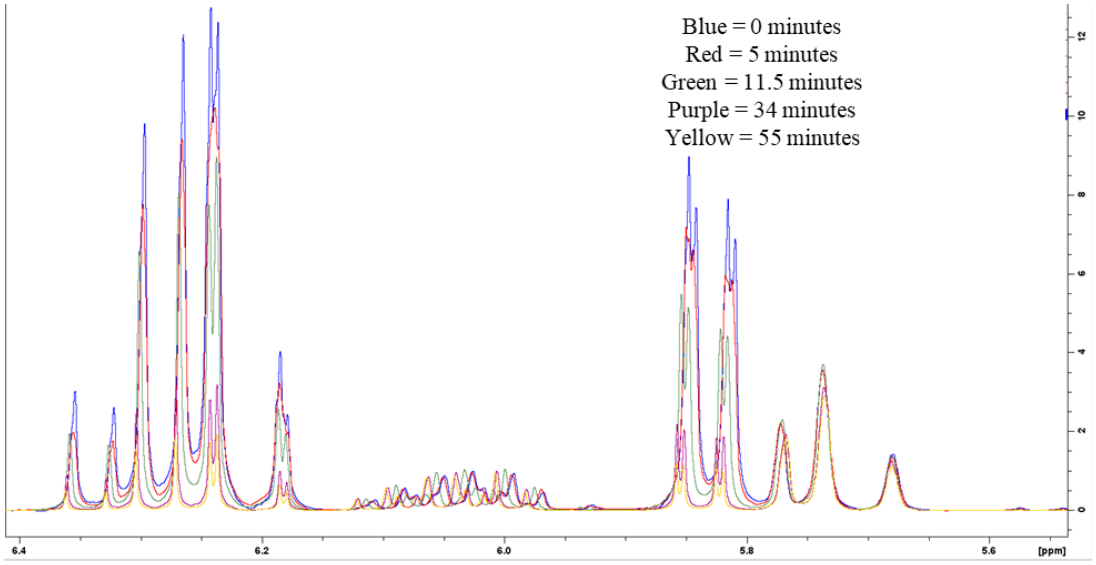

(b)

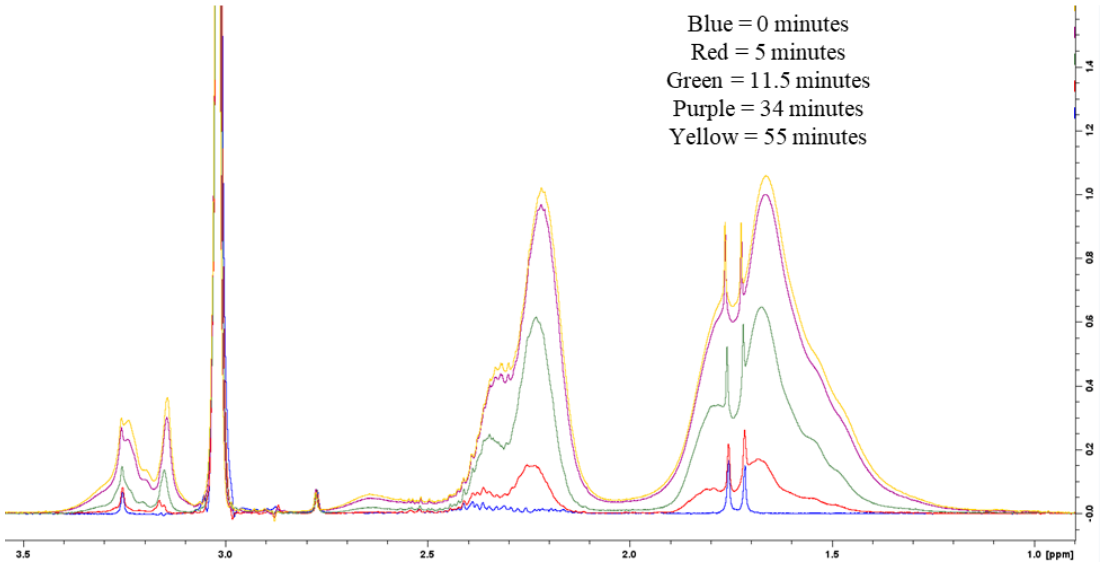

Figure 33: Representative polymerization measurements using in situ ^{1}H NMR in (a) the alkene region and (b) the alkane region; results are shown for a replicate from Run 3 (Table 7)

Five different copolymerization formulations were prepared to determine the impact of ionic strength on reactivity ratio estimates. The feed compositions and ionic strengths vary,

but all samples are prepared at pH 7 and 2.0 M monomer concentration. An example of calculating ionic strength can be seen in Appendix A.1.

Table 7: Feed compositions and ionic strength of copolymerization experiments

Run	$f_{DADMAC,0}$	NaCl (M)	Ionic Strength (M)
1	0.1	0	0.100
2	0.1	0.751	0.851
3	0.1	1.502	1.602
4	0.851	0	0.851
5	0.851	0.751	1.602

5.2.2. Reactivity Ratio Estimation

All formulations were selected to facilitate ionic strength comparisons between reactivity ratio estimates. For example, 0.751 M NaCl was added to Run 2 to ensure that an AAm-rich and DADMAC-rich feed composition (Runs 2 and 4) have the same ionic strength (0.851 M). In the same way, the salt concentration for Run 5 was selected to compare the effects of adding the same amount of NaCl as in Run 2 (0.751 M). All combinations are summarized in Table 8, and are used in what follows to elucidate the effects of ionic strength on DADMAC – AAm reactivity ratio estimates.

Table 8: Copolymerization combinations for DADMAC – AAm and resulting reactivity ratio estimates

Pair	IS (M) (DADMAC-Rich)	IS (M) (AAm-Rich)	r_{DADMAC}	r_{AAm}
(1,4)	0.851	0.100	0.063	5.85
(2,4)	0.851	0.851	0.070	6.47
(3,4)	0.851	1.602	0.094	7.97
(2,5)	1.602	0.851	0.20	6.67
(3,5)	1.602	1.602	0.24	8.32

For each run, there were 4 replicates. Figure 34 demonstrates the repeatability of the conversion vs. time data collection, as the four data sets are shown for Run 2 of Table 7. The 4 replicates shown here were completed over a 2-month span.

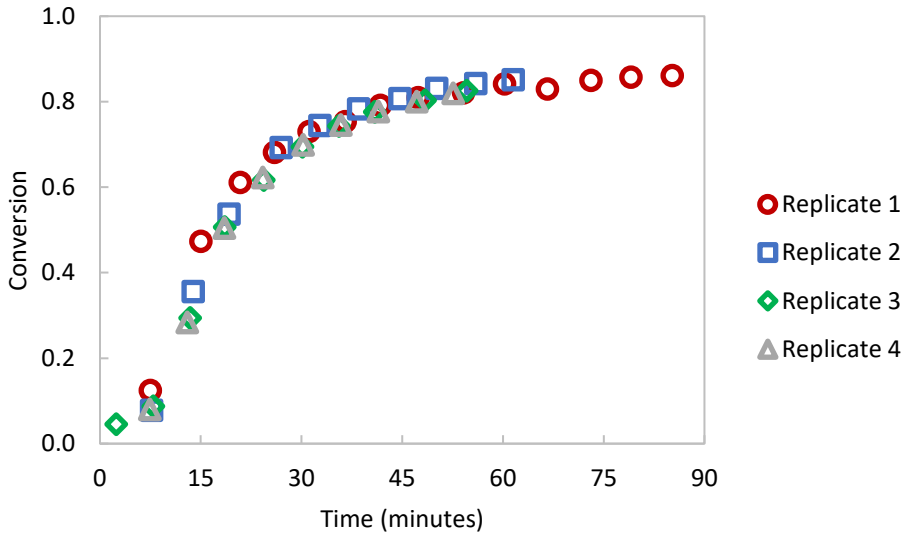

Figure 34: Representative repeatability of in situ ^{1}H NMR for Run 2 (DADMAC – AAm copolymerization with $f_{DADMAC,0}$ = 0.1 and IS = 0.851 M)

The reactivity ratio estimation results of DADMAC – AAm copolymerization with no ionic strength adjustments (that is, Runs (1,4)) are different than the initial estimate from the

literature, especially for r_{DADMAC}. Bi and Zhang [17] estimated reactivity ratios of r_{DADMAC} = 0.14 and r_{AAm} = 6.11, compared to r_{DADMAC} = 0.063 and r_{AAm} = 5.85 in the current study. These differences may be attributed to differences in monomer concentration, temperature, and mixing. Also, Bi and Zhang used a linear method of estimating reactivity ratios whereas in this study EVM (a non-linear method) was used. Despite these differences, the current reactivity ratio estimates are similar to estimates from other studies, including references [15,49,51]. For example, Wandrey et al. reported reactivity ratios of r_{DADMAC} = 0.05 and r_{AAm} = 6.06 [49]. Wandrey et al. used a monomer concentration of 3 M, polymerized at 35°C, and the pH was not adjusted/measured. Relevant literature data are shown in Figure 35 [15,49,51].

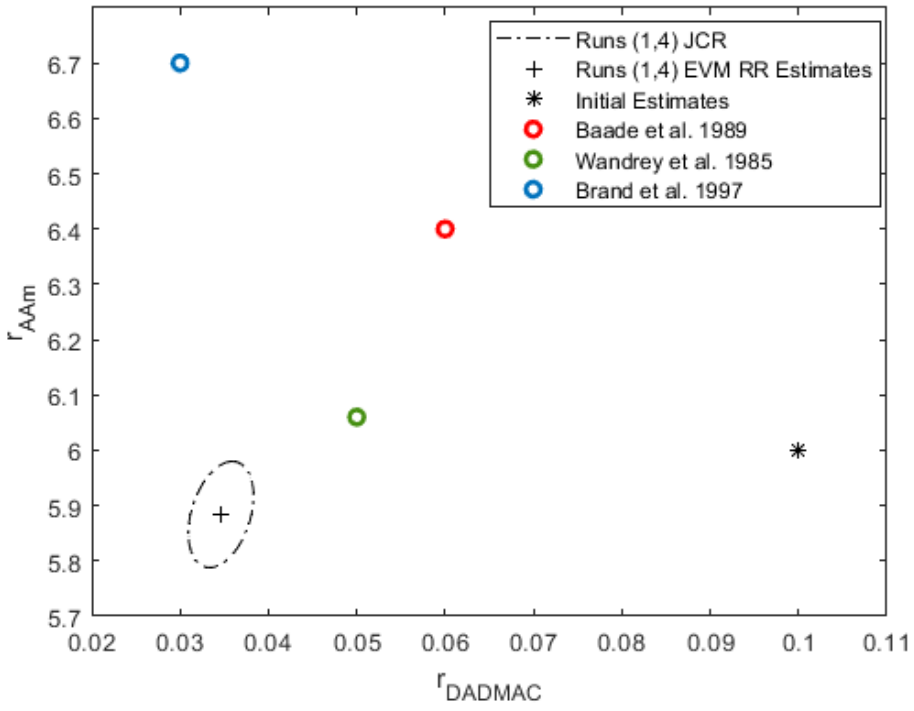

Figure 35: Reactivity ratio estimates and JCR for Runs (1,4) (no ionic strength adjustment); initial estimates from Bi and Zhang [17]; data points from the literature also shown [15,49,51]

5.2.2.1. Varying Ionic Strength in AAm-rich Feeds

When ionic strength of the AAm-rich feed is increased (but the IS of the DADMAC-rich feed remains constant), both reactivity ratios increase, as shown in Figure 36. The increase in r_{DADMAC} aligns with physicochemical expectations; as ionic strength increases, the electrostatic repulsion decreases via an ionic shielding effect and homopropagation of DADMAC (k_{11}) increases. Since r_{AAm} also increased with increasing ionic strength, that may mean that cross-propagation (k_{21}) decreased; k_{22} is not expected to be impacted by ionic strength. The decrease in k_{21} is likely the result of an increase in k_{11}, as these would be competing reactions. When ionic strength in the AAm-rich feed is increased further to 1.602 M, a further increase in r_{AAm} and r_{DADMAC} is observed (see Figure 36).

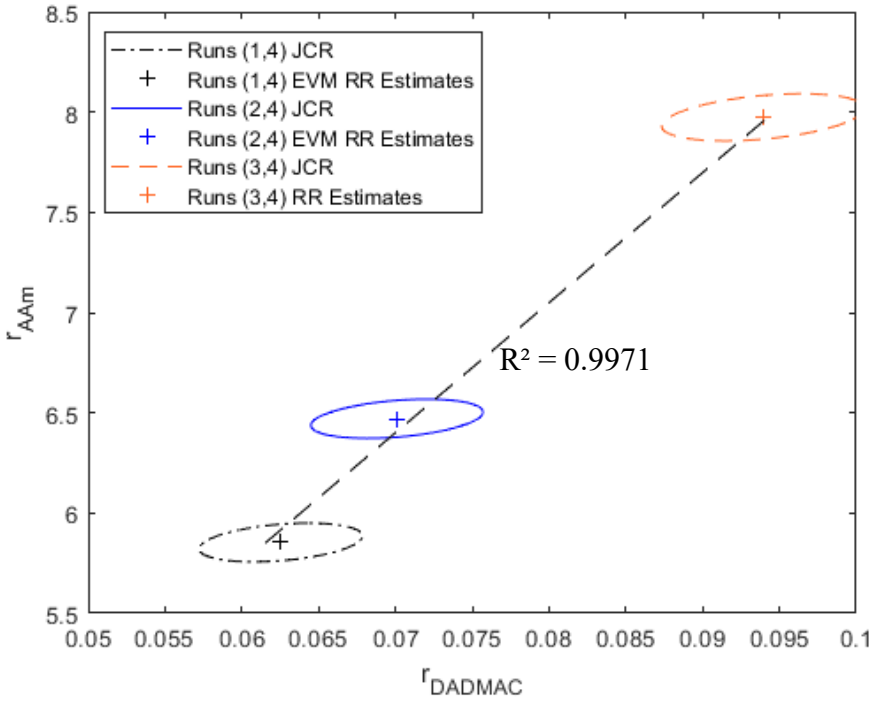

Figure 36: Reactivity ratio estimates and JCRs for Runs (1,4), Runs (2,4), and Runs (3,4); all DADMAC-rich data collected with IS = 0.851 M, with AAm-rich data collected at varying IS

Using Equation 13, if k_{11} increases, k_{21} would decrease due to competing reactions. Looking at the reactivity ratio equations, $r_{AAm} = k_{22}/k_{21}$ and $r_{DADMAC} = k_{11}/k_{12}$. Therefore, when increasing ionic strength, it is expected that k_{11} would increase and k_{21} would decrease. Since k_{21} is in the denominator of r_{AAm}, r_{AAm} increases with decreased k_{21}. If competing reactions are the main cause of the change in r_{AAm}, it would be expected that r_{AAm} would vary linearly. In Figure 36, it is evident that there is a very strong linear trend between r_{AAm} and r_{DADMAC} as ionic strength increases, which suggests that the increase in r_{AAm} is likely due to competing reactions between k_{21} and k_{11}.

5.2.2.2. Varying Ionic Strength in DADMAC-rich Feeds

As shown in Figure 37, changing the ionic strength in the DADMAC-rich feed (for example, comparing Runs (3,4) vs. Runs (3,5) and Runs (2,4) vs. Runs (2,5)) has a stronger effect on the reactivity ratios than changing the ionic strength of the AAm-rich feed (for example, comparing Runs (2,4) to Runs (3,4) vs. Runs (2,4) to Runs (2,5)). This result is as expected, as DADMAC is the ionic monomer and AAm homopropagation is not expected to be significantly affected by ionic strength. The driving force for changes in r_{DADMAC} is ionic shielding, whereas r_{AAm} is primarily impacted by competing reactions. The increase in r_{DADMAC} under the specified conditions is over 180%, compared to r_{AAm} which increased by approximately 11%, as seen in Figure 37. The increase in r_{AAm} from Runs (2,5) to Runs (3,5) serves as validation that increasing the ionic strength in the AAm-rich feed increases r_{AAm} as it follows the same trend as Runs (2,4) to Runs (3,4). It is worth noting that although the relative increase in r_{DADMAC} is higher than r_{AAm}, the absolute increase is higher for r_{AAm}. For example, r_{AAm} increases by 1.5, whereas r_{DADMAC} increases by 0.13.

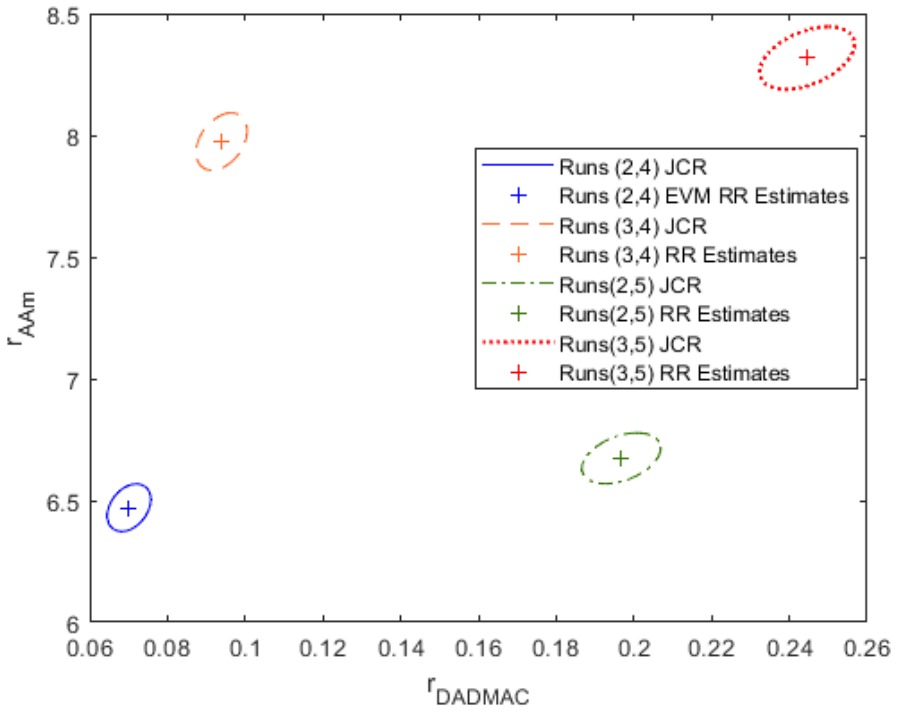

Figure 37: Reactivity ratio estimates and JCRs for Runs (2,4), Runs (2,5), Runs (3,4), and Runs (3,5); impact of varying the IS of AAm-rich and DADMAC-rich formulations on reactivity ratios

The effect of changing the IS in the DADMAC-rich feed can also be observed in the instantaneous copolymer composition predictions in Figure 38; the differences are especially noticeable at high DADMAC fractions. When the DADMAC fraction in the monomer phase is below ≈0.6, the instantaneous copolymer composition is the same. However, once the DADMAC composition in the feed is above 0.6, the formulations with increased ionic strength in the DADMAC-rich feed (Runs (2,5) for example) have a higher instantaneous copolymer composition than the lower ionic strength formulations, suggesting that DADMAC is more likely to propagate as ionic strength increases. This is in agreement with the significant increase in r_{DADMAC} as ionic strength increases.

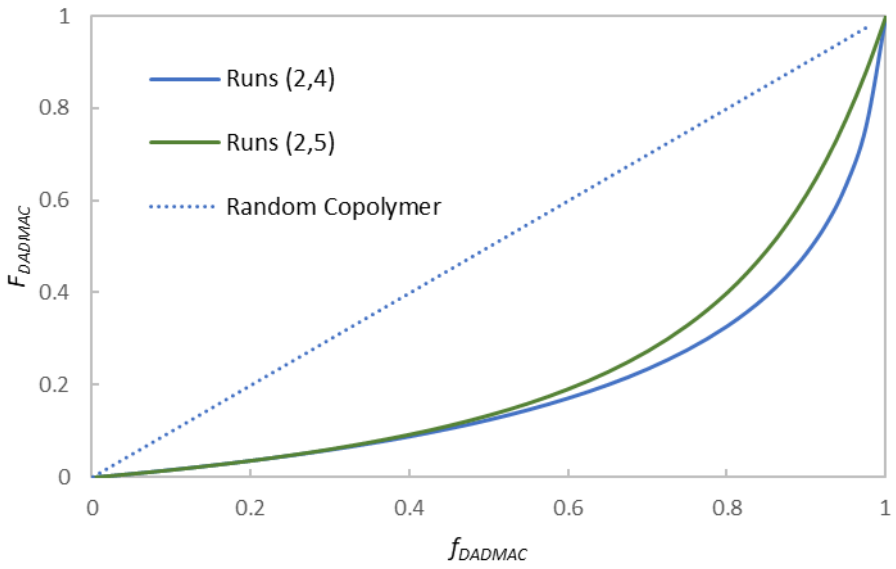

Figure 38: Instantaneous copolymer composition vs. monomer composition predicted using reactivity ratios from Runs (2,4) and Runs (2,5); both data sets have an AAm-rich feed IS of 0.851 M, while the DADMAC-rich feed IS is 0.851 M for Runs (2,4) and 1.602 M for Runs (2,5)

The impact of ionic strength on DADMAC – AAm copolymerization is also evident when looking at the predicted triad fractions, as shown in Figure 39 and Figure 40. Triad fractions have been calculated (as per Equations 32 through 34) for samples with and without ionic strength adjustments (Runs (3,5) and Runs (1,4), respectively). For the DADMAC-centered triads (Figure 39), there is a significant shift with ionic strength adjustment; controlling ionic strength results in a higher fraction of A_{111} triads (where monomer 1 = DADMAC and monomer 2 = AAm). This indicates that the copolymer prepared under controlled IS conditions will be more 'blocky' or have a gradient microstructure. In contrast, without ionic strength adjustment, the triad fractions are generally dominated by A_{212}, suggesting that an alternating-type copolymer will form.

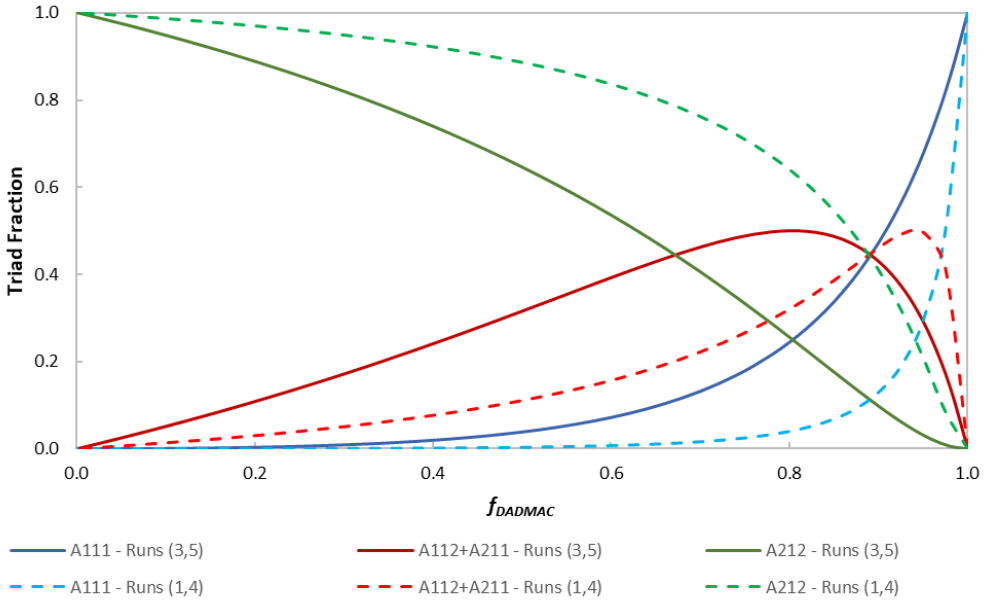

Figure 39: DADMAC-centered triad fraction predictions for Runs (1,4) (no IS adjustment) and Runs (3,5) (both adjusted to IS = 1.602 M)

The acrylamide-centered triads (shown in Figure 40) are not as significantly impacted by IS adjustment as the DADMAC-centered triads. However, this is expected, as AAm triad fraction calculations only use r_{AAm} estimates. Therefore, since r_{AAm} only increased by 11% with increased ionic strength, the change would be relatively small compared to the DADMAC triads, where r_{DADMAC} increased by 180%. However, we again see slightly higher 'blocky' fractions (A_{222}) for the formulation with IS adjustment. This is an important result for future application studies, as block copolymers may be more effective flocculants [5,14,63]; this demonstrates that higher (controlled) ionic strength has the potential to positively impact flocculation properties.

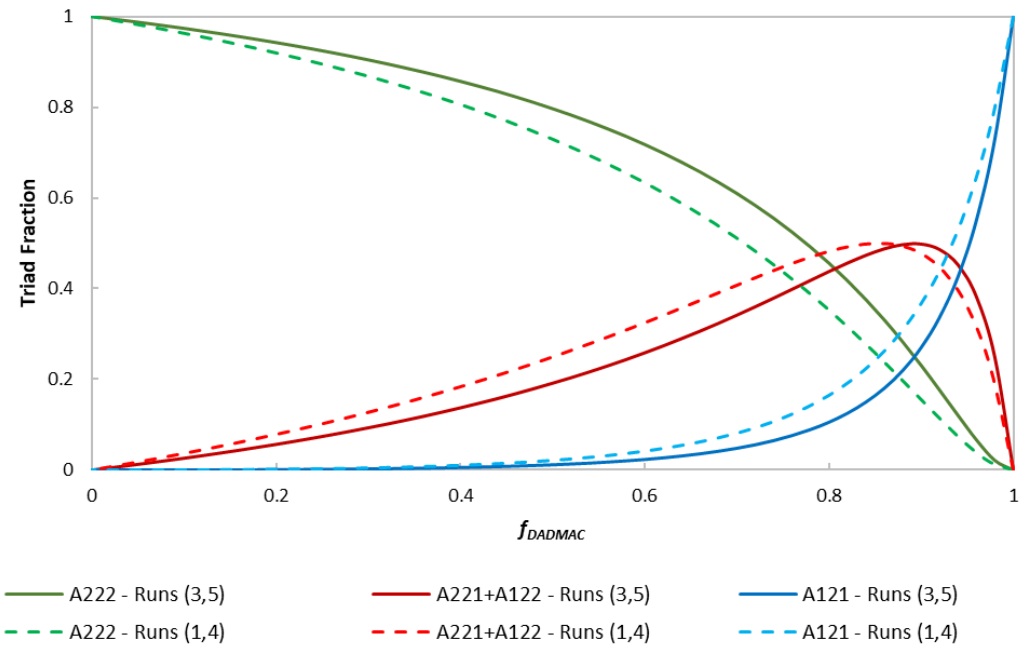

Figure 40: AAm-centered triad fraction predictions for Runs (1,4) (no IS adjustment) and Runs (3,5) (both adjusted to IS = 1.602 M)

5.2.2.3. Constant Ionic Strength

Finally, reactivity ratios were estimated from the copolymerization data where samples were adjusted to constant ionic strength (that is, AAm-rich feed and DADMAC-rich feed had the same ionic strength). As shown in Table 8, the ionic strengths were 0.851 M (Runs (2,4)) and 1.602 M (Runs (3,5)). The difference between the resulting reactivity ratio estimates is significant; increasing ionic strength increased both r_{AAm} and r_{DADMAC}, and especially r_{DADMAC}. r_{DADMAC} increased from 0.070 to 0.24, whereas r_{AAm} increased from 6.47 to 8.32 (see Figure 41). As mentioned above, the increase in r_{DADMAC} is likely due to the ionic shielding effect, meaning that there is a reduced electrostatic repulsion between the cations on the DADMAC monomer and the cations incorporated into the DADMAC-containing macroradical.

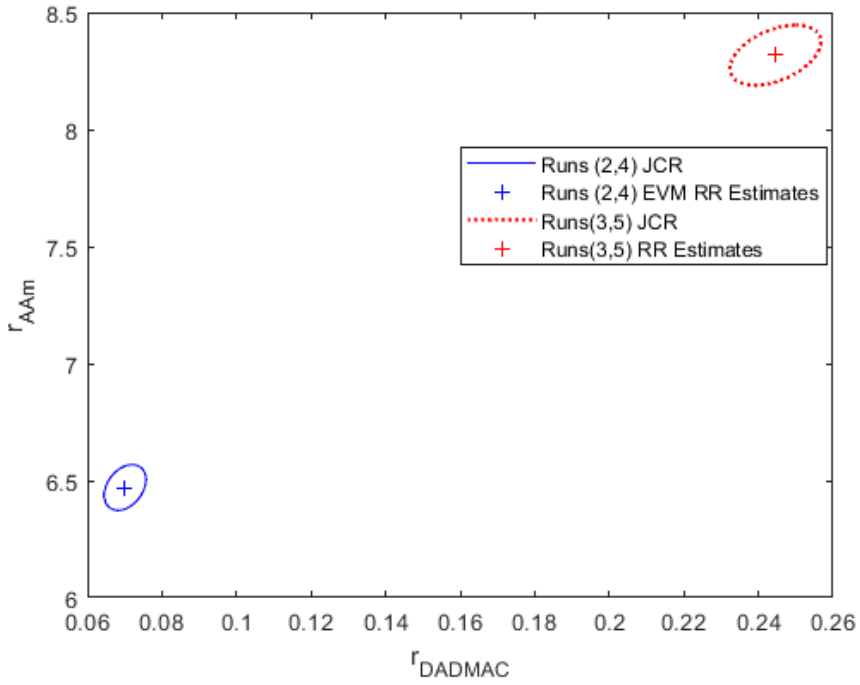

Figure 41: Reactivity ratio estimates and JCRs for Runs (2,4) and Runs (3,5); constant IS of 0.851 M (Runs (2,4)) and 1.602 M (Runs (3,5))

The impact of increasing (constant) ionic strength on cumulative copolymer composition is shown in Figure 42. In comparing the cumulative composition model predictions at different ionic strengths, differences between the high and low IS at $f_{DADMAC,0}$ = 0.1 are minimal. However, at $f_{DADMAC,0}$ = 0.851, the ionic strength has a significant impact on cumulative copolymer composition, especially below 60% conversion. At low conversions, the higher ionic strength formulation has a higher DADMAC incorporation compared to the copolymer without ionic strength adjustment. This result, combined with the triad fraction models, suggests that not only is it more likely for DADMAC to be incorporated, but there is also an increase of A_{111} triads and decrease in A_{212} triads. As such, it is more likely that the resulting polymer microstructure synthesized at higher ionic strength will have gradient characteristics.

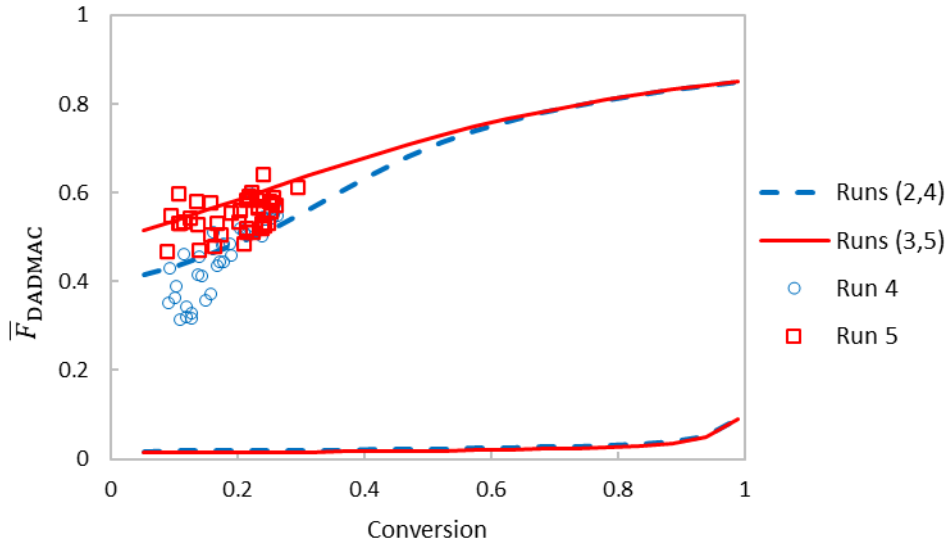

Figure 42: Estimated and measured cumulative copolymer composition vs. conversion, using reactivity ratios estimated from Runs (2,4) and (3,5); data points represent experimental results

5.2.3. Molecular Weight Characterization

Molecular weights were measured using gel permeation chromatography (GPC); the protocol is explained in Section 3.5. Molecular weight distribution is an important characteristic for flocculation, as it is important for the bridging mechanism. It is also important that the polydispersity (PDI) is as low as possible, as high PDI would indicate a wide range of polymer chain lengths, including many small polymers that would not be as effective as the longer chains. The copolymers characterized herein were the same samples used in flocculation testing (Section 5.2.4), and one GPC replicate per formulation was evaluated.

For Runs 1 to 3 (which all had the same feed composition of $f_{DADMAC,0}$ = 0.1) there were minimal differences in terms of $\overline{M}_w$ and polydispersity; differences can be attributed to

experimental error. The $\overline{M}_w$ for all three samples were in the range of 4.5E6 to 5.12E6 g/mol as seen in Table 9 and Figure 43. This was similar to the predicted $\overline{M}_n$ based on earlier calculations at 14×10^6 g/mol, which relied on propagation rate data from a study by Abdollahi et al. [3]. Sample calculations can be seen in Appendix A.2.

Table 9: $\overline{M}_w$ and polydispersity of AAm-rich DADMAC – AAm copolymers

	NaCl added (M)	$\overline{M}_w$	PDI
Run 1	0	5.12E+06	1.17
Run 2	0.751	4.93E+06	1.10
Run 3	1.502	4.50E+06	1.08

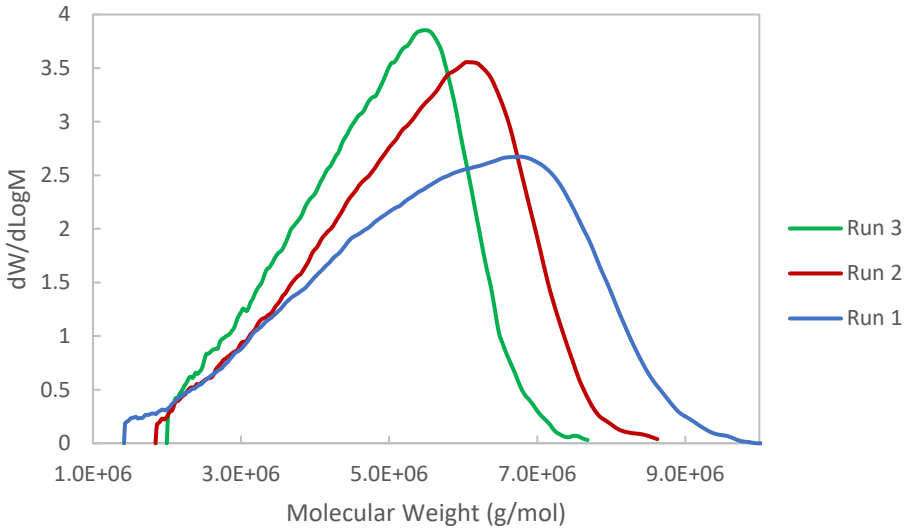

Figure 43: Molecular weight distribution of AAm-rich samples measured by GPC

With increased ionic strength in the polymerizing mixture, there was a loss of polymer mass during GPC characterization, as seen in Figure 44. For all three formulations, the percentage of remaining polymer mass (as measured by the GPC) decreased with increased

ionic strength. For example, Run 2 was prepared to have a polymer concentration of 0.26 mg/mL, but the GPC-measured concentration at the detectors was 0.084 mg/mL (based on the input dn/dc value of 0.187 at $\overline{F}_{DADMAC} = 0.1$ [88]).

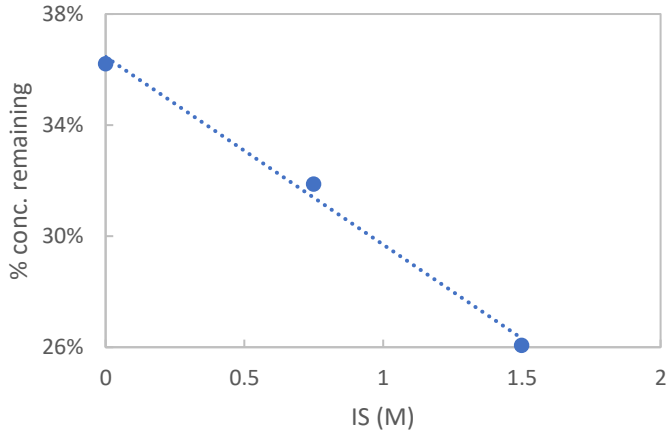

Figure 44: Ionic strength during synthesis vs. the percent of mass remaining (that is, polymer concentration measured/prepared concentration before filtration) for AAm-rich samples

It is possible that residual salt within the copolymer product is creating small flocs that are being retained in the filters used for GPC sample preparation. This result could also be due to solubility issues during solution preparation, or due to polymers sticking to the GPC column. At higher IS, the copolymer chains may become more intertwined due to low electrostatic repulsion, therefore creating small flocs in solution.

For the DADMAC-rich samples, the $\overline{M}_w$ were also close to the predicted values and in the range of 3.98E5 to 5.65E5 g/mol, as seen in Table 10. Abdollahi et al. [3] reported that the $\frac{k_p}{k_t^{0.5}}$ for $f_{DADMAC,0} = 0.851$ is approximately one tenth of the $\frac{k_p}{k_t^{0.5}}$ for $f_{DADMAC,0} = 0.1$, therefore it was expected that the $\overline{M}_w$ of AAm-rich copolymers would be higher than the $\overline{M}_w$ of DADMAC-rich copolymers by a factor of 10.

Table 10: $\overline{M}_w$ and polydispersity of DADMAC-rich DADMAC – AAm copolymers

	NaCl added (M)	$\overline{M}_w$	PDI
Run 4	0	3.98E+05	1.20
Run 5	0.75	5.65E+05	1.15

As before, when copolymers were synthesized at higher ionic strengths, a loss of mass in the GPC filtration step was observed. While there was 19% of the prepared polymer sample remaining/measured in Run 4, only 6.4% of the polymer mass remained in Run 5 (based on the input dn/dc value of 0.176 at $\overline{F}_{DADMAC} = 0.85$ [88]). DADMAC-rich copolymers may be more impacted by residual salt, as the copolymer has a higher concentration of ions. It is worth noting that both DADMAC polymers had a somewhat bimodal distribution, as shown in Figure 45. This is likely a characterization issue, especially as a low percent of the polymer was remaining and below an ideal polymer concentration for molecular weight measurements.

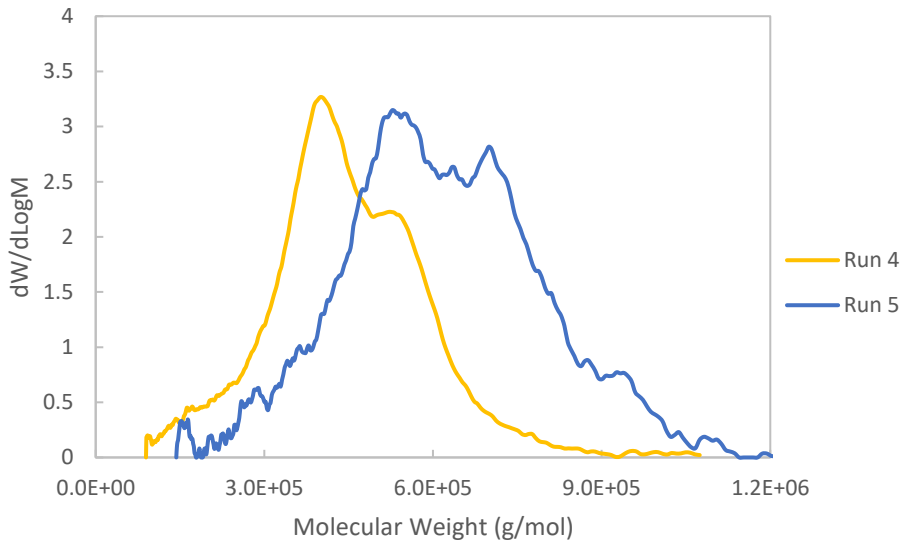

Figure 45: Molecular weight distribution of DADMAC-rich samples measured by GPC

The molecular weight distributions of commercial cationic polymer flocculants (obtained from Dr. Amina Stoddart, Department of Civil and Resource Engineering, Dalhousie University) were also measured, as shown in Table 11 and Figure 46; note that the y-axis in Figure 46b) is larger than in Figure 46a). The commercial flocculants were used for comparison to the custom-made polymers synthesized in the current work. The PDI is estimated to be very low for the Commercial Polymer #3, which is likely due to the molecular weight averages reaching the maximum limit of the column (10×10^6 g/mol).

Table 11: $\overline{M}_w$ and polydispersity of commercial flocculants

	$\overline{M}_w$ (g/mol)	PDI
Commercial Polymer #1	3.79E+06	1.35
Commercial Polymer #2	2.79E+06	1.49
Commercial Polymer #3	7.01E+06	1.00

It is worth noting that the measured concentrations of the commercial flocculants were below the prepared (expected) concentrations, as was the case for the synthesized copolymers. Commercial Polymer #1, #2, and #3 had 26.8%, 6.7%, and 5.5 % remaining concentration, respectively. The dn/dc was estimated to be 0.18, which was the average of the two DADMAC-AAm feeds. Additionally, an assumption was made that the cationic structural unit in the commercial flocculant is DADMAC, since this information was not provided by the supplier.

(a) (b)

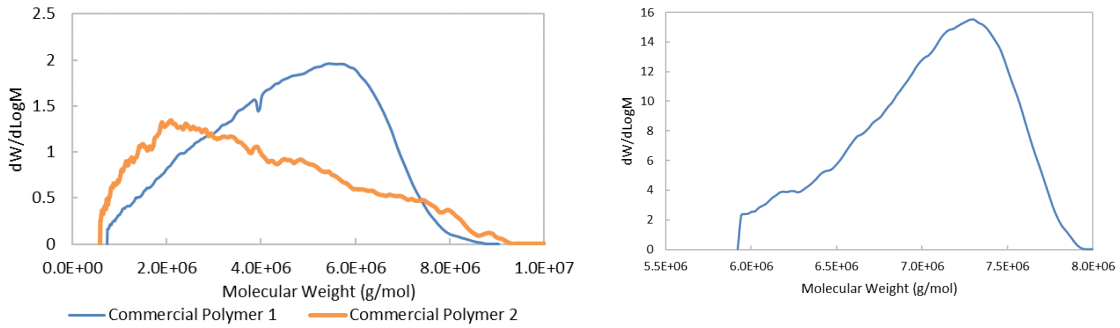

Figure 46: a) Commercial polymers 1 and 2 and b) Commercial polymer 3 molecular weight distributions measured by GPC

The commercial polymers #1 and #2 had molecular weights between the AAm-rich and DADMAC-rich flocculants. It is also likely that the copolymer composition of these polymers are in between AAm-rich and DADMAC-rich copolymers. It is believed that having copolymer composition around 50% is ideal [13]. Commercial flocculant #3 had the highest molecular weight, it is likely a high copolymer composition of AAm.

5.2.4. Flocculation Results

The protocol for flocculation trials is explained in Section 3.6. Flocculation trials were performed to relate copolymer microstructure to application performance. Flocculation trials for this study were performed at the Dartmouth Wastewater Treatment Facility on October 3, 2023, and the influent was collected for the day at ~9:30 am. Experiments and measurements were performed with the assistance of Carolina Ontiveros and Kayleigh Dunphy.

For flocculation trials, the influent was characterized with minimal treatment (post coarse screen, fine screen, and grit removal) as a baseline condition; the results are shown in Table 12. This is an important step for wastewater treatment studies, as the wastewater characteristics are always changing. The influent sample was taken post coarse screen, fine screen, and grit removal from the Dartmouth Wastewater Treatment Plant, and influent with properties as shown in Table 12 was used for all flocculation trials within Chapter 5. All measurements related to flocculation were collected with two replicates.

Table 12: Measured influent properties from the Dartmouth Wastewater Treatment Plant on October 3, 2023

Temperature (°C)	pH	Alkalinity (mg/L $CaCO_3$)	Turbidity (NTU)	UVT254 (%Transmission)
19.2	6.85	110	57.9	29.5
Zeta Potential (mV)	Conductivity (mS/cm)	TSS (mg/L)	BOD (mg/L)	COD (mg/L)
-14.19	1.954	133	160.3	319.5
UVT=ultraviolet transmission, TSS= total suspended solids, BOD= biochemical oxygen demand, and COD= chemical oxygen demand				

When dissolving the polymers for flocculation tests (as described in Section 3.6), the polymer sample from Run 3 was particularly difficult to dissolve; after 12 hours of mixing, the solution was diluted from 1 mg/mL to 0.33 mg/mL (final concentrations in jar tests were the same as 3 times the flocculant solution was added). Since the tests did not include adding any coagulant, the flocs from the trials did not become large or dense enough to settle effectively. This was observed for all samples, including the commercial flocculants. As such, a large portion of the flocs in solution floated to the top of the graduated cylinder, and settling velocity was not calculated. Representative results are shown in Figure 47.

Figure 47: Jar tests using commercial polymer flocculant #2 (left), commercial polymer #3 (middle), and commercial flocculant #1 (right); the flocs floated to the top and are circled in red

From Figure 48, it is evident that all polymer samples synthesized at high ionic strength conditions demonstrate improved flocculation over the polymer samples synthesized without ionic strength adjustment. Polymers synthesized during Runs 2 and 3 (AR, [IS] = 0.851 M and AR, [IS] = 1.602 M) result in lower settled water turbidity during wastewater

treatment than polymers synthesized during Run 1 (AR, [IS] = 0.1 M, note that Runs 1 through 5 are the same runs described in Section 5.2.1). Similarly, polymers synthesized during Run 5 (DR, [IS] = 1.602 M) result in lower settled water turbidity during wastewater treatment than polymers synthesized during Run 4 (DR, [IS] = 0.851 M). The lowest settled water turbidity observed when employing the custom-made polymers was obtained when using samples synthesized during Run 2. The best performing material overall (that is, the polymer that lowered settled water turbidity most substantially) was Commercial Polymer #2. The next lowest settled water turbidity was from Run 2, followed by Commercial Polymer #1. For the Commercial Polymer #3, the large flocs that formed were suspended in front of the turbidity detector, therefore the measurement was 152 NTU. This measurement was taken as an outlier and was not used in the average, although it was left for the standard deviation, which explains the large error bars. The commercial flocculants performed very well, especially Commercial Flocculant #2. During flocculation trails, it was very noticeable that the flocs from the commercial flocculants were significantly larger than those from the custom-made flocculants. Ultimately, the polymer compositions for the DADMAC – AAm copolymers were chosen for optimal estimation of reactivity ratios, not optimal flocculation performance. Commercial flocculants are likely in the range of 0.3 to 0.7 copolymer composition, as this is the optimal composition [13].

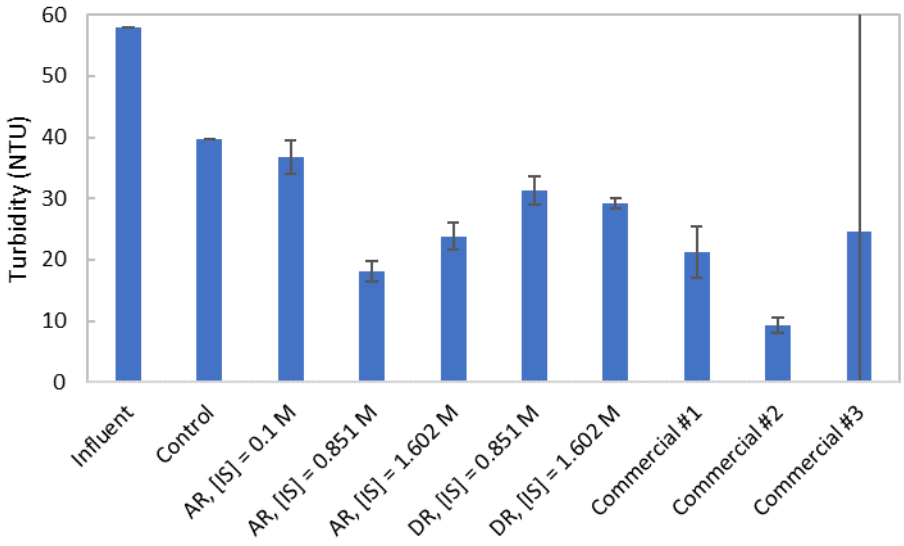

Figure 48: Settled water turbidity measurements for all flocculants tested; error bars represent standard deviation (n = 2). AR = acrylamide-rich, DR = DADMAC-rich, and [IS] = ionic strength concentration

Among the DADMAC – AAm copolymers, improvement in removing suspended solids (that is, reducing settled water turbidity) by increasing ionic strength during polymer synthesis is likely due to a higher fraction of A_{222} triads along the polymer backbone, giving these polymers a gradient or blocky microstructure. Both polymers synthesized in Run 2 and Run 3 have higher A_{222} triads than polymers synthesized in Run 1, as shown in Figure 49.

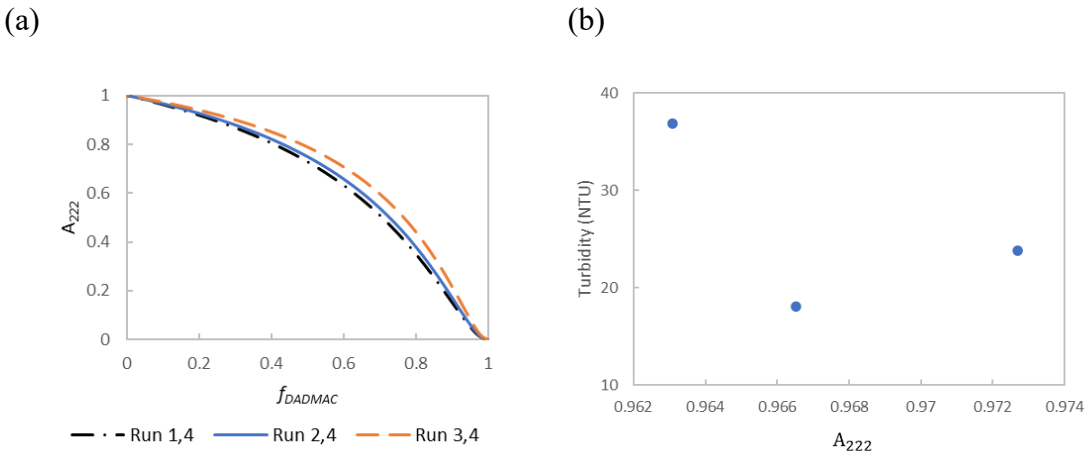

Figure 49: (a) A_{222} triads versus DADMAC monomer fraction for all AAm-rich measurements; (b) A_{222} triads at $f_{DADMAC,0} = 0.1$ for each formulation versus turbidity measurements

An explanation of why samples from Run 2 performed better than samples from Run 3 may be attributed to the difficulties observed when dissolving Run 3 samples. The concentration of polymers from Run 3 was one third of the concentration of other polymer samples, and dissolution was still difficult. During flocculation trials, it was visually observed that trials using Run 3 polymers were producing inconsistent floc sizes. This may be due to undissolved polymeric material in solution creating large flocs. Figure 50 demonstrates an example where there are some large flocs compared to most of the others within the same jar. It is possible that not having the polymer fully dissolved would reduce its flocculation effectiveness.

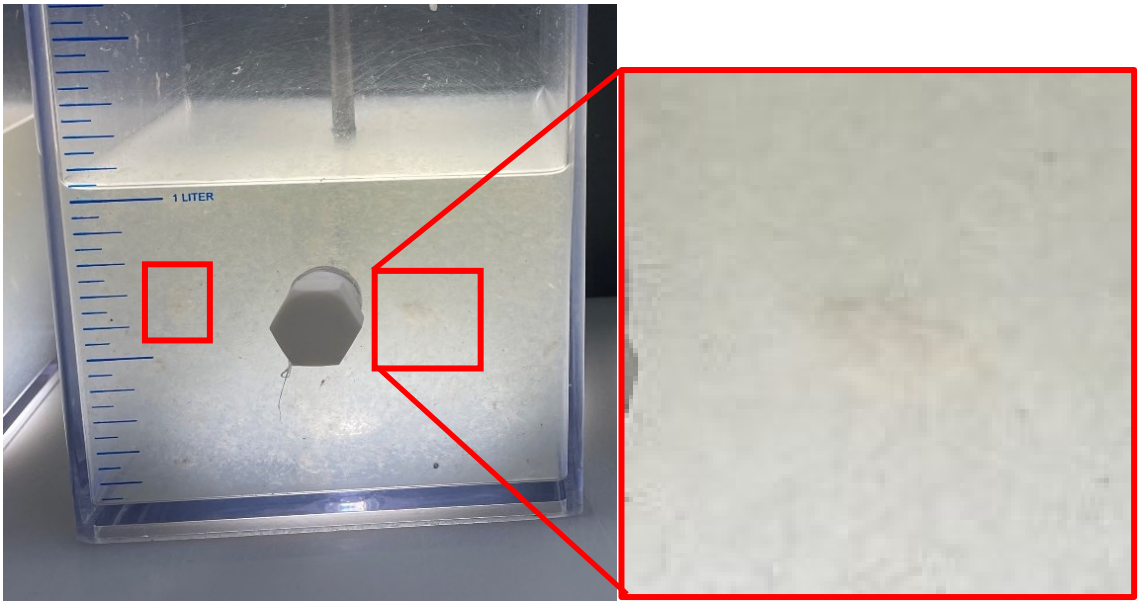

Figure 50: Flocculation trial using Run 3 samples, during slow mixing stage; two larger flocs are identified with red squares, and a zoomed-in image is on the right

In contrast, an example of consistent floc sizes is provided in Figure 51, where polymeric material from Run 2 produces minimal visual variation in floc sizes, as expected.

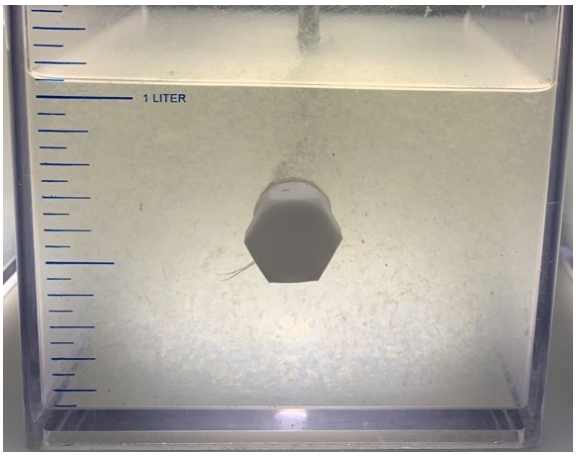

Figure 51: Flocculation trial using Run 2 samples, during slow mixing stage; minimal visual variation in floc sizes

For settled water UVT254 measurements, the best performing custom polymers were the ones synthesized without any ionic strength adjustment (that is, samples from Run 1 and Run 4). Settled water UVT254 measurements are an indicator of the amount of organic

matter in solution [89]. The mean settled water UVT254 measurement for DADMAC-rich flocculants is 39.8% transmission with a standard deviation of 1.2% and the same measurement for AAm-rich flocculants is 40.9% transmission with a standard deviation of 0.8%, meaning DADMAC and AAm rich flocculants had statistically equal performance for removing organic matter.

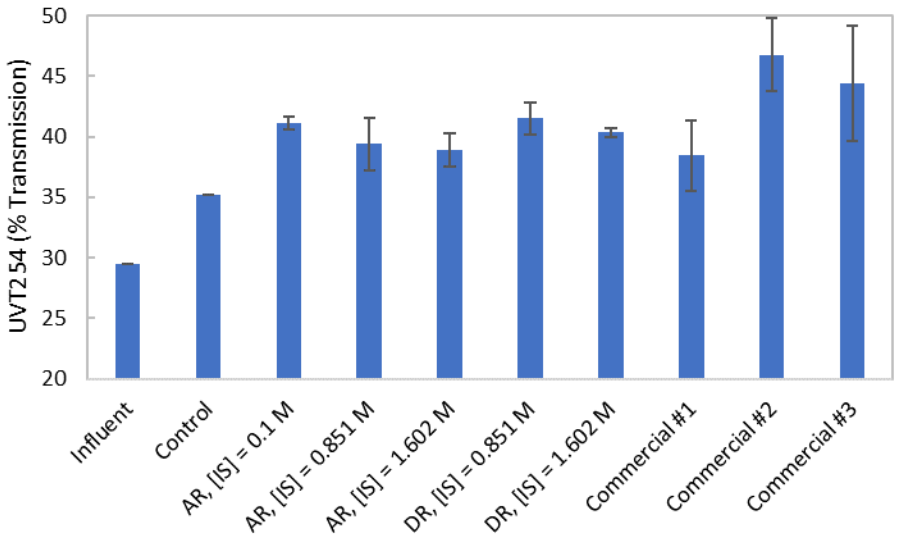

Figure 52: Settled water UVT254 measurements for all flocculants tested; error bars represent standard deviation (n = 2)

The relationship between A_{212} fractions and settled water UVT254 measurements is shown in Figure 53. Figure 53 indicates that having a higher fraction of A_{212} improves the removal of organic matter. This suggests that it is better to have an alternating or periodic copolymer for organic matter removal; this allows the DADMAC to be more evenly spaced throughout the polymer chain to remove organic contaminants.

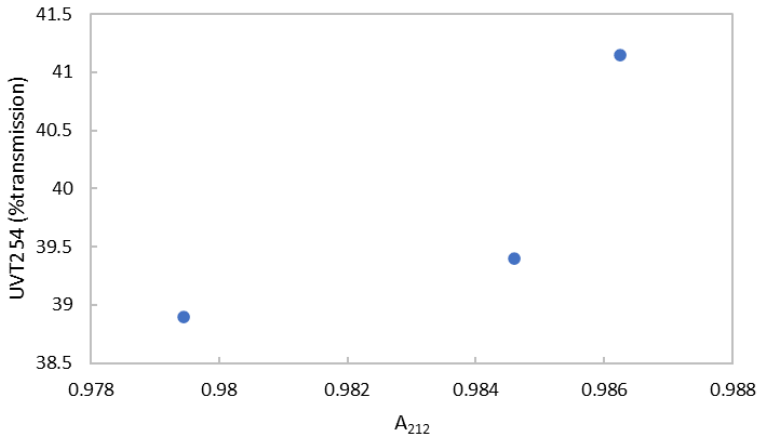

Figure 53: A_{212} triads at $f_{DADMAC,0} = 0.1$ for each synthesis run vs. settled water UVT254 measurements

Finally, by measuring the zeta potential, it was shown that Run 2 was (again) the best performing custom-made flocculant. This can also be attributed to higher A_{222} triads. This further demonstrates the importance of having 'blocky' sections in copolymer flocculants.

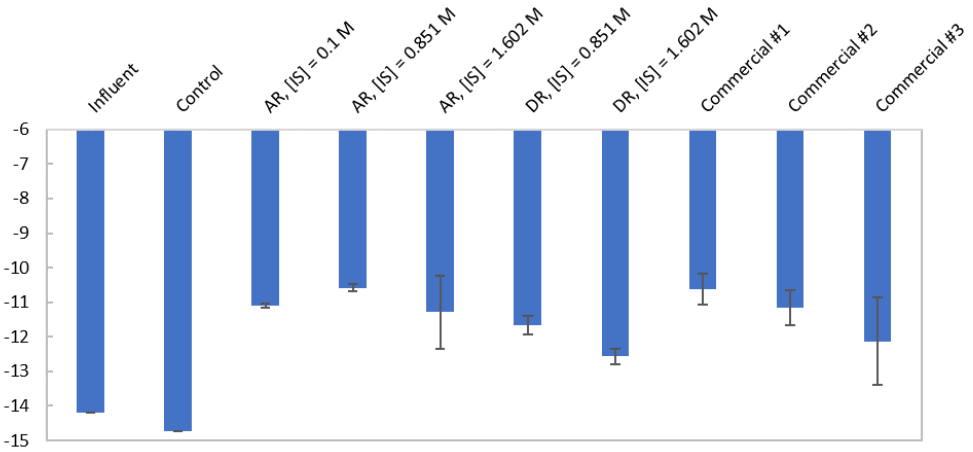

Figure 54: Settled water zeta potential measurements for all flocculants tested; error bars represent standard deviation (n = 2)

5.3. Conclusion

To conclude this study, it was found that the addition of NaCl to increase ionic strength during copolymer synthesis had significant impacts on the microstructure and flocculation performance for DADMAC – AAm copolymers. It was found that reactivity ratios were $r_{DADMAC} = 0.063$ and $r_{AAm} = 5.85$ with no ionic strength adjustment, but when both feeds had an ionic strength of 1.602 M, the reactivity ratios increased to $r_{DADMAC} = 0.24$ and $r_{AAm} = 8.32$. When studying the triad fraction predictions (based on reactivity ratio estimates), it was found that increasing ionic strength in the feed increased both A_{111} and A_{222} triad fractions, creating a more 'blocky' copolymer.

From GPC experiments, it was found that DADMAC-rich copolymers had a $\overline{M}_w$ of approximately 5×10^5 g/mol and AAm-rich copolymers had MW of approximately 5×10^6 g/mol, as expected based on rate constants, monomer concentration, and initiator concentration. It was found that altering ionic strength during synthesis had negligible effects on the MW.

Finally, all samples prepared at different comonomer compositions and ionic strengths were tested for flocculation performance. From flocculation results, it was found that polymers from Run 2 were the most effective synthesized flocculants. Run 2 is an AAm-rich flocculant synthesized with an ionic strength of 0.851 M. The good flocculation performance is attributed to a high fraction of A_{222} triads.

6. Penultimate vs. Terminal Model: Predicting Copolymerization Behaviour of Large Ionic Monomers

In Chapter 6, different copolymerization models, the penultimate and terminal model, are studied to understand the relative prediction accuracies when copolymerizing two monomers that have differences in size and charge. AMPS and DADMAC were both copolymerized with AAm. AMPS is a large anionic monomer, DADMAC is a large cationic monomer, and AAm is a small non-ionic monomer. Design of experiments was used to obtain optimal feed compositions for both models. Using in situ ^{1}H NMR, reactivity ratios were estimated using the two models. Finally, the cumulative copolymer composition predictions for both models were compared to experimental results, and triad fraction estimates were compared for the two models.

6.1. Reactivity Ratio Estimation

To estimate reactivity ratios using the penultimate model, a non-linear least squares program was developed using MATLAB. The parameters were evaluated using the shuffled complex evolution (SCE) method. In the current study, the optimum point is the lowest sum of residuals squared between the experimental measurements and the predicted cumulative copolymer composition (based on reactivity ratio estimates within the cumulative model); see Section 2.3.1.2, Section 2.3.4, and Equations 23 and 24 for additional information.

To facilitate estimation, initial estimates of the reactivity ratios are obtained from the literature and provided to the program. For each iteration, the next estimates of reactivity ratios are used to calculate the instantaneous copolymer composition using the extended

Mayo-Lewis equation (recall Equation 16). The differential copolymer composition equation (Equation 24) is then used to calculate the next monomer composition (f_n) at the experimental molar conversion (X_n). Since we are using the cumulative copolymer composition to estimate reactivity ratios, each polymerization is done individually due to slight differences in feed compositions. For example, if the data input contains data from 8 copolymerizations, one set of reactivity ratios is used for all 8 copolymerizations, but the cumulative copolymerization composition is estimated for each run individually (again, all with the same set of reactivity ratios). After solving for f_1, $\bar{F}_1$ is then calculated using the Skeist equation, which is shown in Equation 23.

The sum of residuals squared is then taken between the measured cumulative copolymer compositions and the associated estimated values. The SCE will continue iterations until optimal reactivity ratios are found (that is, until the lowest possible error is identified).

Four runs at two feed compositions were employed for the terminal model estimation and two runs at four feed compositions were employed for penultimate model estimation, for all cases. Two of the replicates from $f_{AMPS,1,0} = 0.10$, $f_{AMPS,2} = 0.84$, and $f_{DADMAC,3,0} = 0.851$ (as described in Chapters 4 and 5) were also used in the penultimate model as the required feeds were the same or very close to data collected previously. The replicates from previous terminal copolymerization studies that were used in the penultimate model estimation were chosen at random.

6.2. Design of Experiments

The method used to estimate optimal feed compositions for reactivity ratio estimation is described in Section 2.3.5. The DOE program used for this study was first validated by

comparing the results to those reported by Burke et al. [72]. As shown in Table 13, using the D-optimality program for DOE (created in MATLAB), results were almost identical to those reported by Burke et al. for both styrene/acrylonitrile and styrene/butyl acrylate copolymer systems. The reactivity ratios used to validate the DOE program were styrene/acrylonitrile (where styrene is monomer 1 and acrylonitrile is monomer 2) with r_{11} = 0.229, r_{21} = 0.634, r_{22} = 0.039, and r_{12} = 0.091 [72]. The other reactivity ratios used to validate the DOE program were for styrene/butyl acrylate (where styrene is monomer 1 and butyl acrylate is monomer 2) with r_{11} = 0.551, r_{21} = 0.937, r_{22} = 0.225, and r_{12} = 0.130 [72,90].

Table 13: Comparison of optimal feed compositions for styrene/acrylonitrile and styrene/butyl acrylate copolymerizations for RRE using the penultimate model; Burke et al. [72] vs. this study.

	Styrene/Acrylonitrile		Styrene/Butyl Acrylate	
	[72]	This study	[72]	This Study
$f_{2,1}$	0.9890	0.9890	0.9624	0.9624
$f_{2,2}$	0.8974	0.8974	0.8412	0.8411
$f_{2,3}$	0.0629	0.0629	0.4929	0.4929
$f_{2,4}$	0.4390	0.4390	0.1198	0.1198

Once the DOE program was validated, the next step was to use it for our AMPS – AAm copolymerization system. The MATLAB program described in Section 2.3.5 was used to estimate the optimal feed compositions (according to D-optimality) for reactivity ratio estimation using the penultimate model. The results were $f_{AMPS,1,0}$ = 0.10, $f_{AMPS,2}$ = 0.34, $f_{AMPS,3,0}$ = 0.62, $f_{AMPS,4,0}$ = 0.90. To the best of our knowledge, reactivity ratios have not been estimated using the penultimate model in the literature for AMPS – AAm copolymerization. Therefore, initial estimates of the penultimate model reactivity ratios were estimated using the data that were used to estimate reactivity ratios via the terminal

model (that is, using only 2 feed compositions). The ionic strength for both AMPS- and AAm-rich feeds was 1.58 M (Runs (3,5) from Chapter 4 for the terminal model). The preliminary estimates for penultimate AMPS – AAm reactivity ratios were $r_{11} = 0.195$, $r_{21} = 3.46$, $r_{22} = 1.07$, and $r_{12} = 0.390$, where species 1 is AMPS. These preliminary reactivity ratio estimates were only used to calculate optimal feed compositions for further reactivity ratio estimation. This might be seen as a disadvantage of using the penultimate model: preexisting data are far less available compared to the terminal model. In contrast, for the terminal model, reactivity ratios from McCormick et al. [42] were used as initial estimates for DOE, where $r_{AMPS} = 0.50$ and $r_{AAm} = 1.02$.

For DADMAC – AAm copolymerization, initial reactivity ratio estimates were acquired from Wandrey et al. [49], who estimated penultimate reactivity ratios for DADMAC – AAm copolymerization of $r_{11} = 0.032$, $r_{21} = 0.021$, $r_{22} = 7.19$, and $r_{12} = 2.97$, where species 1 is DADMAC. Once again, the MATLAB program used D-optimality to estimate the optimal feed compositions for reactivity ratio estimation using the penultimate model. The results were $f_{DADMAC,1,0} = 0.41$, $f_{DADMAC,2,0} = 0.72$, $f_{DADMAC,3,0} = 0.86$, and $f_{DADMAC,4,0} = 0.90$. As explained in Section 5.1, it was found that the optimal feed fractions for the terminal model were $f_{DADMAC,0} = 0.851$ and $f_{DADMAC,0} = 0.1$ (recall Figure 30). The ionic strength for all feeds was 1.602 M to compare to Runs (3,5) from Chapter 5 (to compare to the terminal model). This is important for comparing between the terminal and penultimate models.

An important aside is that AMPS-rich copolymerization at IS = 1.58 M has a higher rate of propagation than AAm-rich copolymerization under the same ionic strength conditions, as seen in Figure 55(a). This means that when polymerization occurs in the NMR, and data is collected every ~6 minutes, fewer data points will be collected at lower conversions of

$f_{AMPS,0}$ = 0.84 if there are only 2 experimental replicates (compared to 4 replicates at that feed composition with the terminal model). For example, for the AMPS-rich runs shown in Figure 55a) there is only one data point between 0.2 and 0.4 conversion; increasing the number of replicates would increase the chances of having more data at low conversion. Figure 55(b) demonstrates the conversion vs. time data from 4 replicates for the same AMPS-rich feed, where there are significantly more data points between 0.2 and 0.4 conversion. The trade-off is that you will likely have data points between 0.2 and 0.4 conversion at 0.72 feed fraction for the penultimate model, whereas for the terminal model only 2 feed fractions are used. Note that the 2 replicates for the feeds of $f_{AMPS,1,0}$ = 0.10 and $f_{AMPS,2}$ = 0.84 (required for the penultimate model) were taken from terminal model experiments and chosen at random. Although the penultimate DOE suggested using $f_{AMPS,0}$ = 0.9, data collected previously at $f_{AMPS,0}$ = 0.84 were used to save time and resources.

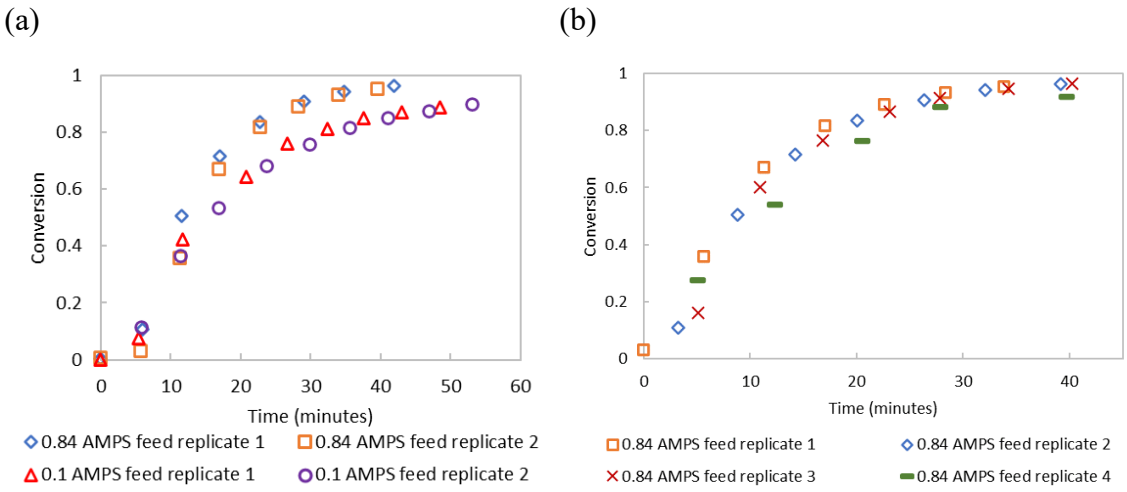

Figure 55: Depiction of the rate of polymerization (and importance of replication) for $f_{AMPS,0}$ = 0.84 and $f_{AMPS,0}$ = 0.1

6.3. Results and Discussion

6.3.1. AMPS – AAm Copolymerization

As described in detail in Section 4.2, reactivity ratio estimates for AMPS – AAm copolymerization using the terminal model (with both formulations adjusted to IS =1.58 M) are r_{AMPS} = 0.465 and r_{AAm} = 0.815, and the joint confidence region has been shown previously in Figure 25 and Figure 27. For the penultimate model, the reactivity ratio estimates using the 4 optimal feed compositions are shown in Table 14. The penultimate reactivity ratios were estimated using the 4 feeds suggested in Section 6.2. It is interesting to note that both of the AMPS reactivity ratios obtained using the penultimate model are higher than the r_{AMPS} estimate from the terminal model (r_{11} and $r_{21} > r_{AMPS}$). Similarly, the AAm reactivity ratios obtained using the penultimate model are also higher than the r_{AAm} estimate from the terminal model (r_{22} and $r_{12} > r_{AAm}$). For estimating terminal and penultimate model reactivity ratios, all data sets included a total of eight experiments.

Table 14: Penultimate reactivity ratios for AMPS – AAm copolymerization

r_{11}	r_{21}	r_{22}	r_{12}
0.695	0.775	0.868	1.259

Using the reactivity ratios, the cumulative copolymer composition can be estimated as a function of conversion using the Skeist equation (recall Equation 23). The estimated cumulative copolymer composition using both the terminal and penultimate models and the experimental data are shown in Figure 56. In Figure 56, 5 different feed compositions are shown: $f_{AMPS,0}$ = 0.1, 0.36, 0.42, 0.66, and 0.85. The feed composition of $f_{AMPS,0}$ = 0.42 was an unintended result, as the aim was to make a formulation at $f_{AMPS,0}$ = 0.36. However,

it is included herein to demonstrate the model prediction performance. Results show that both the terminal and penultimate model yielded similar predictions, and are in good agreement with the experimental data.

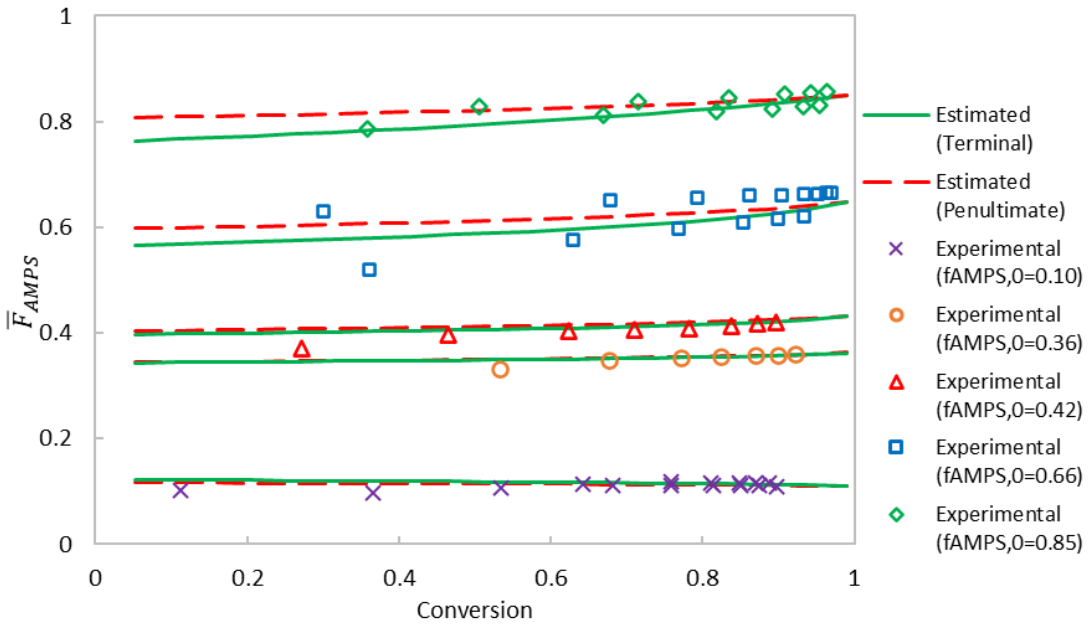

Figure 56: Cumulative copolymer composition predictions for AMPS – AAm using the terminal and penultimate copolymerization models

At low feed fractions of AMPS, both the terminal and penultimate models yield almost identical cumulative copolymer composition predictions. However, at higher AMPS feed fractions, the two models demonstrate some differences in the cumulative copolymer composition predictions. At higher AMPS feed fractions, the penultimate model predicts a higher cumulative copolymer composition of AMPS than the terminal model. Although there are some differences between the models, they are likely within experimental error. Overall, the experimental data are in agreement with both models, showing that penultimate model yields similar results to the terminal model for predicting cumulative copolymer composition in AMPS – AAm copolymerization.

The instantaneous copolymer composition versus monomer composition is shown in Figure 57 for the terminal model, the penultimate model, and for a random copolymer ($r_1 = r_2 = 1.0$). The instantaneous copolymer composition is calculated from Equations 14 and 16, using the terminal and penultimate models, respectively. Figure 57 shows that below a monomer composition of $f_{AMPS} = 0.5$, the terminal and penultimate model predictions are almost identical (this agrees with the predictions shown in Figure 56). However, above $f_{AMPS} = 0.5$, the penultimate model predicts higher instantaneous copolymer composition (F_{AMPS}) than the terminal model.

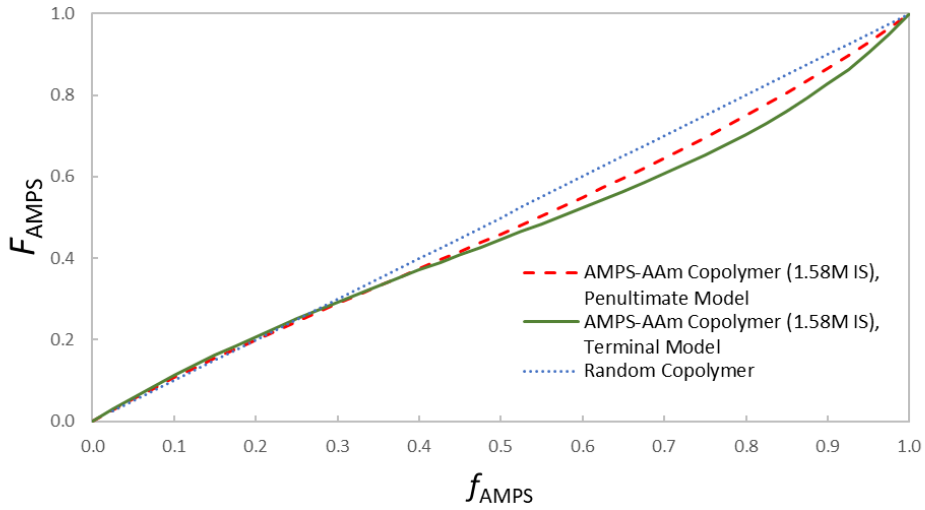

Figure 57: Instantaneous copolymer composition for AMPS – AAm copolymerization estimated by terminal and penultimate models

Finally, triad fractions were calculated using the equations outlined in Section 2.3.6 for the terminal and penultimate models. There are some differences between the model predictions, as the penultimate model predicts more A_{111} triads and fewer $A_{112}+A_{211}$ triads, meaning a more 'blocky' copolymer is predicted. The importance of picking the correct model is shown in Figure 58, where the differences in the models for some triad fractions

is almost 20%. The triad fraction predictions were validated using C^{13} NMR. Based on the experimental data, the penultimate model provides the more accurate estimate. The measured A_{111} fraction is between the two models, but the A_{112}+A_{211} and A_{212} fractions are closer to the penultimate model. This indicates that the penultimate model is more accurate at predicting the copolymer microstructure than the terminal model. This result is reasonable, as AMPS is a large and charged monomer, and therefore penultimate effects are expected.

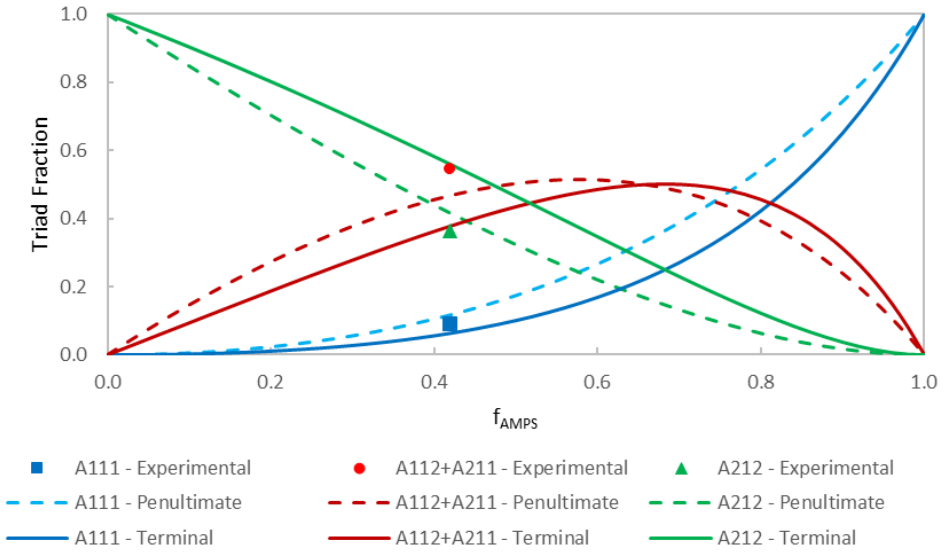

Figure 58: AMPS-centered triad fractions estimated using terminal and penultimate models

In Figure 59, a representative C^{13} NMR spectrum is shown for a feed of $f_{AMPS,0} = 0.42$. The A_{111} peak is at 179 ppm, the A_{112}+A_{211} peak is at 176 ppm, and the A_{212} peak is at 172 ppm. The A_{222} peak is at 22.5 ppm, the A_{221}+A_{122} peak is at 31.5 ppm, and the A_{121} peak is at 38.5 ppm. The A_{222} peak was determined from AAm homopolymerization data at 22.5 ppm, while the A_{221}+A_{122} and A_{121} peaks were identified based on how close they were to A_{111}. For example, A_{121} has two AMPS monomers surrounding the acrylamide centre, and

therefore is assigned the peak closest to A_{111} within the cluster from 22 to 39 ppm. Figure 60 shows the peaks measured.

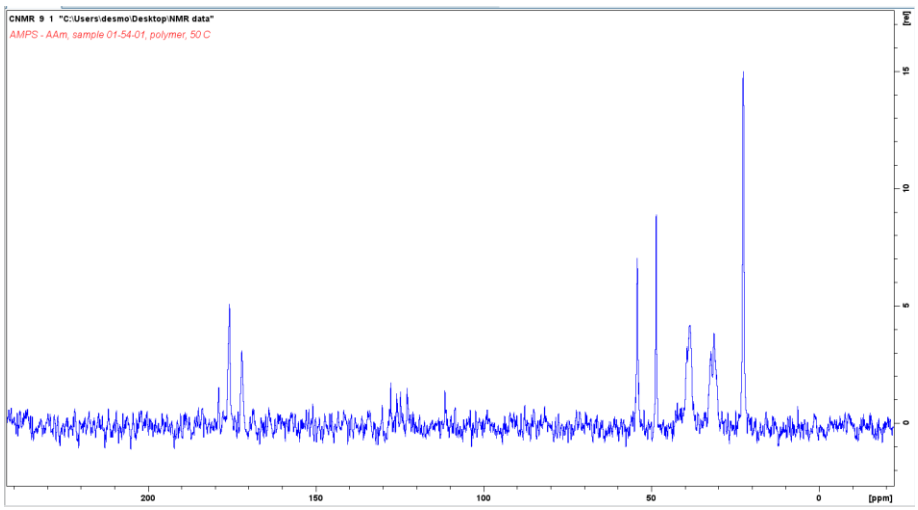

Figure 59: C^{13} NMR scan for AMPS – AAm copolymer synthesized at $f_{AMPS,0} = 0.42$; used to calculate triad fraction data

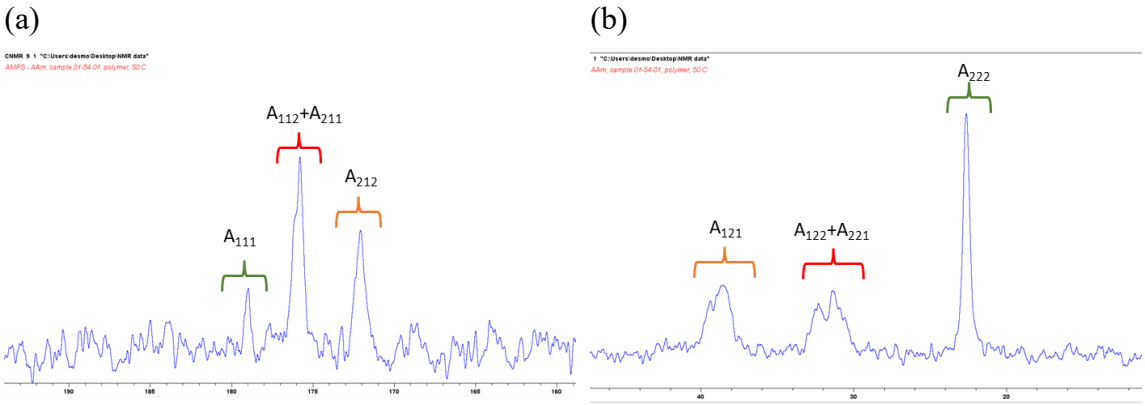

Figure 60: Zoomed-in C^{13} NMR scan for measuring triad fractions for AMPS – AAm copolymerization

The AAm-centered triad fractions were also estimated using both copolymerization models, as shown in Figure 61. The models predicted similar results, which is reasonable since AAm is a small and non-ionic monomer. Both models overpredicted $A_{122}+A_{221}$, although the rest of the triad predictions match the experimental data well. The terminal

model was slightly closer for predicting $A_{122}+A_{221}$ and A_{121}, although the difference may not be statistically significant.

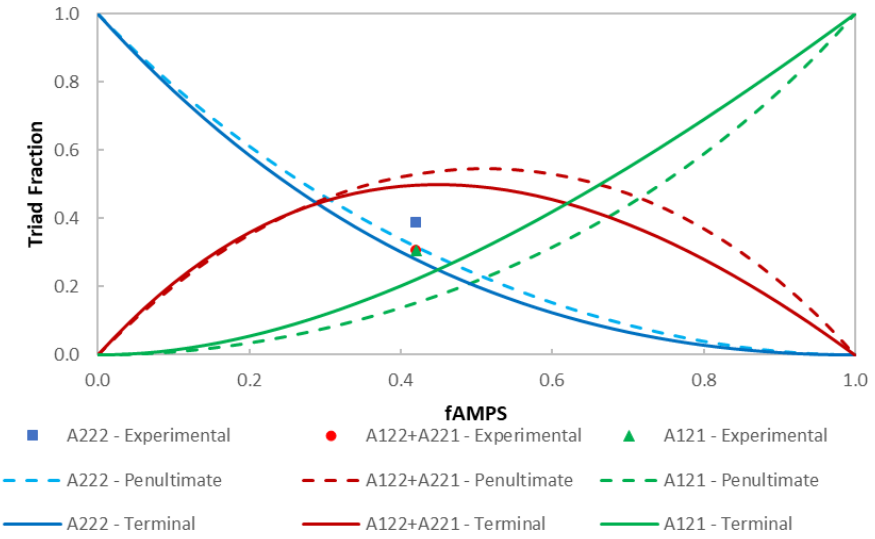

Figure 61: AAm-centered triad fractions estimated using terminal and penultimate models.

6.3.2. DADMAC – AAm Copolymerization

Based on data from Chapter 5, this study again examines DADMAC – AAm copolymerization with 1.602 M ionic strength in both the DADMAC-rich and AAm-rich feeds. Using the terminal model, it was previously determined that $r_{DADMAC} = 0.24$ and $r_{AAm} = 8.32$; recall the reactivity ratios and JCRs shown in Figure 37 and Figure 41. Using the penultimate model and additional experimental data, it was determined that $r_{11} = 0.131$, $r_{21} = 1.16$, $r_{22} = 6.67$, and $r_{12} = 29.6$, where DADMAC is monomer 1. The fact that $r_{21} > 1$ is surprising, as it suggests that k_{211} is higher then k_{212}, meaning it is more likely for DADMAC to propagate when the chain sequence is AAm and then DADMAC; this is

especially interesting when we compare this result to the very low r_{DADMAC} estimated by the terminal model. This suggests significant penultimate effects.

Table 15: Penultimate reactivity ratios for DADMAC – AAm copolymerization

r_{11}	r_{21}	r_{22}	r_{12}
0.131	1.16	6.67	29.6

Five estimated cumulative copolymer compositions, along with experimental data, are shown in Figure 62. It is important to note that the feed composition of $f_{DADMAC,0}$ = 0.1 is shown, even though it was not used to estimate the reactivity ratios using the penultimate model. The $f_{DADMAC,0}$ = 0.1 feed composition was only used for estimation using the terminal model because the goal of this study was to compare models, therefore only the feeds that were calculated using the DOE in Section 6.2 were used for penultimate reactivity ratio estimation. In comparing the model predictions in Figure 62, it is noticeable that the terminal model predicts lower cumulative copolymer compositions ($\overline{F}_{DADMAC}$) than the penultimate model at lower feed compositions. At $f_{DADMAC,0}$ = 0.42, it seems like the experimental data is closer to the terminal model prediction, but at $f_{DADMAC,0}$ = 0.1, the penultimate model prediction may be slightly closer to the experimental data at higher DADMAC feed fraction. At higher feed fractions such as $f_{DADMAC,0}$ = 0.85 and $f_{DADMAC,0}$ = 0.9, the penultimate model predictions are closer to the experimental cumulative copolymer composition. It seems that at high DADMAC feed fractions, the terminal model over-predicts the cumulative copolymer composition. It is not surprising that the penultimate model was less accurate at predicting the cumulative copolymer composition at low

DADMAC feed compositions, since the lowest feed composition within the data set for estimation was $f_{DADMAC,0} = 0.42$.

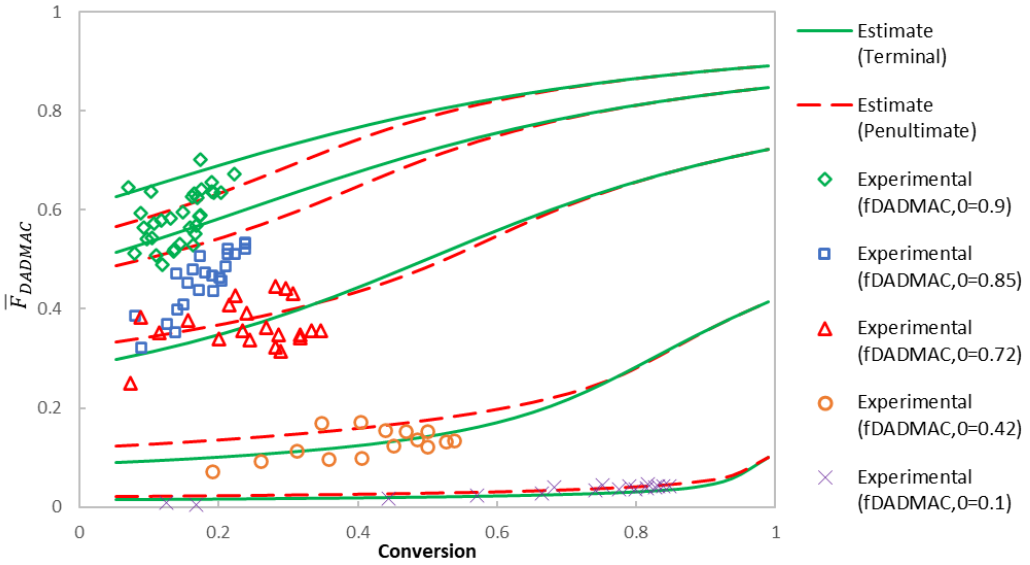

Figure 62: Cumulative copolymer compositions predictions for DADMAC – AAm using the terminal and penultimate copolymerization models

The instantaneous copolymer composition versus monomer composition is shown in Figure 63. The penultimate model predicts higher copolymer composition (F_{DADMAC}) below $f_{DADMAC} = 0.81$, meaning DADMAC is more likely to propagate according to the penultimate model compared to terminal model. Above $f_{DADMAC} = 0.81$, the terminal model predicts that DADMAC is more likely to propagate compared to the prediction by the penultimate model. This agrees with what was observed in Figure 62.

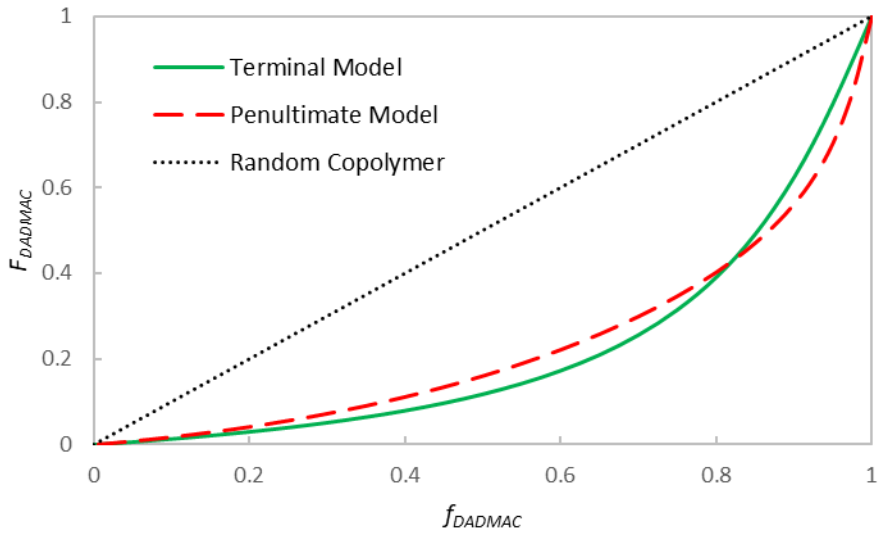

Figure 63: Instantaneous copolymer composition for DADMAC – AAm copolymerization estimated by terminal and penultimate models

When estimating triad fractions with DADMAC centers, there are significant differences between the models (see Figure 64). The largest difference is the A_{112}+A_{211} fraction, where the penultimate model predicts a much higher fraction of A_{112}+A_{211}. This is not surprising, as r_{11} is estimated to be 0.131. This means that the next likely monomer to propagate after a 1-1 sequence is AAm, making A_{112} triads, this is because $k_{111} < k_{112}$ (see Equation 17). Also, since $r_{21} = 1.16$, DADMAC is slightly more likely to propagate than AAm, creating A_{211} triads. In contrast, with the terminal model there is only one reactivity ratio for DADMAC. This means that whether the chain end contains 1-1 or 2-1, the model prediction suggests that it is highly unlikely that DADMAC will homopropagate, therefore predicting a A_{112} or A_{212} triad (only one triad fraction will be included in the $A_{112+211}$ triad calculation). According to the penultimate model, a 1-1 and 2-1 sequence would likely form a A_{112} and a A_{211} triad, respectively (that is, both will be included in the $A_{112+211}$ triad calculation). This behaviour could also explain why the A_{212} triad fraction prediction using

the penultimate model is less than the same triad fraction using the terminal model. For A_{111}, the terminal model prediction has a slightly higher fraction than the penultimate model prediction. This may be because when there is a 1-1 sequence on the chain end, $r_{DADMAC} = 0.245$ from the terminal model, whereas $r_{11}=0.131$ from the penultimate model. Therefore, the reactivity ratio from the terminal model (which is proportional to the rate of DADMAC homopropagation) is higher than the equivalent reactivity ratio from the penultimate model, and therefore predicts higher A_{111} triads.

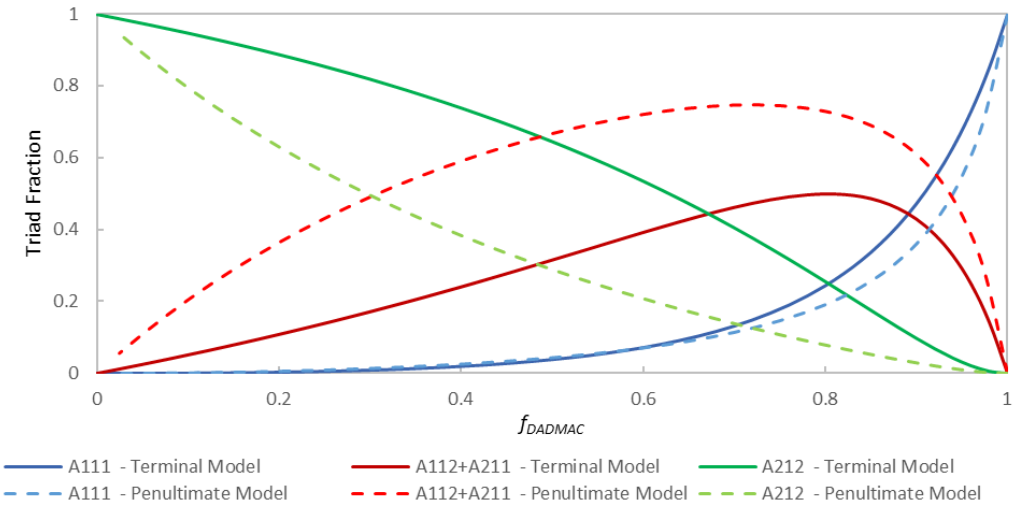

Figure 64: DADMAC-centered triad fractions estimated using terminal and penultimate models

Attempts were made to measure the DADMAC-centered triad fractions of DADMAC–AAm copolymers using C^{13} NMR. A representative measurement is shown in Figure 65. The challenge with the DADMAC – AAm copolymer is that there are 8 peaks, and it is unknown which peak is associated with which triad. Previous work by Brand et al. reported similar issues [51], as polyDADMAC has 6 different diad structures. Following the same approach as the work by Brand et al., only the AAm-centered triads were measured in this

study. Also, only the triads for the copolymer with $f_{DADMAC,0}$=0.1 were determined. With higher fractions of DADMAC, it is difficult to reach high conversions to estimate the triad fractions.

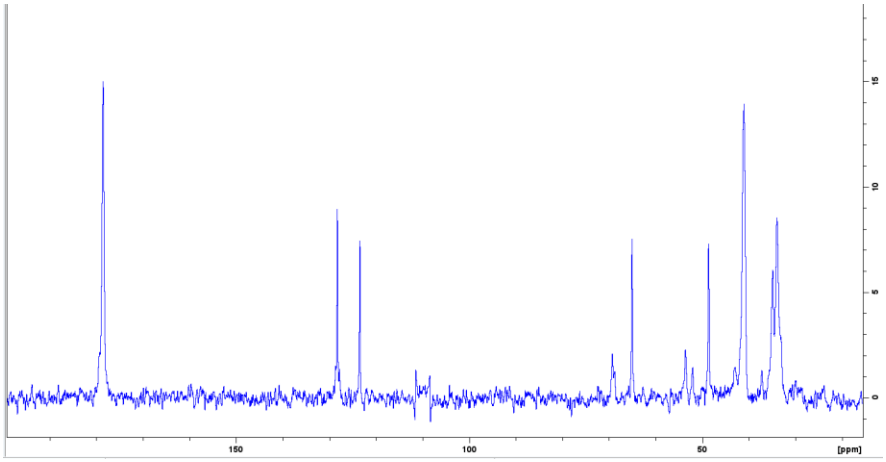

Figure 65: C^{13} NMR scan for copolymer synthesized with f_{DADMAC} = 0.1

A_{222} triads were measured at 34.2 ppm, $A_{122+221}$ triads were measured at 37.6 ppm, and A_{121} triads are measured at 39.3 ppm. These were identified based on information from Brand et al [51]. An example can be seen in Figure 66.

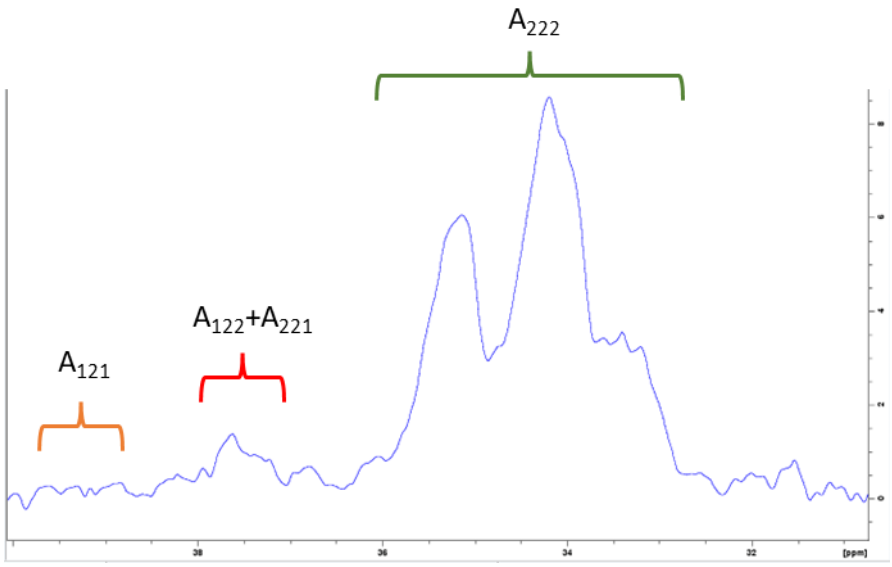

Figure 66: Zoomed-in C^{13} NMR scan for measuring triad fractions for DADMAC – AAm copolymerization

When comparing the AAm-centered triad fractions, the differences between model predictions are not as extreme as the DADMAC-centered triad fractions. For the A_{121} triads, the penultimate model prediction is lower than the terminal model prediction. This is because r_{12}= 29.6, meaning that the penultimate model predicts A_{121} triads are unlikely, except at very high feed compositions of DADMAC. Experimental data are shown to compare to the models in Figure 67; results show that experimental data are slightly closer to the penultimate model. Unfortunately, due to issues with reaching high conversion for DADMAC-rich polymers, only low fractions of DADMAC were used for measuring triad fractions. This resulted in both models having good agreement with each other, and it was not possible to confidently say which model fit the experimental data better.

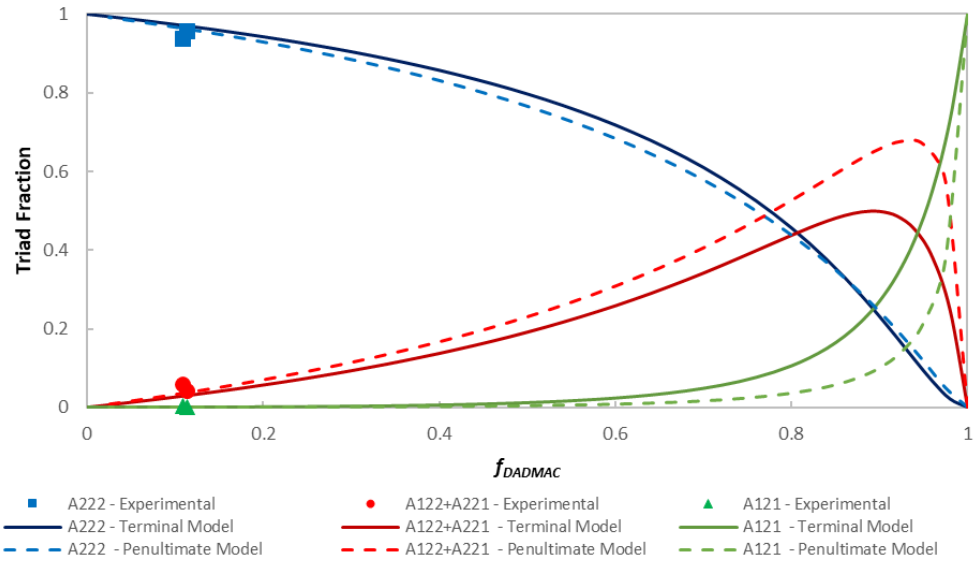

Figure 67: AAm-centered triad fractions estimated using terminal and penultimate models.

6.4. Conclusion

This chapter explored the importance of choosing the correct copolymerization model. When comparing models, each one has its pros and cons. For the penultimate model, there are far fewer reported reactivity ratios compared to the terminal model, therefore using DOE to estimate optimal feed compositions for reactivity ratio estimation can be difficult. Without any reported penultimate reactivity ratios, guessing or trial and error approaches are required to acquire initial reactivity ratio estimates to estimate optimal feed compositions. An advantage of the penultimate model is that more feed compositions are tested: the penultimate model requires four feed compositions instead of the two feed compositions required by the terminal model.

The goal of this study was to understand penultimate effects from large ionic monomers. The reactivity ratio estimates for the penultimate model indicate penultimate effects for

AMPS-AAm copolymerization, as the reactivity ratios for AAm are r_{12} = 0.868 and r_{22} = 1.259, indicating that the more likely monomer to propagate is dependant on the penultimate monomer (more likely to homopropagate when reactivity ratio is greater than 1). The study found that penultimate and terminal models predicted very similar cumulative copolymer compositions for AMPS – AAm copolymerization. However, for the triad fraction predictions, there were differences observed. The measurements show that experimental data for triad fraction measurements are closer to the penultimate model. Although for AMPS-AAm copolymerization the penultimate model may be more accurate, the terminal model is also accurate and requires less experiments.

The reactivity ratio estimates for DADMAC – AAm copolymerization indicate strong penultimate effects. The DADMAC reactivity ratios are r_{11} = 0.131 and r_{21} = 1.16, indicating the next monomer to propagate is highly dependant on the penultimate monomer. The difference in the model predictions for cumulative copolymer composition and triad fractions was more significant for DADMAC-AAm copolymerization compared to AMPS-AAm, especially for triad fractions. Based on the results of penultimate effects, the penultimate model may be the accurate model, although the terminal model is also accurate and should be used if there are time constraints.

7. Effect of pH and Monomer Concentration on DADMAC – AAm Copolymerization Kinetics, Microstructure, and Flocculation Performance

In Chapter 7, the effect of pH and total monomer concentration on the copolymerization of DADMAC – AAm was studied. Specifically, the effect of pH and total monomer concentration on DADMAC – AAm copolymerization reactivity ratios and the resulting copolymer microstructure were investigated. GPC was used to measure the molecular weight distributions of the synthesized copolymers. Additionally, flocculation performance was studied for the resulting copolymers. Flocculation trials were performed at the Dartmouth Wastewater Treatment Facility with support from Halifax Water and the Centre for Water Resources Studies (CWRS).

7.1. Design of Experiments

A 2^2 factorial design with replicated center points was used to study the effects of pH and monomer concentration on the reactivity ratios and subsequent flocculation performance of DADMAC – AAm copolymers. pH 5 and pH 9 were selected as the low and high factor levels for this design, because the pKa of DADMAC is 7.0 [77]. At pH 9, DADMAC is 99% deprotonated, meaning that the cationic charge is neutralized. At pH 5, DADMAC is 99% protonated, meaning that there is a strong cationic charge. At pH 7, DADMAC is 50% protonated, meaning that 50% of the functional groups are charged. An example of calculating the ionic strength is shown in Appendix A.1.

The monomer concentration ([M]) levels chosen were 1 M and 3 M. Initially, the monomer concentration levels chosen were 1 M and 4 M. However, after preliminary experiments,

it was determined that a [M] of 4 M required a high initiator concentration, [I], and the ACVA initiator could not be dissolved at pH 5. As seen previously in Equation 18 (Section 2.3.2), initiator concentration must increase exponentially with increasing [M] to target the same chain length, and ACVA is less soluble in acidic conditions. Once the solution was prepared with [M] = 4 M, [I] = 59 mM and pH 5, the pre-polymerization solution was put in an ice bath during degassing (recall Section 3.3). The mixture became cloudy, and it was then evident that the ACVA had come out of solution. 4 M was initially chosen because a study by Wandrey and Jaeger showed that increasing total [M] increased r_{DADMAC} [49], however this concentration was deemed infeasible using the current polymerization conditions. Therefore, moving forward, the [M] levels for the factorial design were chosen as 1 M and 3 M. Center point replicates were added to protect against curvature in the surface response. Figure 68 demonstrates the 2^2 factorial design with replicated center points. Since reactivity ratios were being calculated, 2 feed compositions were needed. Therefore, a pair of 2^2 factorial designs were employed, as shown in Figure 68. The blue represents DADMAC-rich feed and red represents AAm-rich feed. The purple lines represent the pairs of copolymerization data required for reactivity ratio estimation at the specified reaction conditions (pH and [M]).

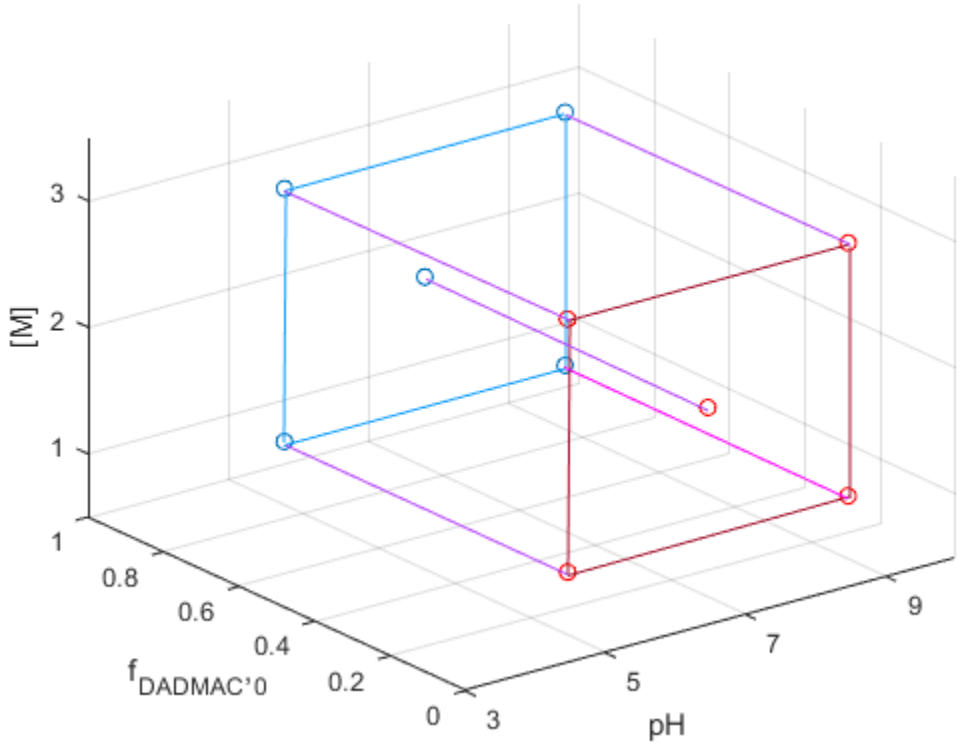

Figure 68: 2^2 factorial design outlining reaction conditions for DADMAC – AAm copolymerization kinetics study

The equation for the second-order response surface model for the 2^2 factorial with center points is shown in Equation 38 [91]. Factorial design was selected as it provides the ability to study the joint effects of multiple factors on a response. This study used pH and monomer concentration as the experimental factors.

$$y = \beta_0 + \sum_{j=1}^{k} \beta_j x_j + \sum \sum_{i<j} \beta_{ij} x_i x_j + \sum_{j=1}^{k} \beta_{jj} x_j^2 + \epsilon \quad \text{Equation 38}$$

β_{jj} represents the pure second order effects calculated using Equation 39.

$$\beta_{jj} = \frac{n_F n_C (\overline{y}_F - \overline{y}_C)}{n_F + n_C} \quad \text{Equation 39}$$

n_F is the number of runs at the factorial points, n_C is the number of runs at the center point, $\overline{y}_F$ is the average of the four factorial points, and $\overline{y}_C$ is the average of the center point [91].

The initiator (ACVA) concentrations ([I]) for this study varied with [M] according to Equation 18: [I] = 1.32 mM for samples at [M] = 1 M, [I] = 5.26 mM for samples at [M] = 2 M, and [I] = 11.84 mM for samples at [M] = 3 M. At the center point, there were 4 replicates of AAm-rich and DADMAC-rich feeds (4 each, 8 total) to fully understand the variance; feed compositions were selected as described previously in Section 5.1 to be $f_{DADMAC,0}$ = 0.851 and $f_{DADMAC,0}$ = 0.1. The center point was reused from Runs (3,5) from Section 5.2.2. The 4 factorial points (non-center points from Figure 68) included 2 replicates at each point, again for both AAm-rich and DADMAC-rich feeds (2 each, 4 total).

7.2. Results and Discussion

7.2.1. Reactivity Ratio Estimation

Reactivity ratios were estimated using the EVM method with the terminal model (discussed in Section 2.3.3) for five different data sets; these are shown in Table 16 and Figure 69. The terminal model was chosen in this chapter for efficiency; although the penultimate model may be somewhat more accurate, terminal model is also still accurate. Figure 69 indicates that the reactivity ratios are significantly impacted by both pH and [M].

Table 16: Copolymerization Combinations and Resulting Reactivity Ratio Estimates for DADMAC – AAm at Varying pH and [M].

pH	[M] (M)	r_{DADMAC}	r_{AAm}	$r_{DADMAC} * r_{AAm}$
5	1	0.0954	4.47	0.427
9	1	0.110	13.6	1.50
5	3	0.194	6.68	1.30
9	3	0.0772	6.06	0.468
7	2	0.0625	5.85	0.366

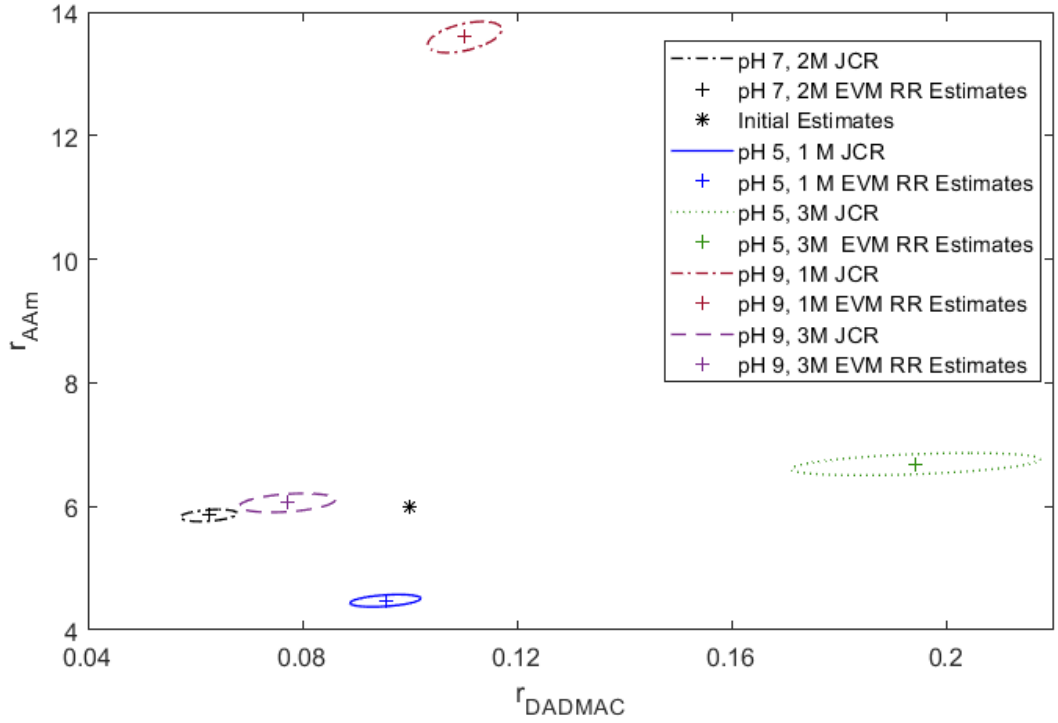

Figure 69: Reactivity ratio estimates for various pH and [M]; initial estimates from [17]

Samples at (pH 7, [M] = 2 M), (pH 5, [M] = 1 M), and (pH 9, [M] = 3 M) are all within a similar range for r_{DADMAC} and r_{AAm}. The center point (pH 7 and [M] = 2 M) has the lowest r_{DADMAC}, whereas r_{AAm} is near the middle. This is likely due to pH effects: since the pKa of DADMAC is 7, DADMAC is protonated and has a positive charge at pH 5, but is deprotonated and neutral at pH 9. This has the potential to create a 'perfect storm': at pH 9, the polymer chains would be randomly coiled in solution due to lack of charges and be

impacted by a 'crowding effect', but would have no electrostatic repulsion. In contrast, at pH 5, the polymer chains in solution would be rigid, eliminating the 'crowding effect' but experiencing electrostatic repulsion between the charged monomers and the growing polymer chain. At the mid-point, pH 7, the copolymer may be experiencing both 'crowding' and electrostatic effects.

The largest difference of reactivity ratios is observed between samples prepared at (pH 9, [M] = 1 M) and samples prepared at (pH 5, [M] = 3 M). These can be seen at the opposite ends of the factorial design (for example, top left and bottom right of Figure 68).

When comparing samples at (pH 5, [M] = 1 M) and (pH 9, [M] = 1 M), changing the pH impacts r_{AAm} significantly as these two formulations represent the lowest and highest r_{AAm}. Based on homopolymerizations of AAm, discussed in Section 2.4.1, it is not expected that homopropagation of AAm (k_{22}) will be impacted between pH 5 and 9. Therefore, the increase in r_{AAm} is likely due to a decrease in cross propagation (k_{21}). Results suggest that at pH 9 and [M] = 1 M, there is a random coil conformation in solution that is causing steric hindrance (or 'crowding') of the large DADMAC monomer, causing k_{21} to decrease and therefore increasing r_{AAm}. At pH 5, the conformation in solution would be a rigid copolymer due to the electrostatic repulsion. Without the steric effects impacting the DADMAC incorporation, we would expect to see an increased k_{21} and a decreased r_{AAm}. r_{DADMAC} at these formulations, (pH 5, [M] = 1 M) and (pH 9, [M] = 1 M), is not impacted significantly due to the pH change; this is likely because at pH 5, there are limited steric effects (due to chain rigidity) but there are significant electrostatic effects, while at pH 9 there are steric effects but limited electrostatic effects. As a result, the r_{DADMAC} estimates are similar for both systems.

Comparing reactivity ratio estimates at (pH 5, [M] = 3 M) and (pH 9, [M] = 3 M), the effects of changing the pH are more prominently shown in r_{DADMAC} at [M] = 3 M. Due to the high concentration of monomers, the steric effects (or 'crowding') would be much more significant than at 1 M. This is suggested by the sample at pH 9 (random coil conformation) having a significantly lower r_{DADMAC} compared to at pH 5 (rigid conformation).

Next, surface response curves were created to understand further how pH and [M] affect reactivity ratios (see Figure 70). At pH 5, the DADMAC is positively charged, creating a rigid copolymer in solution due to electrostatic repulsion, whereas at pH 9, the copolymer has a random coil conformation in solution due to the charge neutralization (recall Figure 12). As mentioned above, r_{DADMAC} is highest at pH 5 and [M] = 3 M; this may be due to low steric effects resulting from the copolymer rigidity and high monomer availability for propagation from the high monomer concentration.

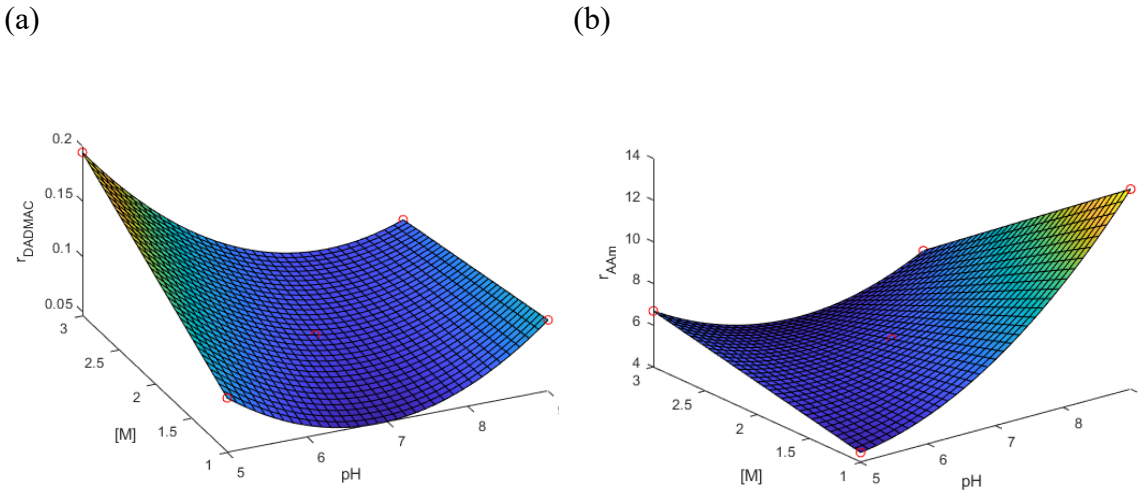

Figure 70: Surface response plots demonstrating the impact of pH and [M] on (a) r_{DADMAC} and (b) r_{AAm}

At pH 9, due to the random coil conformation (occurring due to charge neutralization), it is likely that the large DADMAC monomers may experience crowding effects, causing steric effects and decreasing reactivity ratio at (pH 9, [M] = 3 M) for the DADMAC-rich. The impacts of [M] are more significant at pH 5, since at pH 9 the charges are neutralized.

As mentioned above, the r_{AAm} (Figure 70(b)) variability under different reaction conditions is likely due to changes in cross-propagation, as it is not expected that homopropagation of AAm will be affected by pH or [M] in the ranges used. At (pH 5, [M] = 3 M) the r_{AAm} is likely higher than (pH 5, [M] = 1 M) due to competing reactions. At (pH 5, [M] = 3 M) r_{DADMAC} is at its highest, meaning a high k_{11}, likely causing a decrease in k_{21} due to competing reactions, decreasing k_{21} will increase r_{AAm}; more explanations about competing reactions were provided in Section 5.2.2.1. At (pH 9, [M] = 3 M), the cross-propagation (k_{21}) is likely higher due to the higher availability and more readily available DADMAC for propagation, compared to (pH 9, [M] = 1 M), where DADMAC is not as readily available for propagation due to lower concentration. As discussed in Section 2.4.2, studies show that [M] has minimal effects on AAm homopolymerization, whereas for DADMAC it is expected to increase with higher [M], therefore r_{AAm} will decrease (with higher cross-propagation) at (pH 9, [M] = 3 M) (see Equation 14). r_{DADMAC} does not significantly change when increasing [M] due to (pH 9, [M] = 3 M) having more DADMAC readily available to propagate, but will have more steric effects due to a crowding effect, and therefore counteracting effects.

7.2.2. Molecular Weight Characterization

For all of the samples synthesized at varying pH and [M] conditions, the $\overline{M}_w$ were estimated using GPC; these are summarized in Table 17. The $\overline{M}_w$ for AAm-rich flocculants were in the same range at around 5E6 g/mol, whereas DADMAC-rich flocculants had much more variation, especially at pH 5. This may be because at pH 5, the monomers and propagating polymer chains are charged during synthesis, which could have an effect on $\overline{M}_w$ and polydispersity. At pH 9, where the charges are neutralized, all DADMAC-rich polymers exhibited $\overline{M}_w$ around 1E6 g/mol.

Table 17: Weight-average molecular weights and PDI for all samples to be used in flocculation; data collected using GPC

	$\overline{M}_w$ of DADMAC-Rich Copolymers (g/mol)	PDI of DADMAC-Rich Copolymers	$\overline{M}_w$ of AAm-Rich Copolymers (g/mol)	PDI of AAm-Rich Copolymers
pH5, 1M	5.30E+05	1.86	4.46E+06	1.70
pH9, 1M	9.59E+05	1.32	4.39E+06	1.27
pH5, 3M	1.42E+06	1.08	3.56E+06	1.20
pH9, 3M	1.08E+06	1.69	3.76E+06	1.52
pH7, 2M	3.98E+05	1.20	5.12E+06	1.17

Results show that there is a trend between the weight-average molecular weights and the monomer concentration for the DADMAC-rich copolymers. For example comparing (pH 5, 1 M) to (pH 5, 3 M) the $\overline{M}_w$ increases. Also, at constant pH 9, the $\overline{M}_w$ increases slightly

with increasing [M]. However, the increase is much more substantial at pH 5, where the $\overline{M}_w$ almost triples. In a paper by Akyuz et al. [77] it was found that during homopolymerization of DADMAC, increasing monomer concentration increased the final $\overline{M}_w$, similar to what was observed for the DADMAC-rich copolymers in this study. In the same paper, it was also found that the final $\overline{M}_w$ was the same between samples, despite changing the pH. For AAm-rich polymers, the 1 M polymers had slightly higher $\overline{M}_w$ than the 3 M polymers. However, the copolymers synthesized at the mid-point, [M] = 2 M, had the highest $\overline{M}_w$. This may be due to a more complex system at pH 7, as the DADMAC is 50% protonated. An important difference between the study by Akyuz et al. [77] and the current work is as follows: in the literature study, the initiator was held constant and therefore an increased $\overline{M}_w$ is expected, whereas in this work the initiator concentration was adjusted so that the molecular weight averages would stay (approximately) the same; recall Equation 18. As such, any significant trends are not expected in the current data.

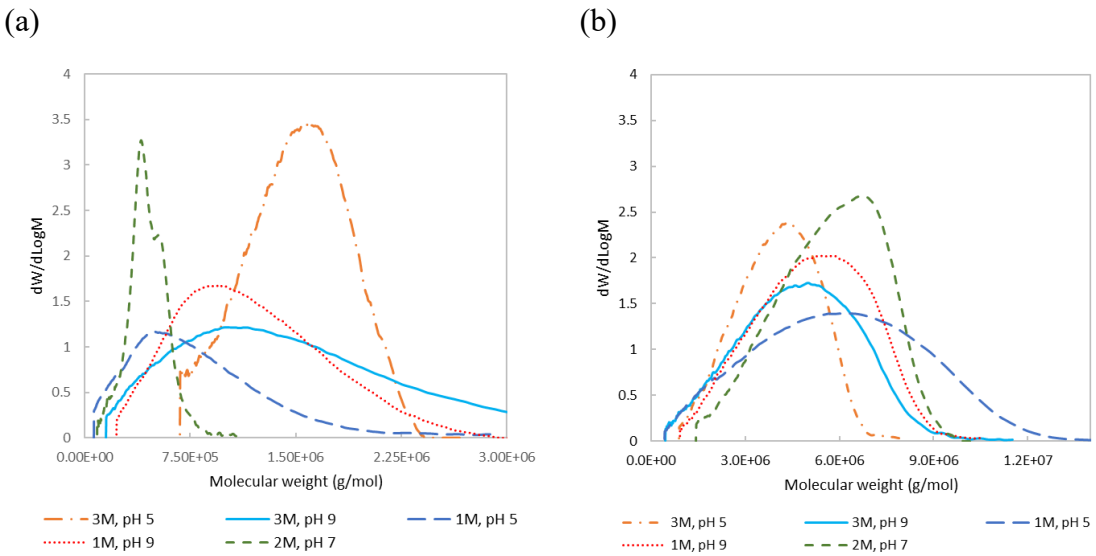

Figure 71: Molecular weight distributions of (a) DADMAC-rich and (b) AAm-rich samples measured by GPC

The PDIs of polymers synthesized under different conditions (as reported in Table 17) were also analyzed. Polymers with lower PDIs are generally more suitable for flocculation; a narrow molecular weight distribution means that there are fewer polymers with chains that are too short for bridging. The PDIs for both AAm- and DADMAC-rich polymers have similar trends, with a high PDI at (pH 5, 1 M) and (pH 9, 3 M). A lower PDI is obtained at (pH 5, 3 M) and (pH 9, 1 M).

(a) (b)

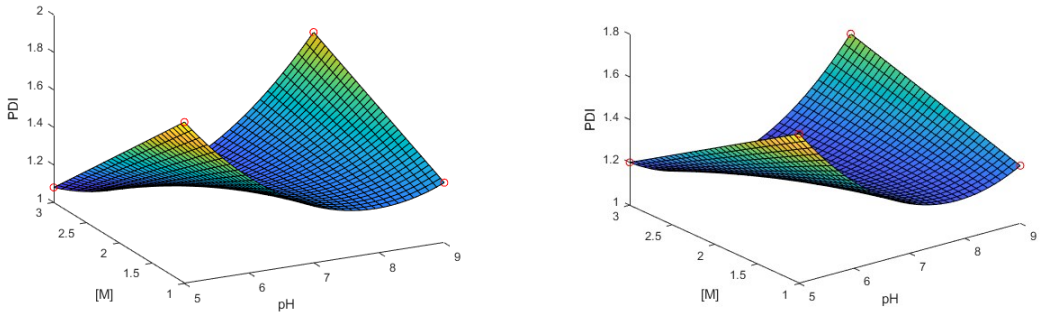

Figure 72: Surface response plots demonstrating the impact of pH and [M] on PDI for (a) DADMAC-rich flocculants and (b) AAm-rich flocculants

7.2.3. Flocculation Results

Flocculation trials at the Dartmouth Wastewater Treatment Facility were performed on October 5, 2023, and the influent was collected for the day at ~8:30 am. Experiments and measurements were done with the assistance of Carolina Ontiveros and Kayleigh Dunphy. Influent data measurements are shown in Table 18. As outlined previously, it is important to characterize the wastewater being tested, prior to treatment, since it is a complex system that is always changing. The flocculation jar test method explained in Section 3.6 was employed. The goal was to understand how copolymer microstructure would impact flocculation performance. Controls were also used in this study, where the controls went through the jar testing experiments without the addition of any polymer. All flocculation-related measurements in this chapter had 2 replicates, and the standard deviation was calculated based on these results.

Table 18: Measured influent properties from the Dartmouth Wastewater Treatment Plant on October 5, 2023

Temperature (°C)	pH	Alkalinity (mg/L $CaCO_3$)	Turbidity (NTU)	UVT254 (%T)
19.9	6.82	119	75.2	29.1
Zeta Potential (mV)	Conductivity (mS/cm)	TSS (mg/L)	BOD (mg/L)	COD (mg/L)
-15.03	2.348	177	99.2	369
UVT=ultraviolet transmission, TSS= total suspended solids, BOD= biochemical oxygen demand, and COD= chemical oxygen demand				

Settled water turbidity measurements (after treatment), including all synthesized copolymers and commercial cationic flocculants, are shown in Figure 73. Overall, the commercial flocculants created larger flocs and exhibited better settling behaviour. Commercial flocculants have been designed for optimal performance, whereas the custom flocculants synthesized in this study were designed to understand how the polymerization kinetics impact microstructure and flocculation performance. Commercial flocculants likely have higher copolymer concentration of cations, and some papers suggest that ideal copolymers have 50% ion composition [13]. Also, it is important to note that inorganic coagulants (such as alum) were intentionally excluded in these flocculation experiments. Typically, flocculants are added after coagulants to cause the flocs to further agglomerate, improving floc size and subsequent settling. Coagulants were intentionally excluded in this study to improve understanding of the flocculation mechanism without any external factors.

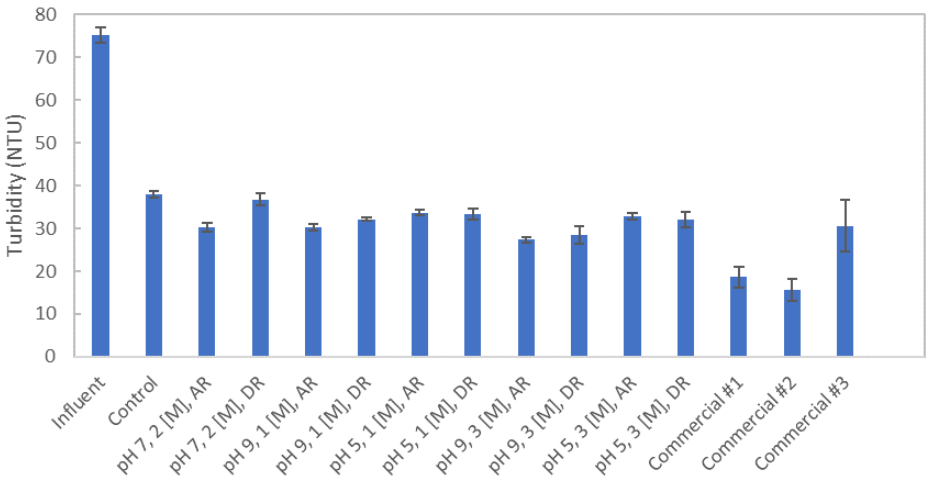

Figure 73: Settled water turbidity measurements for all flocculants tested, with error bars representing standard deviation; AR = acrylamide-rich and DR = DADMAC-rich

AAm-rich samples at each combination of pH and monomer concentration decreased settled water turbidity slightly more than DADMAC-rich samples, except polymerizations at pH 5. For wastewater treatment, a lower settled water turbidity following treatment is better. AAm-rich flocculants also created slightly larger flocs based on visual inspection; this may be due to the higher $\overline{M}_w$ obtained. The DADMAC-rich samples synthesized at pH 5 were better performing than their AAm-rich counterparts, likely due to the high concentration of protonated cations, whereas at pH 9 the cations are deprotonated. The increased fraction of positively charged ions in the DADMAC-rich chains were able to remove suspended solids just as well as or better than the AAm-rich flocculants synthesized under the same conditions. Figure 74 provides a comparison of the AAm-rich and DADMAC-rich flocculant settled water turbidity measurements side by side; this data is the same as that presented in Figure 73.

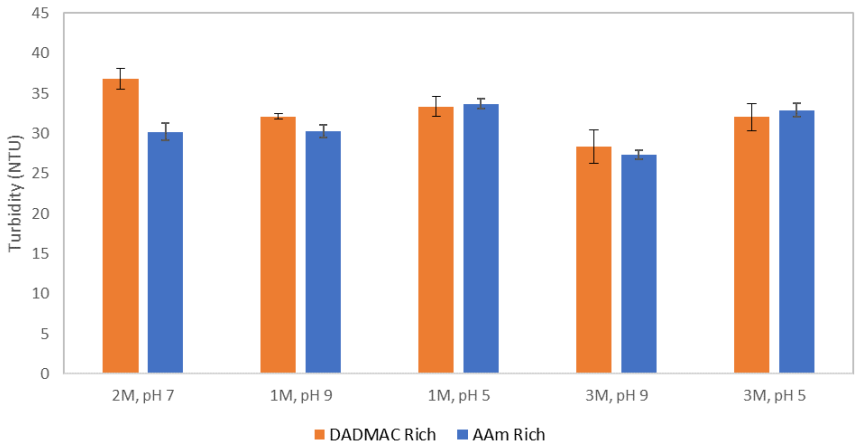

Figure 74: Settled water turbidity measurements for custom-made flocculants, with error bars representing standard deviation.

Surface response plots relating turbidity of the treated wastewater to the polymerization conditions are shown in Figure 75. There appears to be a strong trend between the reactivity ratios (Figure 70) and the settled water turbidity measurements. Results suggest that the lowest settled water turbidity measurements are using polymers synthesized at pH 9, for both DADMAC-rich and AAm-rich flocculants. When comparing the DADMAC-rich flocculant settled water turbidity measurements to r_{DADMAC}, both response surface plots follow a similar arch trend. For the AAm-rich flocculants, the settled water turbidity measurement and r_{AAm} have similar trends where the settled water turbidity decreased with increased pH, and an inverse trend was observed for r_{AAm}. One slight discrepancy is that (pH 9, [M] = 3 M) had the lowest settled water turbidity, but the highest r_{AAm} was at (pH 9, [M] =1 M).

(a) (b)

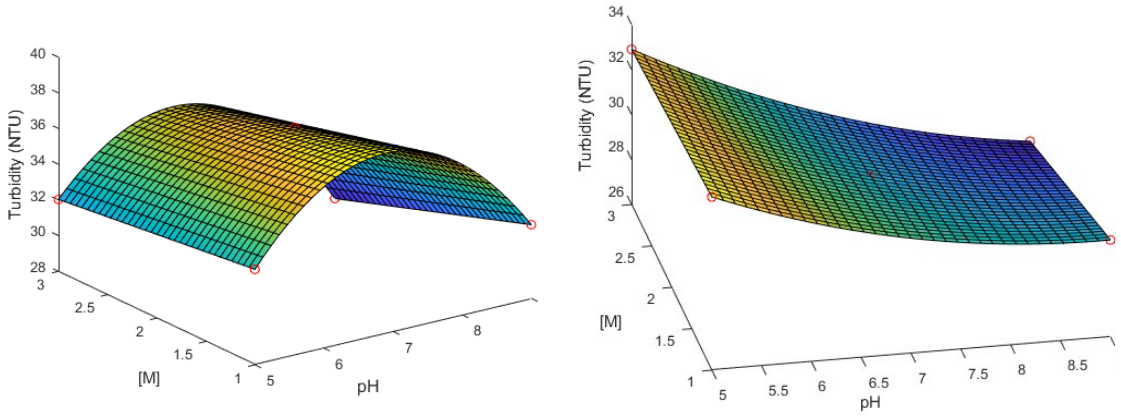

Figure 75: Surface response plots demonstrating the impact of pH and [M] on settled water turbidity for (a) DADMAC-rich flocculants and (b) AAm-rich flocculants

There is also a connection between polymer microstructure and the settled water turbidity of the treated wastewater. The triad fractions were calculated at the feed compositions using reactivity ratio estimates and the equations in Section 2.3.6. Figure 76 shows that for DADMAC-rich flocculants synthesized at pH 9, there was a low fraction of A_{111} triads, but a high fraction of A_{222} triads (1=DADMAC, 2=AAm). When looking at A_{212} triads (Figure 77), the fraction is significantly higher at pH 9 and [M] = 3 M. This suggests that optimal flocculation performance for removing suspended solids is to have AAm comonomers form a blocky microstructure (A_{222}), but for DADMAC comonomers to have an alternating microstructure (A_{212}). This means that it may be ideal to have at least 3 AAm comonomer units in a row, with DADMAC comonomers in between the AAm "blocks".

(a) (b)

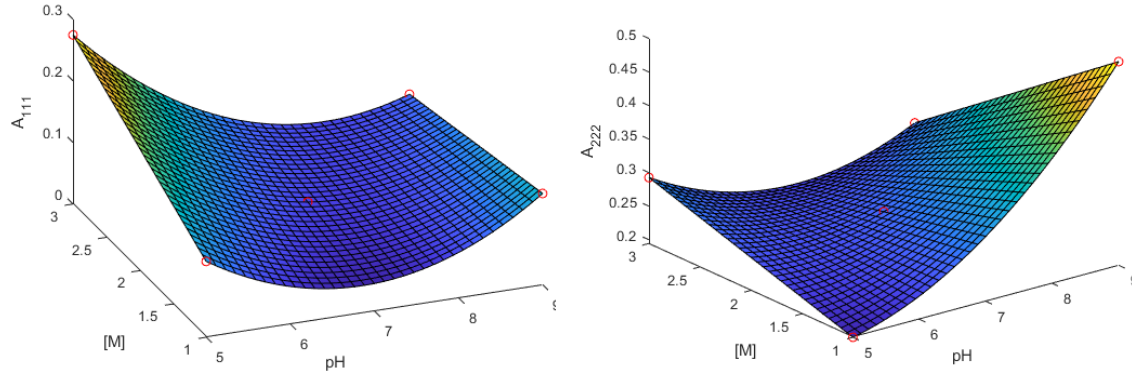

Figure 76: Surface response plots demonstrating the impact of pH and [M] on (a) A_{111} and (b) A_{222} triads for DADMAC-rich flocculants at 0.85 DADMAC copolymer composition

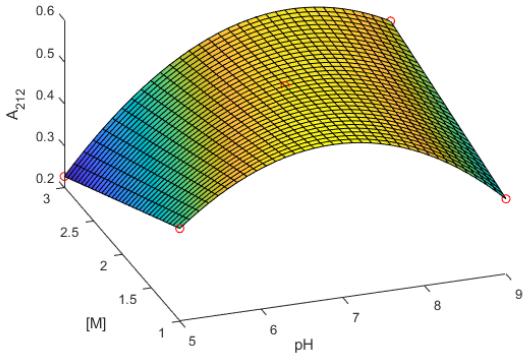

Figure 77: Surface response plots demonstrating the impact of pH and [M] on A_{212} triads for DADMAC-rich flocculants at 0.85 DADMAC copolymer composition

Similar results were observed for AAm-rich flocculants. There is a trend between having high A_{222} and A_{212} triads with reducing turbidity of the supernatant. The A_{222} triads give the copolymer a block-like microstructure, whereas the A_{212} triads indicate that the DADMAC comonomers are distributed throughout the polymer chain, surrounded by AAm. In Figure 78, it is shown that at pH 9, the A_{222} fractions are higher. Also, higher A_{212} fractions were observed for (pH 9, 3 M) than for (pH 9, 1 M). This combination of high

A_{222} and A_{212} could be used to explain why the (pH 9, 3 M) polymerization conditions synthesized the best performing flocculant for removing suspended solids, and (pH 9, 1 M) conditions synthesized the next best sample. If there was a high proportion of A_{111} fractions, that result would result in low A_{212} triads and indicate minimal DADMAC propagation until AAm is depleted or almost depleted. Therefore, a high proportion of A_{212} triads signifies more DADMAC propagation earlier in the reaction and better distribution along the polymer chain.

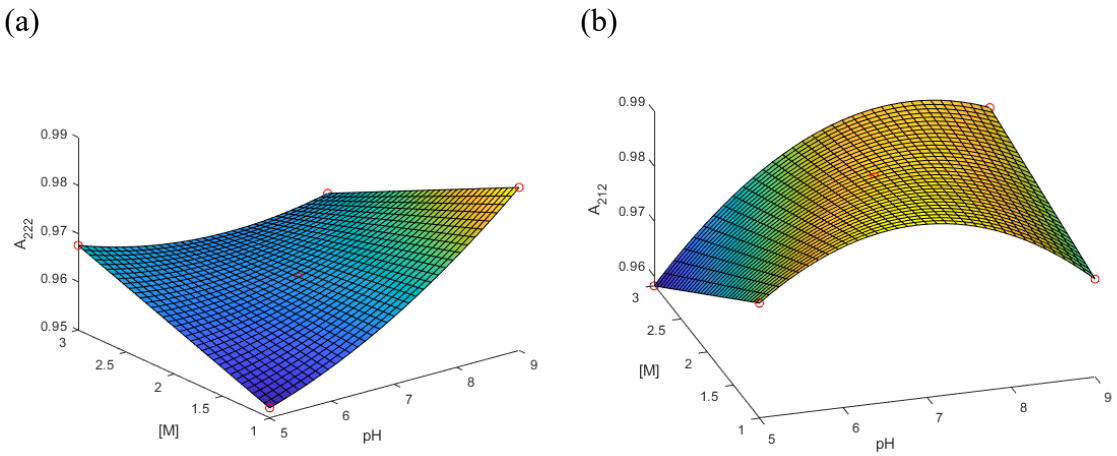

Figure 78: Surface response plots demonstrating the impact of pH and [M] on (a) A_{222} and (b) A_{212} triads for AAm-rich flocculants

Settled water UVT254 is used to indicate the amount of organic matter in solution. As shown in Figure 79(a), the center point for DADMAC-rich flocculant has the lowest transmittance, with the others showing higher and similar results. Although the high transmittance results are similar, the flocculants synthesized at (pH 9, 3 M) and (pH 5, 3 M) had the best performance at removing organic matter. The settled water UVT254 measurements for DADMAC-rich flocculants closely resemble the r_{DADMAC} surface plot in Figure 70(a). On average, the DADMAC-rich flocculants performed better than the AAm-

rich flocculants, as transmittance values were generally higher. This suggests that having a large proportion of charged comonomers is important for removing organic matter.

For the AAm-rich flocculants, all performed similarly (well) except for the flocculant synthesized at (pH 5, 1 M). The flocculant synthesized at (pH 5, 1 M) had low reactivity ratios compared to other formulations (Figure 70), which caused a low fraction of A_{222} triads (recall Figure 78). It is interesting to note that for AAm-rich flocculants, the center point (pH 7, 2 M) is best performing; this is likely related to high A_{212} triads (Figure 78). This could mean that when trying to remove organic matter, having alternating DADMAC is important. This is likely due to the small nature of organic matter compared to suspended solids. As stated earlier, some papers [5,14,39,63] have mentioned that intentionally designed microstructure is critical to avoid 'wasting' charges throughout polyelectrolyte chain.

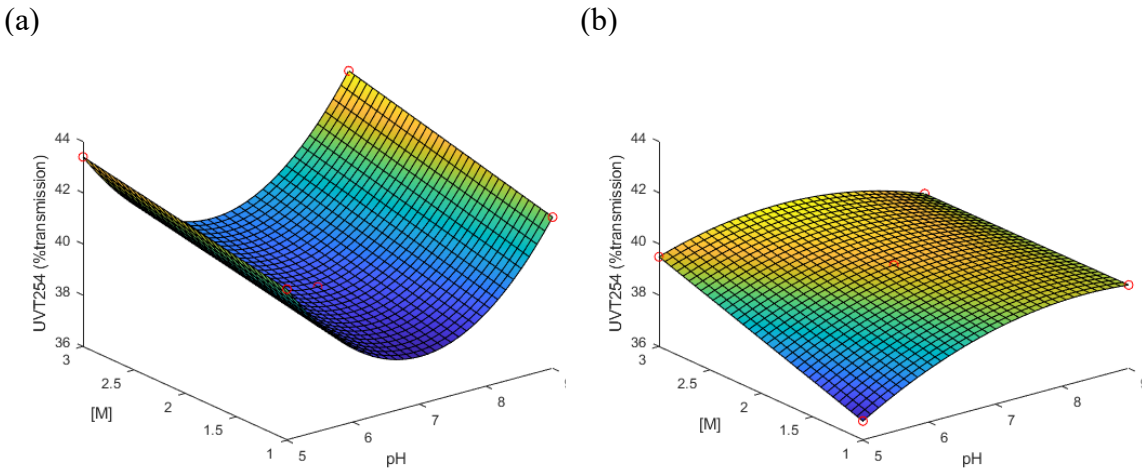

Figure 79: Surface response plots demonstrating the effect of pH and [M] on settled water UVT254 for (a) DADMAC-rich flocculants and (b) AAm-rich flocculants

Zeta potential is another important measurement for water treatment, as zeta potential provides a measure of the charge in the water. It is important to target 0 zeta potential to reduce repulsion between the contaminants and the polymers. For zeta potential measurements, AAm-rich flocculants tended to perform better than DADMAC-rich flocculants, as shown in Figure 80. This is rather surprising as DADMAC-rich flocculants have more cationic charges within the polymer chain, and it would be expected that the high concentration of cations would attract and remove the contaminants. In comparing these results to the triad fraction calculations, it seems like having more 'blocky' copolymer segments is effective for neutralizing charge. As seen for the DADMAC-rich flocculants, the DADMAC-rich polymer with the highest A_{111} triad was synthesized at (pH 5, 3 [M]); this was also the flocculant measurement with the zeta potential closest to 0 (compare Figure 76 and Figure 80). It seems that the DADMAC-rich flocculant zeta potential response is inverse of A_{212} (compare Figure 77 and Figure 80). This shows that certain microstructures may be better for removing specific contaminants. For the AAm-rich flocculant, a similar trend was observed: the A_{222} fraction was highest for the polymer synthesized at (pH 9, 1 [M]), which was also the best performing flocculant in terms of zeta potential. It seems for both flocculants there is a trend with either A_{111} or A_{222}, meaning having both DADMAC blocks and AAm blocks are important to control the zeta potential of treated wastewater.

(a) (b)

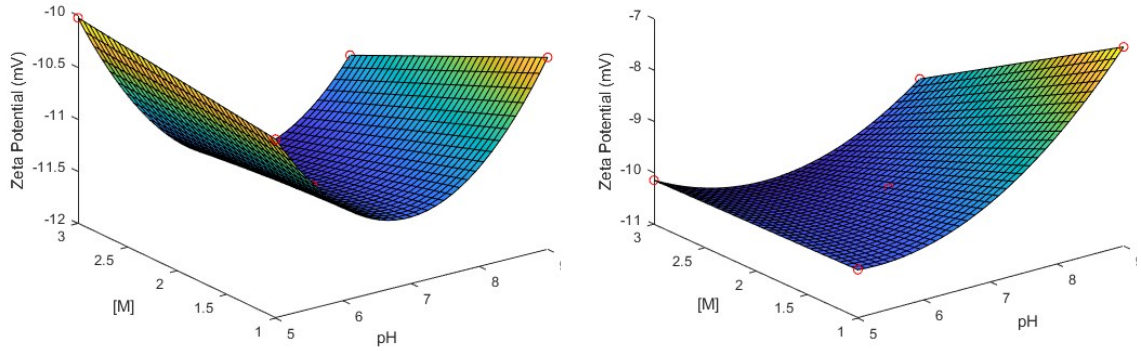

Figure 80: Surface response plots demonstrating the impact of pH and [M] on zeta potential for (a) DADMAC-rich flocculants and (b) AAm-rich flocculants

7.3. Conclusion

From the polymerization kinetics experiments, it was observed that the DADMAC – AAm copolymer microstructure was impacted by the reaction conditions. It was found that the reactivity ratios were statistically (and practically) impacted by changing the pH, monomer concentration, or both. For example, for comonomer solutions that were polymerized at (pH 9, [M] = 1 M), the reactivity ratios were r_{DADMAC}=0.110 and r_{AAm}=13.6. For this solution, the r_{AAm} was significantly higher than for the other formulations evaluated. For comonomer solutions that were polymerized at (pH 5, [M] = 3 M), the reactivity ratios were r_{DADMAC}=0.194 and r_{AAm}=6.68. For this solution the r_{DADMAC} was significantly higher than the other formulations evaluated.

From the flocculation trials, it was observed that the flocculation performance was dependant on the copolymer microstructure. It was found that DADMAC – AAm

copolymer flocculants (both AAm- and DADMAC-rich) made at (pH 9, 3 M) were the best materials to remove suspended solids. This is believed to be due to high triad fractions of A_{222} and A_{212} in the copolymer product. This agrees with other studies that have shown that block copolymers are better for flocculation due to less "wasted" charges (see, for example, [14,39,63]). This study shows that although A_{222} triads are very important, A_{212} triads are also important to distribute DADMAC throughout the polymer chain.

For reducing organic matter, it was found that all DADMAC-rich flocculants synthesized (under a variety of experimental conditions) performed well, except for the center point (pH 7, 2 M). This may have been due to low triad fractions of A_{111} and A_{222}. This suggests that 'blocky' copolymer sections are important for removing organic matter using DADMAC-rich flocculants. It was found that, in general, DADMAC-rich flocculants performed better than AAm-rich flocculants for removing organic matter, meaning that it is important to have a high proportion of charges within polyelectrolytes used for removing organic matter. For the AAm-rich flocculants, all flocculants perform well except those synthesized at (pH 5, 1 M). This was likely due to r_{AAm} being lowest under these reaction conditions, which translates to low fractions of both A_{222} and A_{212} triads.

For zeta potential measurements, it was found that AAm-rich flocculants were able to reduce the charges in the water more effectively than DADMAC-rich flocculants. This was not expected initially, but for AAm-rich flocculants synthesized at pH 9, the settled water turbidity of the treated wastewater was at its lowest. This means that contaminants were removed most effectively using these polymers, and the removal of those contaminants would also affect the zeta potential. This is likely due to the high fraction of A_{111} triads. The 'blocky' sections of DADMAC would create strong, positively charged fields to attract

the negatively charged contaminants. For the AAm-rich flocculants, the zeta potential results seem related to the A_{222} triad fractions, suggesting that the 'blocky' structure is again best for neutralizing zeta potential.

The best formulations in this work for overall flocculation performance were the copolymers synthesized at (pH 9, 3 M), especially the AAm-rich formulation. The AAm-rich copolymer synthesized at (pH 9, 3 M) was the best at lowering settled water turbidity and the second best at lowering zeta potential, but did not perform well in organic matter removal. The DADMAC-rich formulation synthesized at (pH 9, 3 M) was the best material for removing organic matter and the second best for lowering settled water turbidity, but did not perform well in the zeta potential testing. Another promising copolymer was the DADMAC-rich copolymer synthesized at (pH 5, 3M), as it performed reasonably well for all wastewater treatment tests. The best-performing material will also depend on the target contaminants; for this work, settled water turbidity was selected as the most important target for flocculation performance, therefore AAm-rich polymers synthesized at (pH 9, 3 M) were the best-performing materials for flocculation.

8. Thesis Conclusions and Recommendations

Flocculation is used in almost all wastewater treatment plants, therefore polymer flocculants are commonly used in wastewater treatment. Despite numerous publications on the topic, little attention has been paid to how the polymer microstructure impacts flocculation performance. The goal of this study was to establish a connection between copolymerization conditions, copolymer microstructure, and flocculation performance.

In Chapter 4, an in situ ^{1}H NMR copolymerization method was developed. This was possible because the carbon-carbon alkene bonds for both comonomers could be tracked throughout polymerization, making it possible to measure conversion and copolymer composition in parallel. This method also removes error associated with potentially measuring any unreacted monomer, salt, or retained water. The effect of ionic strength on AMPS – AAm copolymerization kinetics was then studied by adding NaCl to prepolymer solutions. It was found that increasing ionic strength altered the copolymer geometry in solution, shifting from a rigid rod conformation to a random coil conformation by ionic shielding. The reactivity ratios for AAm either decreased or increased, depending on the concentration of NaCl added; this is due to interactions of changing polymer geometries in solution and ionic shielding. This is an important result as polymer rigidity and subsequent flocculation performance can depend on ionic strength effects.

In Chapter 5, it was found that changing the ionic strength during DADMAC – AAm copolymerizations also had significant impacts on kinetics, microstructure, and flocculation performance. The reactivity ratios were significantly impacted by ionic strength, especially r_{DADMAC}: r_{DADMAC} increased by over 180%, while r_{AAm} only increased

by 11%. This resulted in significant differences in triad fractions; results showed that increasing ionic strength increased both the AAm and DADMAC 'blocky' fraction (A_{111} and A_{222}). GPC results demonstrated that ionic strength during synthesis had a minimal effect on $\overline{M}_w$. The DADMAC – AAm polymers were tested as flocculants in municipal wastewater treatment, and results showed that AAm-rich flocculants synthesized with 0.76 M NaCl added were the best performing samples for removing suspended solids and increasing zeta potential. It was also found that DADMAC-rich flocculants were best for removing organic matter (settled water UVT254 measurements).

Chapter 6 explored the advantages of the penultimate and terminal copolymerization models for estimating reactivity ratios when large and ionic monomers are involved in the copolymerization. It was found that both models have their advantages and disadvantages. Although very few reactivity ratios are readily available from the literature for the penultimate model, it was found that it may be better at predicting triad fractions for both AMPS – AAm and DADMAC – AAm copolymers. When using the two copolymerization models to estimate the cumulative copolymer composition, minimal differences were observed for AMPS – AAm copolymers, while for DADMAC – AAm copolymers there were significant differences.

In Chapter 7, it was found that changing the pH and [M] of pre-polymerization mixtures impacted the reactivity ratios of DADMAC – AAm copolymers. Unlike changing ionic strength, these factors impacted both r_{AAm} and r_{DADMAC} significantly. It was found from GPC measurements that pH and [M] also impacted the $\overline{M}_w$ and polydispersity, especially for the DADMAC-rich copolymers. From flocculation testing, it was found that the best performing flocculant overall was the AAm-rich copolymer synthesized at pH 9 and [M]

= 3 M. This is likely due to the triad fraction effects, where these polymers are predicted to have high fractions of both A_{212} and A_{222}. This suggests that AAm had long 'blocky' segments and that DADMAC was well-distributed throughout the chain. For Chapter 7, a central composite design can be used to better understand the curvatures in the surface responses. This will results in more accurate surface responses.

To the best of our knowledge, this project highlights the first studies connecting polymerization conditions, copolymer microstructure and flocculation performance in a single effort. This study lays the groundwork for future studies to further optimize polymer flocculants. Improving polymer flocculation will reduce the amount of polymer added and increase settling rates for wastewater treatment plants. This study demonstrates that altering the polymer reaction conditions, microstructure, and conformation will improve flocculation performance.

8.1. Future Work

Future work for AMPS – AAm copolymerization (Chapter 4) would benefit from more studies measuring molecular weight distributions. There are preliminary results for AAm-rich polymers around 5×10^6g/mol. More measurements would determine the effect of ionic strength on molecular weight averages and PDI. Another future study is an in-depth AMPS – AAm flocculation trial. AMPS – AAm copolymers would be used for anionic flocculants.

For future DADMAC – AAm studies (Chapters 5 and 7), it will be important to experiment with different feed fractions of DADMAC ($f_{DADMAC,0}$). In the current work, only 0.1 and 0.851 feed fractions were used. It will be important to investigate more feed fractions between these values that will likely impact flocculation performance. The feed fractions

used in this study were selected to accurately estimate the reactivity ratios, and were therefore not optimized for the flocculation application. One sample was tested from Chapter 6 ($f_{DADMAC,1,0}$ = 0.41), where flocculation trials were done alongside the polymers from Chapter 7. Results showed that it was by far the best at lowering settled water turbidity that day (26.1 NTU) and visually created the largest flocs of all custom-made polymers tested (example shown in Figure 81).

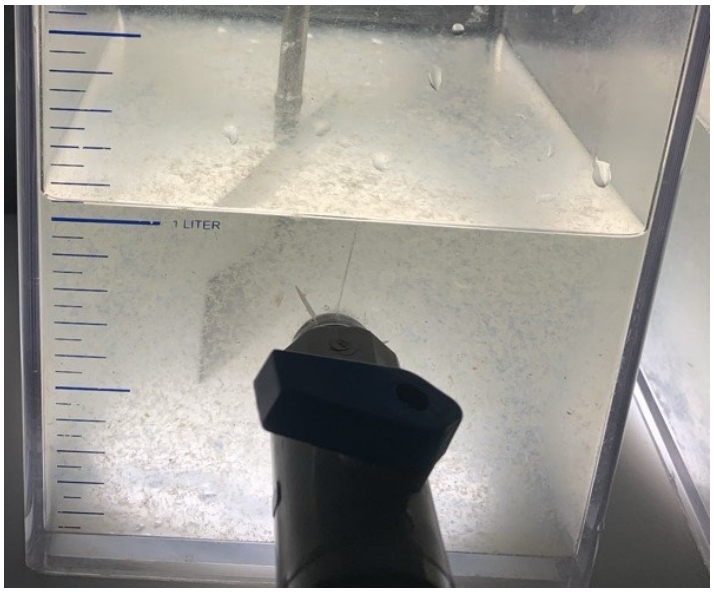

Figure 81: An image during flocculation trials using sample $f_{DADMAC,1,0}$ = 0.41 from Chapter 6.

Another future study (also related to Chapters 5 and 7) would include incorporating coagulants during wastewater treatment trials. In this study, no coagulants were used to eliminate the effects of additional factors. This caused the flocs to have low densities, even when the commercial flocculants were used. As a result, many of the flocs floated instead of settling as expected. Therefore, incorporating coagulants in an effort to improve settling would be an important next step, along with changing the comonomer feed fractions.

One specific issue was the solubility of the copolymer produced from 'Run 3' in Chapter 5. More work could be done to improve solubility, such as using ultrasonicator or diluting further.

Additionally, a lot of future work would benefit Chapter 6 results. One of the biggest opportunities is obtaining more triad fraction results to validate the penultimate model. Currently, minimal triad fraction results have been obtained, and furthering this experimental study is extremely important.

More future work related to Chapter 6 involves estimating joint confidence regions for penultimate reactivity ratios. Understanding the error is important when estimating reactivity ratios, especially in terms of how error impacts potential results.

In Chapter 7, the impact of pH and monomer concentration on reactivity ratios, molecular weight averages, and flocculation performance was studied. The physicochemical relationships between these variables and molecular weight averages were not entirely clear. This study would benefit from further work to better understand how molecular weight averages are impacted.

Initially, there was a desire to explore DADMAC-NVF copolymerization in the current study, for flocculation applications. NVF is considered a more environmentally friendly option than acrylamide [92–95]. However, upon searching the literature, only one pair of reactivity ratio estimates was found, r_{DADMAC}=0.13 and r_{NVF}=1.92 [64]. This is interesting how the reactivity ratio for NVF is smaller than AAm, this allows manipulation of reactivity ratios that are closer together and test other microstructures in flocculation trials.

References

1. Vajihinejad V, Gumfekar SP, Bazoubandi B, Rostami Najafabadi Z, Soares JBP. Water Soluble Polymer Flocculants: Synthesis, Characterization, and Performance Assessment. Macromol Mater Eng. 2019;304:1–43.

2. Chen W, Zheng H, Guan Q, Teng H, Zhao C, Zhao C. Fabricating a Flocculant with Controllable Cationic Microblock Structure: Characterization and Sludge Conditioning Behavior Evaluation. Ind Eng Chem Res. 2016;55:2892–902.

3. Abdollahi M, Alamdari P, Koolivand H, Ziaee F. A comprehensive study on the kinetics of aqueous free-radical homo- And copolymerization of acrylamide and diallyldimethylammonium chloride by online1H-NMR spectroscopy. J Polym Res. 2013;20.

4. Suopaj T. Functionalized nanocelluloses in wastewater treatment applications. 2015.

5. Guan Q, Zheng H, Zhai J, Liu B, Sun Y, Wang Y, et al. Preparation, characterization, and flocculation performance of <scp>P</scp> (acrylamide- co - diallyldimethylammonium chloride) by UV-initiated template polymerization. J Appl Polym Sci. 2015;132:1–7.

6. Ma J, Shi J, Ding H, Zhu G, Fu K, Fu X. Synthesis of cationic polyacrylamide by low-pressure UV initiation for turbidity water flocculation. Chem Eng J. 2017;312:20–9.

7. Salehizadeh H, Yan N, Farnood R. Recent advances in polysaccharide bio-based flocculants. Biotechnol Adv. 2018;36:92–119.

8. Li X, Zheng H, Gao B, Sun Y, Liu B, Zhao C. UV-initiated template copolymerization of AM and MAPTAC: Microblock structure, copolymerization mechanism, and flocculation performance. Chemosphere. 2017;167:71–81.

9. Zhang G, Ran Y, Jiang P, Pei H. A Study on the Thermal Degradation of an Acrylamide and 2-Acrylamido-2-Methylpropanesulfonic Acid Copolymer at High Temperatures. Polymers (Basel). 2023;15:2665.

10. Song H, Zhang S-F, Ma X-C, Wang D-Z, Yang J-Z. Synthesis and application of starch-graft-poly(AM-co-AMPS) by using a complex initiation system of CS-APS. Carbohydr Polym. 2007;69:189–95.

11. Elsaeed SM, Zaki EG, Omar WAE, Ashraf Soliman A, Attia AM. Guar Gum-Based Hydrogels as Potent Green Polymers for Enhanced Oil Recovery in High-Salinity Reservoirs. ACS Omega. 2021;6:23421–31.

12. Durmaz S, Okay O. Acrylamide/2-acrylamido-2-methylpropane sulfonic acid sodium salt-based hydrogels: synthesis and characterization. Polymer (Guildf). 2000;41:3693–704.

13. Vajihinejad V, Guillermo R, Soares JBP. Dewatering Oil Sands Mature Fine Tailings (MFTs) with Poly(acrylamide-co-diallyldimethylammonium chloride): Effect of Average Molecular Weight and Copolymer Composition. Ind Eng Chem Res. 2017;56:1256–66.

14. Zhang Z, Zheng H, Huang F, Li X, He S, Zhao C. Template Polymerization of a Novel Cationic Polyacrylamide: Sequence Distribution, Characterization, and Flocculation Performance. Ind Eng Chem Res. 2016;55:9819–28.

15. Baade W, Hunkeler D, Hamielec AE. Copolymerization of acrylamide with cationic monomers in solution and inverse-microsuspension. J Appl Polym Sci. 1989;38:185–201.

16. Jaeger W, Hahn M, Lieske A, Zimmermann A, Brand F. Polymerization of water soluble cationic vinyl monomers. Macromol Symp. 1996;111:95–106.

17. Bi K, Zhang Y. Kinetic study of the polymerization of dimethyldiallylammonium chloride and acrylamide. J Appl Polym Sci. 2012;125:1636–41.

18. Gumfekar SP, Soares JBP. Polymer reaction engineering tools to design multifunctional polymer flocculants. Chemosphere. 2018;210:156–65.

19. Chatsungnoen T, Chisti Y. Flocculation and electroflocculation for algal biomass recovery. Biofuels from Algae. Elsevier; 2019. p. 257–86.

20. Matsumoto A, Wakabayashi S, Oiwa M, Butler GB. Gelation in the Copolymerization of Diallyldimethylammonium Chloride with Acrylamide. J Macromol Sci Part A - Chem. 1989;26:1475–87.

21. Laskowski JS. Surface chemistry fundamentals in fine coal processing. Coal Handb Towar Clean Prod. Elsevier; 2013. p. 347–421.

22. Hyrycz M, Ochowiak M, Krupińska A, Włodarczak S, Matuszak M. A review of flocculants as an efficient method for increasing the efficiency of municipal sludge dewatering: Mechanisms, performances, influencing factors and perspectives. Sci Total Environ. 2022;820:153328.

23. Haydar S. Chemically Enhanced Primary Treatment of Wastewater. Water Encycl. 2004.

24. Kawahara M, Kato-Negishi M. Link between aluminum and the pathogenesis of Alzheimer's disease: The integration of the aluminum and amyloid cascade hypotheses. Int J Alzheimers Dis. 2011;2011.

25. Aluminum sulfate [Internet]. ChemSpider. Available from: http://www.chemspider.com/Chemical-Structure.23233.html

26. Iron(III) sulfate [Internet]. ChemSpider. Available from: http://www.chemspider.com/Chemical-Structure.23211.html

27. Lacík I, Chovancová A, Uhelská L, Preusser C, Hutchinson RA, Buback M. PLP-SEC Studies into the Propagation Rate Coefficient of Acrylamide Radical Polymerization in Aqueous Solution. Macromolecules. 2016;49:3244–53.

28. Preusser C, Chovancová A, Lacík I, Hutchinson RA. Modeling the Radical Batch Homopolymerization of Acrylamide in Aqueous Solution. Macromol React Eng. 2016;10:490–501.

29. Lin HR. Solution polymerization of acrylamide using potassium persulfate as an initiator: Kinetic studies, temperature and pH dependence. Eur Polym J. 2001;37:1507–10.

30. Xiong B, Loss RD, Shields D, Pawlik T, Hochreiter R, Zydney AL, et al. Polyacrylamide degradation and its implications in environmental systems. npj Clean Water. Springer US; 2018;1:17.

31. Bolto B, Gregory J. Organic polyelectrolytes in water treatment. Water Res. 2007;41:2301–24.

32. Jaeger W, Bohrisch J, Laschewsky A. Synthetic polymers with quaternary nitrogen atoms—Synthesis and structure of the most used type of cationic polyelectrolytes. Prog Polym Sci. Elsevier Ltd; 2010;35:511–77.

33. Ma J, Zheng H, Tan M, Liu L, Chen W, Guan Q, et al. Synthesis, characterization, and flocculation performance of anionic polyacrylamide P (AM-AA-AMPS). J Appl Polym Sci. 2013;129:1984–91.

34. Aguilar MI, Sáez J, Lloréns M, Soler A, Ortuño JF, Meseguer V, et al. Improvement of coagulation–flocculation process using anionic polyacrylamide as coagulant aid. Chemosphere. 2005;58:47–56.

35. Cao CY, Zhao YH, Zhou YJ. A study on oxidative degradation of polyacrylamide in wastewater with UV/FENTON/C4H4O62-. Int J Green Energy. 2016;13:80–4.

36. Beuermann S, Buback M, Hesse P, Junkers T, Lacík I. Free-Radical Polymerization Kinetics of 2-Acrylamido-2-methylpropanesulfonic Acid in Aqueous Solution. Macromolecules. 2006;39:509–16.

37. Kabiri K, Zohuriaan-Mehr MJ, Mirzadeh H, Kheirabadi M. Solvent-, ion- and pH-specific swelling of poly(2-acrylamido-2-methylpropane sulfonic acid) superabsorbing gels. J Polym Res. 2010;17:203–12.

38. Scott AJ, Riahinezhad M, Penlidis A. Optimal design for reactivity ratio estimation: A comparison of techniques for AMPS/acrylamide and AMPS/acrylic acid copolymerizations. Processes. 2015;3:749–68.

39. Feng L, Liu S, Zheng H, Liang J, Sun Y, Zhang S, et al. Using ultrasonic (US)-initiated template copolymerization for preparation of an enhanced cationic polyacrylamide (CPAM) and its application in sludge dewatering. Ultrason Sonochem. Elsevier; 2018;44:53–63.

40. Tian B, Fan B, Peng X, Luan Z. A cleaner two-step synthesis of high purity diallyldimethylammonium chloride monomers for flocculant preparation. J Environ Sci (China). 2005;17:798–801.

41. Vieira HVP, Oliveira PF, Costa JA, de Oliveira LA, Mota LS, Mansur CRE. Thermal stability of polymers based on acrylamide and 2-acrylamido-2-methylpropane sulfonic acid in different temperature and salinity conditions. J Appl Polym Sci. 2021;138:1–14.

42. McCormick CL, Chen GS. Water-soluble copolymers. IV. Random copolymers of acrylamide with sulfonated comonomers. J Polym Sci Polym Chem Ed. 1982;20:817–38.

43. Riahinezhad M, Mcmanus N, Penlidis A. Effect of monomer concentration and pH on reaction kinetics and copolymer microstructure of Acrylamide/Acrylic acid copolymer. Macromol React Eng. 2015;9:100–13.

44. Aggour YA. Thermal stability of poly(2-acrylamido-2-methylpropanesulphonic acid) and polymer complexes of 2-acrylamido-2-methylpropanesulphonic acid with some transition metal salts. Acta Polym. 1993;44:97–9.

45. Farag RK, Labena A, Fakhry SH, Safwat G, Diab A, Atta AM. Antimicrobial activity of hybrids terpolymers based on magnetite hydrogel nanocomposites. Materials (Basel). 2019;12.

46. Mao R, Huglin MB. A new linear method to calculate monomer reactivity ratios by using high conversion copolymerization data: terminal model. Polymer (Guildf). 1993;34:1709–15.

47. Tüdös F, Kelenm T. Analysis of the Linear Methods for Determining Copolymerization Reactivity Ratios. V. Planning of Experiments. J Macromol Sci Part A - Chem. 1981;16:1283–97.

48. Scott AJ, Penlidis A. Computational package for copolymerization reactivity ratio estimation: Improved access to the error-in-variables-model. Processes. 2018;6.

49. Wandrey C, Jaeger W. Copolymerization of dimethyl diallyl ammonium chloride and acryl amide. Acta Polym. 1985;36:100–2.

50. Tanaka H. Copolymerization of cationic monomers with acrylamide in an aqueous solution. J Polym Sci Part A Polym Chem. 1986;24:29–36.

51. Brand F, Dautzenberg H, Jaeger W. Polyelectrolytes with various charge densities: Synthesis and characterization of diallyldimethylammonium chloride-acrylamide copolymers - Brand - 2003 - Die Angewandte Makromolekulare Chemie - Wiley Online Library. Die Angew …. 1997;248:41–71.

52. Wang X, Yue Q, Gao B, Si X, Sun X, Zhang S. Dispersion copolymerization of acrylamide and dimethyl diallyl ammonium chloride in ethanol-water solution. J Appl Polym Sci. 2011;120:1496–502.

53. Losada R, Wandrey C. Copolymerization of a cationic double-charged monomer and electrochemical properties of the copolymers. Macromolecules. 2009;42:3285–93.

54. Scott AJ. Design of Polymeric Materials: Novel Functionalized Polymers for Enhanced Oil Recovery & Gas Sorption Applications. University of Waterloo, Thesis; 2019.

55. Su W-F. Radical Chain Polymerization. Princ Polym. Hoboken, NJ, USA: John Wiley & Sons, Inc.; 2013. p. 198–349.

56. Rudin A, Choi P. Elements of Polymer Science and Engineering. Elsevier; 2013.

57. Chanda M. Chain Copolymerization. Introd to Polym Sci Chem. CRC Press; 2013. p. 405–50.

58. Kazemi N. Reactivity Ratio Estimation in Multicomponent Polymerizations Using the Error-in-Variables-Model (EVM) Framework. University of Waterloo, Thesis; 2014.

59. Riahinezhad M, Kazemi N, McManus N, Penlidis A. Effect of ionic strength on the reactivity ratios of acrylamide/acrylic acid (sodium acrylate) copolymerization. J Appl Polym Sci. 2014;131:1–7.

60. Mayo FR, Lewis FM. Copolymerization. I. A Basis for Comparing the Behavior of Monomers in Copolymerization; The Copolymerization of Styrene and Methyl Methacrylate. J Am Chem Soc. 1941;147:1594–601.

61. Dube M, Sanayei RA, Penlidis A, O'Driscoll KF, Reilly PM. A microcomputer program for estimation of copolymerization reactivity ratios. J Polym Sci Part A Polym Chem. 1991;29:703–8.

62. Cabaness WR, Lin TY-C, Párkányi C. Effect of pH on the reactivity ratios in the copolymerization of acrylic acid and acrylamide. J Polym Sci Part A-1 Polym Chem. 1971;9:2155–70.

63. Zhao C, Zheng H, Feng L, Wang Y, Liu Y, Liu B, et al. Improvement of sludge dewaterability by ultrasound-initiated cationic polyacrylamide with microblock structure: The role of surface-active monomers. Materials (Basel). 2017;10.

64. Tanaka M, Tanaka H, Pelton R. Amine-derivatized poly(diallyldimethylammonium chloride) from N -vinylformamide copolymerization. J Appl Polym Sci. 2007;104:1068–75.

65. Shaikh S, Puskas JE, Kaszas G. A new high-throughput approach to measure copolymerization reactivity ratios using real-time FTIR monitoring. J Polym Sci Part A Polym Chem. 2004;42:4084–100.

66. Tidwell PW, Mortimer GA. An improved method of calculating copolymerization reactivity ratios. J Polym Sci Part A Gen Pap. 1965;3:369–87.

67. Burke AL, Duever TA, & Penlidis A. (1994). Model discrimination via designed experiments: Discriminating between the terminal and penultimate models based on triad fraction data. Macromolecular Theory and Simulations, 1994;3:1005–1031.

68. Burke AL, Duever TA, Penlidis A. Model discrimination via designed experiments: discriminating between the terminal and penultimate models on the basis of composition data. Macromolecules. 1994;27:386–99.

69. Duan QY, Gupta VK, Sorooshian S. Shuffled complex evolution approach for effective and efficient global minimization. J Optim Theory Appl. 1993;76:501–21.

70. Kazemi N, Duever TA, Penlidis A. Design of experiments for reactivity ratio estimation in multicomponent polymerizations using the error-in-variables approach. Macromol Theory Simulations. 2013;22:261–72.

71. Burke AL, Duever TA, Penlidis A. An experimental verification of statistical discrimination between the terminal and penultimate copolymerization models. J Polym Sci Part A Polym Chem. 1996;34:2665–78.

72. Burke AL, Duever TA, Penlidis A. Revisiting the design of experiments for copolymer reactivity ratio estimation. J Polym Sci Part A Polym Chem. 1993;31:3065–72.

73. Huang J, Turner SR. Recent advances in alternating copolymers: The synthesis, modification, and applications of precision polymers. Polymer (Guildf). Elsevier Ltd; 2017;116:572–86.

74. Kurenkov VF, Myagchenkov VA. Effects of reaction medium on the radical polymerization and copolymerization of acrylamide. Eur Polym J. 1980;16:1229–39.

75. Currie DJ, Dainton FS, Watt WS. The effect of pH on the olymerization of acrylamide in water. Polymer (Guildf). 1965;6:451–3.

76. Atta AM, El-Mahdy GA, Allohedan HA, Abdullah MMS. Synthesis and Application of Poly Ionic Liquid-Based on 2-Acrylamido-2-methyl Propane Sulfonic Acid as Corrosion Protective Film of Steel. Int J Electrochem Sci. 2015;10:6106–19.

77. Akyüz A, Buyukunsal G, Paril A. Online monitoring of diallyldimethylammonium chloride polymerization. Polym Eng Sci. 2014;54:1350–6.

78. Preusser C. Kinetics and Modeling of Free Radical Aqueous Phase Polymerization of Acrylamide with Acrylic Acid at varying Degrees of Ionization. Thesis. Queen's University, Thesis; 2015.

79. Paril A, Giz A, Catalgil-Giz H. Composition control through pH and ionic strength during acrylic acid/acrylamide copolymerization. J Appl Polym Sci. 2013;127:3530–6.

80. Scott AJ, Duever TA, Penlidis A. The role of pH , ionic strength and monomer concentration on the terpolymerization of 2-acrylamido-2-methylpropane sulfonic acid , acrylamide and acrylic acid. Polymer (Guildf). Elsevier; 2019;177:214–30.

81. Cutie SS, Henton DE, Powell C, Reim RE, Smith PB, Staples TL. The effects of MEHQ on the polymerization of acrylic acid in the preparation of superabsorbent gels. J Appl Polym Sci. 1997;64:577–89.

82. Mckay RT. How the 1D-NOESY suppresses solvent signal in metabonomics NMR spectroscopy: An examination of the pulse sequence components and evolution. Concepts Magn Reson Part A. 2011;38A:197–220.

83. Preusser C, Hutchinson RA. An In-Situ <scp>NMR</scp> Study of Radical Copolymerization Kinetics of Acrylamide and Non- <scp>I</scp> onized Acrylic Acid in Aqueous Solution. Macromol Symp. 2013;333:122–37.

84. How to Work Safely with - Hazardous Products using "Gas Cylinder" Pictogram [Internet]. Can. Cent. Occup. Heal. Saf. 2017. Available from: https://www.ccohs.ca/oshanswers/chemicals/howto/gas_cylinder.html

85. Feng J, Oyeneye OO, Xu WZ, Charpentier PA. In-Situ NMR Measurement of Reactivity Ratios for Copolymerization of Methyl Methacrylate and Diallyl Dimethylammonium Chloride. Ind Eng Chem Res. 2018;57:15654–62.

86. Ponratnam S, Kapur SL. Reactivity ratios of ionizing monomers in aqueous solution. Copolymerization of acrylic and methacrylic acids with acrylamide. Die Makromol Chemie. 1977;178:1029–38.

87. He G, Wen G, Skandalis A, Pispas S, Liu D. Effects of ionic strength and ion-specificity on the interface behavior of PDMAEMA-b-PLMA-b-POEGMA triblock terpolymer. Colloids Surfaces A Physicochem Eng Asp. Elsevier B.V.; 2023;658:130659.

88. Wandrey C, Hernandez-Barajas J, Hunkeler D. Diallyldimethylammonium Chloride and its Polymers. 1999;123–83.

89. Blatchley ER, Weng S, Afifi MZ, Chiu H, Reichlin DB, Jousset S, et al. Ozone and UV 254 Radiation for Municipal Wastewater Disinfection. Water Environ Res. 2012;84:2017–29.

90. Burke AL, Duever TA, Penlidis A. Model discrimination via designed experiments: Discrimination between the terminal and penultimate models based on rate data. Chem Eng Sci. 1995;50:1619–34.

91. Montgomery DC. Design and Analysis of Experiments. 8th ed. Joh Wiley & Sons; 2013.

92. Yao K, Wang S, Wang Q, Yang X. Synthesis and Characterization of Functional Monomer N -Vinyl Formamide (NVF). Macromol Chem Phys. 2022;223:1–10.

93. Marhefka JN, Marascalco PJ, Chapman TM, Russell AJ, Kameneva M V. Poly(N -vinylformamide)A Drag-Reducing Polymer for Biomedical Applications. Biomacromolecules. 2006;7:1597–603.

94. Gu L, Zhu S, Hrymak AN. Acidic and basic hydrolysis of poly(N-vinylformamide). J Appl Polym Sci. 2002;86:3412–9.

95. Gu L, Zhu S, Hrymak A., Pelton R. Kinetics and modeling of free radical polymerization of N -vinylformamide. Polymer (Guildf). 2001;42:3077–86.

Appendix A: Sample Calculations

A.1 Ionic Strength Concentration

The degree of ionization is calculated using Equation 40. pKa for DADMAC is 7 [77] and AMPS is 2.3 [76]. For this example, DADMAC – AAm comonomer solution with a feed fraction of f_{DADMAC} =0.851 at pH 7 was used.

$$\alpha = \frac{10^{pH-pKa}}{10^{pH-pKa}+1} \qquad \text{Equation 40}$$

$$\alpha = \frac{10^{7-7}}{10^{7-7}+1}$$

$$\alpha = 0.5$$

A monomer stock solution is made of 55.032 g of DADMAC (or 84.67 g of 65% DADMAC solution) and 4.236 g of AAm is used in 100 mL HPLC grade H_2O. A 10 mL sample is then taken from the stock.

$$\frac{55.032g * 10\ mL}{100\ mL} = 5.503g\ DADMAC$$

$$\left(\frac{5.503g\ DADMAC}{161.67\frac{g}{mol}DADMAC}\right) * 0.5 = 0.01702\ mol\ ions$$

Sample is diluted to a 20 mL solution.

$$\frac{0.01702\ mol\ cations}{0.020\ L} = 0.851\frac{mol}{L}\ ions$$

A.2 Chain Length Estimation

Chain length is estimated using Equation 18 and 19. For this example, DADMAC – AAm comonomer solution with a feed fraction of f_{DADMAC} =0.851 at pH 7 was used. Abdoulahi et al. reported a $\frac{k_p}{k_t^{.5}}$ = 0.558 (L·mol·s)$^{0.5}$ for 0.851 feed fraction of DADMAC [3]. For k_d, Preusser et al. gave Equation 41 for ACVA [28].

$$k_d(s^{-1}) = 8.96 \times 10^{16} \exp\left(\frac{-17080}{T}\right) \qquad \text{Equation 41}$$

$$k_d(s^{-1}) = 8.96 \times 10^{16} \exp\left(\frac{-17080}{50 + 273.15}\right)$$

$$k_d(s^{-1}) = 9.949 \times 10^{-7}\ s^{-1}$$

The chain length (v) is then calculated using Equation 18.

$$v = \frac{(0.558)(2)}{2\left((0.8)(9.949 \times 10^{-7})0.00526\right)^{\frac{1}{2}}}$$

$$v = \frac{1.116}{2(4.187 \times 10^{-9})^{\frac{1}{2}}}$$

$$v = \frac{1.116}{1.294 \times 10^{-4}}$$

$$v = 8624$$

$$\overline{DP}_n = 2v$$

$$\overline{DP}_n = 17248$$

Calculate average monomer molecular weight. A DADMAC copolymer composition of 0.851 is used in this example.

$$M_0 = 0.851(161.67) + (1 - 0.851)(71.08)$$

$$M_0 = 148.2\ g/mol$$

Calculate number average molecular weight:

$$\overline{M}_n = M_0\overline{DP}_n$$

$$\overline{M}_n = (148.2)(17248)$$

$$\overline{M}_n = 2.556 \times 10^6\ g/mol$$

A.3 Surface Response Methodology

In this example we will use settled water turbidity measurements for AAm-rich polymer flocculants from Chapter 7. The data is measured turbidity of the supernatant of the treated wastewater. Data can be seen in Table A.1.

Table A.1: Monomer concentration, pH, and resulting turbidity measurements from Chapter 7.

[M]	pH	Turbidity (NTU)
2	7	30.179
1	9	30.304
1	5	33.704
3	9	27.329
3	5	32.904

Using Equation 38:

$$y = \beta_0 + \sum_{j=1}^{k} \beta_j x_j + \sum\sum_{i<j} \beta_{ij} x_i x_j + \sum_{j=1}^{k} \beta_{jj} x_j^2 + \epsilon$$

β_0 is the center point (pH 7, 2 [M])

$$\beta_0 = 30.179$$

$$\beta_j = \frac{\frac{(27.329 + 30.304)}{2} - \frac{(33.704 + 32.904)}{2}}{2}$$

$$\beta_j = -2.244$$

$$\beta_i = \frac{\frac{(27.329 + 32.904)}{2} - \frac{(30.304 + 33.704)}{2}}{2}$$

$$\beta_i = -0.944$$

$$\beta_{ij} = \frac{\frac{(27.329 - 30.304)}{2} - \frac{(32.904 - 33.704)}{2}}{2}$$

$$\beta_{ij} = -0.5438$$

i represents the monomer concentration and *j* represents the pH. These results show us that reducing both pH and monomer concentration decreases turbidity since β_i and β_j are negative.

Equation 39 was used next to calculate β_{jj}. At each formulation, 1 polymer was tested in flocculation with 2 replicates, therefor $n_F = n_C = 2$.

$$\beta_{jj} = \frac{n_F n_C (\overline{y}_F - \overline{y}_C)}{n_F + n_C}$$

$\overline{y}_F$ is the average of the 4 responses at the factorial points.

$$\overline{y}_F = \frac{27.329 + 30.304 + 32.904 + 33.704}{4}$$

$$\overline{y}_F = 31.06$$

$\overline{y}_C$ is the center point.

$$\overline{y}_C = 30.179$$

$$\beta_{jj} = \frac{2 * 2 * (31.06 - 30.179)}{2 + 2}$$

$$\beta_{jj} = 0.8813$$

Calculate x_j using Equation 42

$$x_j = \frac{x - \frac{\left(pH_{low} + pH_{high}\right)}{2}}{\frac{pH_{high} - pH_{low}}{2}} \qquad \text{Equation 42}$$

$$x_j = \frac{x - \frac{(5+9)}{2}}{\frac{9-5}{2}} = \frac{x-7}{2}$$

Same for [M]:

$$x_i = \frac{z - \frac{(1+3)}{2}}{\frac{3-1}{2}} = \frac{z-2}{1} = z - 2$$

The resulting equation for the 2^2 factorial design was used for AAm-rich flocculant settled water turbidity measurements.

$$y = 30.179 + (-2.244) * \left(\frac{x-7}{2}\right) + (-0.944) * (z-2) + (-0.5438) * \left(\frac{x-7}{2}\right)$$

$$* (z-2) + (0.8813) * \left(\frac{x-7}{2}\right)^2$$

Plotting in MATLAB gives the following plot:

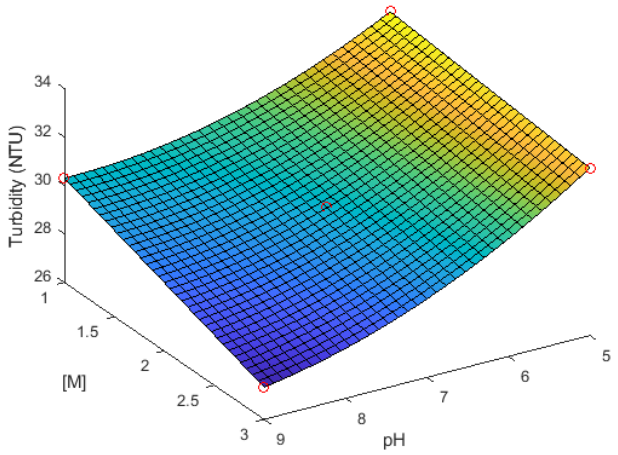

Figure A.1: Surface response for acrylamide-rich flocculant turbidity measurements. Note that the orientation is different than Figure 75